Technical University of Denmark

DTU

Quantitative studies of antimicrobial peptide-lipid membrane interactions

Kristensen, Kasper; Andresen, Thomas Lars; Henriksen, Jonas Rosager

Publication date:
2013

Document Version
Publisher's PDF, also known as Version of record

Link back to DTU Orbit

DTU Library
Technical Information Center of Denmark

Quantitative studies of antimicrobial peptide-lipid membrane interactions

PhD thesis
October 2013

Kasper Kristensen

Supervisor: Thomas L. Andresen
Co-supervisor: Jonas R. Henriksen

Quantitative studies of antimicrobial peptide-lipid membrane interactions

Preface

This thesis is submitted as part of the requirements for obtaining the degree of Doctor of Philosophy (PhD) at the Technical University of Denmark. The PhD project was funded by grants from the Innovation Consortium NanoMorph and the Technical University of Denmark. The work was carried at the Department of Micro- and Nanotechnology, DTU Nanotech, in the Colloids & Biological Interfaces Group in the period from September 2010 to October 2013, except for a three-month period from April 2012 to July 2012 in which I went abroad to visit the lab of Professor Petra Schwille at the Technical University of Dresden, Germany. The project was supervised by Professor Thomas L. Andresen (main supervisor) and Assistant Professor Jonas R. Henriksen (co-supervisor).

There are many people without whom this project would not have been possible. First and foremost, I am grateful to Thomas L. Andresen for giving me the opportunity to join his group and for providing valuable guidance and help throughout the course of the project. I am also indebted to Jonas R. Henriksen for his extensive help in the lab and for always finding time to discuss my ideas, thoughts, and problems. I also thank Nicky Ehrlich for a great collaboration on developing the assay for studying antimicrobial peptide-induced leakage on the single-vesicle level. In addition, I thank Rasmus Irming Jølck, Lise Nørkjær Bjerg, Rasmus Eliasen, and Lotte Nielsen for their help with the preparative and analytical HPLCs, and I thank Lars Linderoth and Sofie Trier from Novo Nordisk for carrying out the peptide concentration measurements on the chemiluminescent nitrogen detection system. Moreover, I thank all of my colleagues in the Colloids & Biological Interfaces Group for creating an inspiring, helpful, friendly, and humorous working atmosphere on a day-to-day basis.

In connection with my stay in Dresden, I would like to thank Petra Schwille for giving me the opportunity to visit her lab. Additionally, I would also like to express my deep gratitude to the people in her lab for welcoming me and for giving me a memorable and eventful stay in the fantastic city of Dresden. I also thank Augustinus Fonden and Rudolph Als Fondet for providing financial support for my stay in Dresden.

Last, but not least, I would like to thank my friends, my family, and my girlfriend, Nadia, for their loving support and for their patience with me in the final period of the project.

Abstract

The increasing occurrence of multi-drug-resistant bacteria poses a serious threat to modern society. Therefore, novel types of anti-infective therapeutics are highly warranted. Antimicrobial peptides are a class of naturally occurring host-defense molecules that potentially might be developed into such novel therapeutics. However, limited understanding of the mechanisms underlying microbicidal activity of antimicrobial peptides has slowed down this development.

A central step toward understanding the microbicidal mechanisms of action of antimicrobial peptides is to understand the mechanisms by which antimicrobial peptides interact with phospholipid membranes. Motivated by that fact, the scope of this thesis is to study these antimicrobial peptide-lipid membrane interactions. In particular, we attempt to study these interactions with a quantitative approach. For that purpose, we consider the three archetypal α-helical antimicrobial peptides mastoparan X, melittin, and magainin 2 as model peptides. These three peptides are investigated by three different experimental techniques.

The first of these experimental techniques is analytical HPLC. We use this technique to document an effect that might pose a significant problem for quantitative studies of antimicrobial peptide-lipid membrane interactions; namely that antimicrobial peptides adsorb to surfaces of glass and plastic. Specifically, we demonstrate that under standard experimental conditions, this effect is significant for mastoparan X, melittin and magainin 2. Consequently, we conclude that investigators should always take this adsorptive effect into account when designing and interpreting their experiments on antimicrobial peptides.

The second experimental technique is fluorescence correlation spectroscopy (FCS). We optimize this technique so that it can be used to quantify antimicrobial peptide-induced leakage of fluorescent markers from large unilamellar lipid vesicles in solution. For that purpose, we derive the mathematical framework required to calculate leakage from the FCS data, and we identify a number of experimental pitfalls that might lead to inaccurate conclusions, or even completely wrong conclusions, when interpreting the FCS data. We show that, if all of the pitfalls are avoided, then FCS is a technique with a large potential for quantitative studies of antimicrobial peptide-induced leakage of fluorescent markers from large unilamellar lipid vesicles in solution. Particularly interesting is our finding that FCS might be used for studying peptide-induced leakage of markers of different sizes, thereby providing a novel approach for rapid sizing of transmembrane pores formed by antimicrobial peptides. We demonstrate

the applicability of FCS by using the technique to study partial transient leakage induced by mastoparan X, melittin, and magainin 2. The leakage data demonstrate that magainin 2 forms larger and/or more stable transmembrane pores in POPC/POPG (3:1) lipid bilayers than do mastoparan X and melittin.

The third and final technique is confocal imaging. Specifically, we use this technique to visualize fluorescently-labeled surface-tethered large unilamellar lipid vesicles. We design an experimental protocol that allows us to directly correlate antimicrobial peptide-induced leakage of fluorescent markers from these surface-tethered vesicles to antimicrobial peptide-induced leakage of fluorescent markers from lipid vesicles in solution. Thereby, we have developed a direct and flexible approach for quantitative evaluation of antimicrobial peptide-induced leakage from large unilamellar lipid vesicles on the single-vesicle level, allowing us an unprecedented level of insight into the leakage process. For example, the surface-tethered lipid vesicles can be used to directly visualize how the single-vesicle leakage profiles depend on the marker size. We employ the surface-tethered vesicles to study partial transient leakage induced by mastoparan X, melittin and magainin 2 from POPC/POPG (3:1) large unilamellar lipid vesicles. The results show that on the single-vesicle level, all three peptides induce heterogenous leakage in the sense that they induce complete emptying of some vesicles and only partly emptying of other vesicles. This heterogenous leakage profile is observed regardless of the size of the lumen dye.

Resumé

Den stigende forekomst af antibiotika-resistente bakterier udgør en alvorlig trussel mod det moderne samfund. Nye typer af antiinfektive lægemidler er derfor højt eftertragtede. Antimikrobielle peptider er en klasse af naturligt forekommende molekyler, der potential kan udvikles til at blive en sådan ny type af lægemidler. Denne udvikling er dog indtil videre blevet bremset af en begrænset viden om virkemåden af antimikrobielle peptider.

Et centralt skridt mod at forstå virkemåden af antimikrobielle peptider er at forstå de mekanismer, hvormed antimikrobielle peptider vekselvirker med fosfolipidmembraner. Motiveret af denne kendsgerning er målet for nærværende afhandling at studere disse vekselvirkninger. I særdeleshed er målet for afhandlingen at studere disse vekselvirkninger med en kvantitativ indgangsvinkel. Til det formål anvender vi de tre α-heliske antimikrobielle peptider mastoparan X, melittin og magainin 2. Disse tre peptider studeres ved hjælp af tre forskellige eksperimentelle teknikker.

Den første eksperimentelle teknik er analytisk HPLC. Vi anvender denne teknik til at dokumentere en effekt, der potentielt kan udgøre et alvorligt problem for kvantitative studier af vekselvirkningen mellem antimikrobielle peptider og lipidmembraner - nemlig at antimikrobielle peptider adsorberer til overflader i glas- eller plastikbeholdere. Vi demonstrerer at denne effekt er signifikant for både mastoparan X, melittin og magainin 2 ved almindeligt anvendte eksperimentelle koncentrationer. Følgelig konkluderer vi at det er vigtigt at tage højde for denne effekt ved design og fortolkning af experimentelle studier af antimikrobielle peptider.

Den anden eksperimentelle teknik er fluorescens korrelations spektroskopi (FCS). Vi optimerer denne teknik, så den kan anvendes til kvantitative studier af peptid-induceret frigivelse af fluorescerende markører fra store unilamellære lipidvesikler i opløsning. Til det formål udleder vi den nødvendige matematik, og vi identificere et antal eksperimentelle faldgruber, der kan føre til upræcise eller decideret forkerte konklusioner ved fortolkningen af FCS data. Vi viser, at hvis alle disse faldgruber undgås, er FCS en teknik med et stort potentiale for kvantitative studier af peptid-induceret frigivelse af fluorescerende markører fra store unilamellære lipidvesikler. I denne forbindelse er det en særlig interessant observation at FCS kan bruges til at studere frigivelse af markører af forskellige størrelser. Derved kan FCS anvendes til hurtige størrelsesbestemmelser af peptid-inducerede transmembranporer. Vi demonstrerer anvendeligheden af FCS ved at benytte teknikken til at studere partiel transient frigivelse af indholdet af lipidvesikler induceret af mastoparan X, melittin og magainin 2. Vores resultater

demonstrerer at magainin 2 danner større og/eller mere stabile porer i POPC/POPG (3:1) lipidmembraner end mastoparan X og melittin.

Den tredje og sidste teknik er konfokal mikroskopi. Vi anvender denne teknik til at visualisere fluorescensmærkede store unilamellære lipidvesikler, der er immobiliserede til en glasoverflade. Vi designer en eksperimentel protokol, så vi direkte kan korrelere peptid-induceret frigivelse af fluorescerende markører fra de immobiliserede lipidvesikler til peptid-induceret frigivelse af fluorescerende markører fra lipidvesikler i opløsning. Derved har vi udviklet en direkte og fleksibel metode til kvantitativ evaluering af peptid-induceret frigivelse af fluorescerende markører fra store unilamellære lipidvesikler på enkelt-vesikel niveau. Denne metode giver os en hidtil uset indsigt i frigivelsesprocessen. For eksempel kan vi ved hjælp af de immobiliserede vesikler studerer hvordan frigivelsesprocessen på enkelt-vesikel niveau afhænger af størrelsen af den fluorescerende markør. Vi anvender de immobiliserede lipid-vesikler til at studere partiel transient frigivelse induceret af mastoparan X, melittin og ma-gainin 2 fra POPC/POPG (3:1) store unilamellære lipidvesikler. Resultaterne viser, at på enkelt-vesikel niveau inducerer alle tre peptider en heterogen frigivelsesprofil i den forstand, at de inducer fuldstændig tømning af nogle vesikler og kun delvis tømning af andre vesikler. Denne heterogene frigivelsesprofil observeres uanset størrelses af den indkapsulerede markør.

Contents

Introduction

1.1 Why study antimicrobial peptides?

The 20th century was a period that brought a series of revolutionary, technological breakthroughs to mankind. The discovery and development of antibiotics to fight infectious diseases was one of these breakthroughs. Indeed, contemporary healthcare would not be what it is today were it not for these wonder drugs.

However, ever since the introduction of the first antibiotic agents, the problem of microbial pathogen resistance to antibiotics has been well-known. Today, the problem of antibiotic resistance has turned into a regular resistance crisis that poses a grave menace to modern healthcare systems (1). To mitigate this emerging resistance crisis, novel alternatives to the conventional antibiotics are needed (2). Unfortunately, in spite of this pressing demand for novel antibiotics, only a few new antibiotic drugs have been approved for clinical use in recent years (3). Furthermore, new antibiotic drug candidates in pipeline are scarce (4). This is where antimicrobial peptides come into the picture.

Antimicrobial peptides are a class of host defense molecules that is ubiquitously present in a variety of life forms across the evolutionary spectrum (5). Since one of their principal biological roles is to protect their host organism by killing a broad spectrum of invading microbial pathogens (6), antimicrobial peptides have also attracted considerable scientific attention as candidates to become a novel class of antibiotics. As a matter of fact, antimicrobial peptides as anti-infective therapeutic candidates display several advantages over conventional antibiotics. One important example of these advantages is the capability of antimicrobial peptides to kill microbes that are resistant to conventional antibiotics. Another example is that antimicrobial peptides do not evoke resistance in pathogens to the same extent as conventional antibiotics, probably because the peptides act via multiple mechanisms of action (7, 8).

As of today, a few antimicrobial peptides, such as polymyxin B and gramicidin S, have successfully found their way into products on the pharmacy shelf, primarily for topical applications. Moreover, a number of antimicrobial peptides and peptidomimetics for mostly topical applications are currently in preclinical or clinical trials (8, 9). However, in spite of

these facts, a number of obstacles remain for the development of antimicrobial peptides into effective profitable drugs, especially in relation to drugs with systemic applications. These obstacles include high manufacturing cost, unknown toxicity profiles, and susceptibility to proteolytic degradation (7). Yet another obstacle limiting the development of antimicrobial peptides into successful cost-effective therapeutics is the lack of understanding of their mechanism of action (10). To be more specific, enhancing the understanding on the mechanisms by which antimicrobial peptides kill microbes would greatly aid the rational design of novel antimicrobial peptide-based drug formulations. Indeed, to overcome the above-mentioned obstacles, there is still plenty of need to study antimicrobial peptides.

1.2   Thesis scope

There are two predominant hypotheses to explain the microbicidal mode of action of antimicrobial peptides. The first predominant hypothesis suggests that antimicrobial peptides kill microbes by disrupting the structural integrity of the microbial cytoplasmic membrane (11). The second predominant hypothesis suggests that the peptides translocate across the cytoplasmic membrane to target intracellular processes (12). Either way, the microbial cytoplasmic membrane is at the center of action. To understand the microbicidal mode of action of antimicrobial peptides, it is, therefore, essential to understand their interactions with phospholipid membranes (10). That takes us to the scope of this thesis; the scope of this thesis is to quantitatively study the interactions between antimicrobial peptides and phospholipid membranes. The fact that these interactions are studied quantitatively, and not only qualitatively, should be emphasized. As opposed to qualitative information, quantitative information will provide a direct basis for comparing the effect of different antimicrobial peptides under varying experimental conditions. In addition, quantitative information will essentially also allow the formulation of more detailed models to correlate the mode of membrane interactions of antimicrobial peptides directly to the physicochemical characteristics of the peptides.

1.3   Thesis outline

The thesis consists of one introductory chapter, three manuscripts in preparation, and a final concluding chapter. The introductory chapter, Chapter 2, reviews the state of the research field of antimicrobial peptides as of today. In particular, emphasis is put on reviewing the current knowledge about antimicrobial peptide-lipid membrane interactions. Chapter 2 also contains a more elaborate discussion about the thesis scope than provided in Section 1.2. Chapters 3-5 contains each of the three manuscripts. The common denominator of these three manuscripts is quantitative studies of antimicrobial peptide-lipid membrane interactions. The lay-out of each of the manuscripts is adapted to fit the lay-out of the thesis. The final concluding chapter, Chapter 6, summarizes the findings of the thesis and briefly discusses future directions of research.

1.4 Publications

The work conducted during this PhD study have resulted in three article manuscripts (contained in Chapters 3-5) and two conference contributions.

1.4.1 Articles

1. K. Kristensen, J. R. Henriksen, and T. L. Andresen. Adsorption of cationic membrane-active peptides to glass and plastic surfaces. *Manuscript under preparation. To be submitted.*

2. K. Kristensen, J. R. Henriksen, and T. L. Andresen. Quantification of antimicrobial peptide-induced leakage from large unilamellar vesicles by FCS. *Manuscript under preparation. To be submitted.*

3. K. Kristensen, N. Ehrlich, J. R. Henriksen, and T. L. Andresen. Single-vesicle analysis of leakage induced by cationic membrane-active peptides. *Manuscript under preparation. To be submitted.*

1.4.2 Conference contributions

1. K. Kristensen, J. R. Henriksen, and T. L. Andresen. Quantitative studies of antimicrobial peptide pore formation in large unilamellar vesicles by fluorescence correlation spectroscopy (FCS). Platform presentation at Biophysical Society 57th Annual Meeting, 2-6 February 2013, Philadelphia, PA, USA. Abstract published in *Biophysical Journal*, 104(2; Suppl 1):21a, 2013.

2. K. Kristensen, N. Ehrlich, J. R. Henriksen, and T. L. Andresen. Quantitative single-vesicle analysis of antimicrobial peptide-induced leakage. Poster presented at 9th European Biophysics Congress, 13-17 July 2013, Lisbon, Portugal. Abstract published in *European Biophysics Journal*, 42(Suppl 1):S167, 2013.

Antimicrobial peptides

The research field of antimicrobial peptides has been thriving for decades. Combined cross-disciplinary efforts have provided valuable insight into the structure and function of these peptides, but have also left the field with a number of open questions. This chapter reviews the state of the research field as of today. In Sections 2.1-2.3, the functional and structural properties of antimicrobial peptides are described. In Section 2.4, special emphasis is put on interactions between antimicrobial peptides and phospholipid membranes, and a number of popular interaction models are reviewed. Next, in Section 2.5, questions about antimicrobial peptides that still remain to be answered are discussed. Subsequently, in Section 2.6, a brief introduction is given to the three antimicrobial peptides that are studied in this thesis: mastoparan X, melittin and magainin 2. At last, in Section 2.7, the chapter is concluded by revisiting the thesis scope in the light of the information found in this chapter.

2.1   Functions in immunity

Antimicrobial peptides are a class of naturally occurring host defense molecules. To date, more than 2000 peptides with antimicrobial activity have been identified in a broad range of organisms across the biological world, including bacteria, fungi, plants, and animals (13, 14). Antimicrobial peptides are also abundantly present in mammals where they, inter alia, are expressed in mast cells, monocytes, macrophages, neutrophils, epithelial cells, and keratinocytes (8).

Antimicrobial peptides are thought to function as an important part of the innate immune system, providing an effective protective machinery against infectious pathogens. Indeed, the protective role of antimicrobial peptides has been implied in several studies on animal models. For example, mice in which the gene encoding the antimicrobial peptide CRAMP was knocked out were more susceptible to necrotic skin infection caused by the Gram-positive bacterium Group A *Streptococcus* than were wild-type mice (15). In another example, transgenic mice expressing the human Paneth cell antimicrobial peptide HD-5 were far more resistant to oral challenge of the Gram-negative bacterium *Salmonella typhimurium* than were wild-type mice (16). In fact, the transgenic mice expressing HD-5 completely recovered from oral doses that

```
┌─────────────────────────┐
│   Antimicrobial peptides │
│     in innate immunity   │
└─────────────────────────┘
```
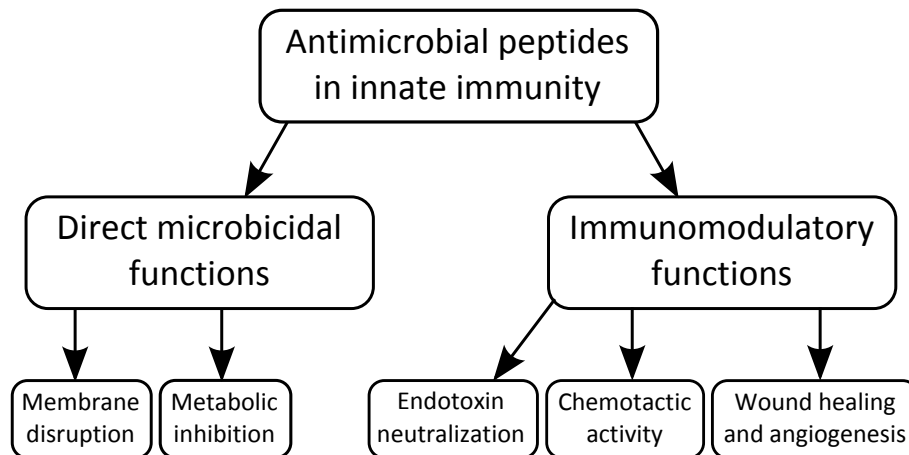
Figure 2.1: Non-comprehensive overview of the roles that antimicrobial peptides have been proposed to play in innate immunity. Generally, antimicrobial peptides are thought to act through direct microbicidal activities as well as immunomodulatory activities.

caused $100\,\%$ mortality in the wild-type mice, thus illustrating the protective capabilities of HD-5.

Indications of the protective role of antimicrobial peptides, however, not only come from observations in animal models, but also from observations in human patients. For instance, patients with Kostmann disease, a severe congenital neutropenia, were devoid of the antimicrobial peptide LL-37, and this deficiency correlated to the occurrence of frequent infections and periodontal disease (17). The protective functions of antimicrobial peptides were also implied by the increasing peptide expression levels in patients with inflammatory conditions such as cystic fibrosis, bronchiolitis, and psoriasis (8).

Many different suggestions as to the specific functions by which antimicrobial peptides defend their host organism from invading microbial pathogens have been put forward. These functions are generally divided into two categories: direct microbicidal functions and immunomodulatory functions (8), see Fig. 2.1.

2.1.1 Direct microbicidal functions

Direct killing of infectious microbial pathogens is thought to be one of the principal biological functions of antimicrobial peptides (5). Indeed, there is plenty of evidence that antimicrobial peptides are capable of directly killing a broad spectrum of Gram-positive and Gram-negative bacteria, fungi, and viruses (6, 8).

The mechanisms by which antimicrobial peptides kill these microbes are still a topic for debate (14). One predominant idea suggests that antimicrobial peptides act by disrupting the structural integrity of the microbial cell membrane (11). Accordingly, the literature is rich with *in vitro* examples showing that peptide action is associated with membrane disruption and cell lysis. For example, bactericidal activity of the antimicrobial peptides magainin 2 and cecropin P1 against the Gram-negative bacterium *Escherichia coli* was coupled to

cell lysis (18, 19). In another example, the human antimicrobial peptide LL-37, as well as truncated peptide analogues, induced lateral separation of membrane components and leakage of proteins and nucleotides from the cytoplasm when acting on the fungus *Candida albicans*. In yet another illustrative example, the insect antimicrobial peptide defensin A permeabilized the cytoplasmic membrane of the Gram-positive bacterium *Micrococcus luteus*, causing leakage of potassium ions (20).

There are, however, also *in vitro* indications that antimicrobial peptides might kill microbes without damaging the cell membrane itself (12). Thus, the antimicrobial peptide buforin II rapidly killed *Escherichia coli* without lysing the cell membrane (18). Instead, buforin II accumulated in the cytoplasm. Furthermore, buforin II was found to bind to DNA and RNA, and it was hypothesized that this binding is important for the *in vivo* mechanism of buforin II. PR-39, a peptide from the pig small intestine, did not kill *Escherichia coli* by cell lysis either (19). Rather, data indicated that the peptide induced a halt in protein and DNA synthesis, possibly due to PR-39-induced proteolytic activity. The fungal antimicrobial peptide plectasin was involved in another interesting example of non-lytic peptide activity (21). To be more specific, plectasin was shown to inhibit cell-wall biosynthesis in the Gram-positive bacteria *Bacillus subtilis* and *Staphylococcus simulans*, rather than perforating the cell membrane (21). Detailed experiments further indicated that the cell-wall precursor Lipid II was the target of plectasin. Finally, in a last example of non-lytic peptide action, fungicidal activity of the peptide histatin 5 against *Candida albicans* was suggested to be related to non-lytic efflux of ATP or generation of reactive oxygen species (22).

2.1.2 Immunomodulatory functions

In recent years, the idea that antimicrobial peptides exhibit other functions than just their direct microbicidal functions has become increasingly widespread. More specifically, it is now clear that antimicrobial peptides can also modulate the immune response of their host organism. For instance, it is recognized that some antimicrobial peptides display chemotactic activities. That is, some antimicrobial peptides can enhance pro-inflammatory responses by chemoattracting immune cells to sites of infection, either by direct chemoattraction or by stimulation of chemokine release (8, 23). Also, in another example of immunomodulatory activities, some antimicrobial peptides have been suggested to neutralize the effect of endotoxins by direct high-affinity lipopolysaccharide binding or by stimulation of the expression of anti-inflammatory compounds (8, 23). In addition to these examples, antimicrobial peptides have also been hypothesized to be involved in a plethora of other immunomodulatory functions, including wound healing and angiogenesis (8, 23).

It has been even suggested that the immunomodulatory functions represent the principal biological role of many antimicrobial peptides, as many peptides are found to be devoid of direct microbicidal activities under physiological conditions. To more precisely describe their complex involvement in immunity, it was, therefore, suggested that the peptides should be termed "host defense peptides" instead of "antimicrobial peptides" (8). In this thesis, we will however stick to the term "antimicrobial peptides".

2.2   Structural categorization

Antimicrobial peptides are a diverse class of peptides with great variability in amino acid sequence among individual peptides. However, despite this sequence variability, it is possible to classify the peptides into a few groups based on their membrane-bound conformation.

The largest and most well-studied group of antimicrobial peptides is the α-helical peptides (14). These peptides are often in random coil conformation in aqueous solution and only fold into helical conformation upon partitioning into phospholipid bilayers. Non-polar, polar and charged amino acid residues are generally arranged in a characteristic pattern which upon peptide folding creates an amphipathic helix. At low peptide-to-lipid ratios, this helix typically reside at the bilayer interface with the long axis oriented parallel to the plane of the bilayer (24), often with a small bend at the center of the peptide (25). Mastoparan X, melittin and magainin 2, which are the three antimicrobial peptides to be investigated in this thesis, are all prominent examples of the α-helical antimicrobial peptides.

Another prominent example of the α-helical antimicrobial peptides is the human antimicrobial peptide LL-37. Interestingly, one study on LL-37 indicated the importance of helicity for peptide antimicrobial activity (26). In that study, different types and concentrations of ions was used to promote helix formation in LL-37, and a strong correlation between the helicity of LL-37 and its antibacterial activity against both the Gram-negative bacterium *Escherichia coli* and the Gram-positive bacterium *Bacillus megaterium* was established. However, it should also be mentioned that there are also examples that show that helicity is not always a requirement for antimicrobial peptide. Diastereomers of melittin thus retained high antibacterial activity against both Gram-positive and Gram-negative bacteria in spite of lacking the α-helical secondary structure of native melittin (27).

β-sheet antimicrobial peptides represent another large conformational group. In contrast to the α-helical peptides, the β-sheet peptides are generally more rigid structures stabilized by intermolecular disulfide bonds (25). Therefore, these peptides are often both ordered in aqueous solution and when partitioned into lipid bilayers. Like the α-helical peptides, the β-sheet peptides are typically amphipathic in nature. Some of the most well-known examples of β-sheet antimicrobial peptides are the defensins and protegrins (14, 28).

A large number of antimicrobial peptides do not belong to the classical α-helical or β-sheet categories. Instead, these peptides can sometimes be characterized by their enrichment in one or more amino acid types. A well-known example of a peptide enriched in one type of amino acid is the bovine neutrophil peptide indolicidin, in which the amino acid tryptophan is strongly over-represented. The proline-arginine-rich peptides represent another example of peptides enriched in certain amino acids (25, 28).

2.3   Physicochemical characteristics

A number of physicochemical characteristics pertaining to charge, hydrophobicity, and amphipathicity appear to be common for most antimicrobial peptides. Altering each of these parameters for a given peptide might confer altered antimicrobial activities and selectivities on that peptide.

2.3.1 Charge

Most antimicrobial peptides carry a net positive charge between $+2$ to $+9$ (28). Especially, the cationic amino acids lysine and arginine are highly abundant in antimicrobial peptides. In contrast, the anionic amino acids aspartic acid and glutamic acid are generally scarce (14).

Several papers have report that the net peptide charge correlates to *in vitro* antimicrobial activity. For example, one study considered a number of magainin 2 amide analogues in which the net charge was varied while hydrophobicity, helicity and amphipathicity were kept largely constant (29). For these magainin 2 amide analogues, increasing the net charge from $+3$ to $+5$ lead to an increase in antibacterial activity against *Escherichia coli* and *Bacillus subtilis*. A similar dependence on charge was also observed for a collection of synthetic model peptides in which, as for the magainin 2 amide analogues, the net charge was varied while hydrophobicity, helicity, and amphipathicity were kept constant (30). Thus, for these synthetic model peptides, it was found that charge was a prerequisite for antimicrobial activity toward a broad spectrum of Gram-positive and Gram-negative bacteria, and fungi, and for peptides of charge $+1$ to $+5$, there were even indications that activity only depended on the overall peptide cationicity and not on the specific positioning of charges along the amino acid sequence *per se*. In yet another example on the importance of cationicity, a study on a large number of C3a peptide analogues demonstrated that antibacterial activity against *Escherichia coli* and *Staphylococcus aureus* and antifungal activity against *Candida albicans* also correlated to net positive charge (31).

However, it should be noted that not all studies unambiguously show that antimicrobial activity correlates directly to cationicity. For instance, adding four lysine residues to the N-terminus of magainin 2 decreased the *in vitro* activity of the peptide against the bacteria *Escherichia coli*, *Pseudomonas aeruginosa*, and *Staphylococcus aureus* (32).

It should also be noted that even though antimicrobial activity of a given peptide is often increasing with increasing net charge, it can not unambiguously be said that the properties of that particular peptide are improved when its net charge is increased. More specifically, increasing charge of a peptide will also often increase undesired host cell toxicity of that peptide, typically gauged by the hemolytic activity of the peptide (29, 30). In other words, increasing the charge will often not only change the antimicrobial activity of a given peptide but also the selectivity of that peptide. Therefore, there is typically an optimum net charge at which antimicrobial selectivity is maximal.

Finally, it should be mentioned that anionic antimicrobial peptides with a charge of -1 to -7 do also exist (24). However, these anionic peptides are not as well-studied as the cationic peptides and will not be discussed any further in this thesis.

2.3.2 Hydrophobicity

Antimicrobial peptides typically contain around $50\ \%$ hydrophobic amino acid residues (28). These hydrophobic residues are thought to play an important role for the interaction of antimicrobial peptides with cellular membranes, and, thereby, also for antimicrobial activity.

Accordingly, in many *in vitro* experiments, it has been found that hydrophobicity is an important parameter for microbicidal activity of antimicrobial peptides. Equally important

though, many experiments have also found hydrophobicity to be an important parameter for hemolytic activity (24). As an example on the importance of hydrophobicity, four different magainin 2 analogues in which hydrophobicity was varied while other physicochemical parameters were kept constant displayed increasing antibacterial activity against *Escherichia coli* and to a lesser extent against *Pseudomonas aeruginosa* as a function of hydrophobicity, but also increasing hemolytic activity as a function of hydrophobicity (33). Consequently, the most hydrophobic magainin 2 analogues were still selective against *Escherichia coli* but not against *Pseudomonas aeruginosa*. Similarly, analogues of the antimicrobial peptide V13K$_\text{L}$ with systematic substitutions of alanine and leucine residues also displayed poor selectivity against different *Pseudomonas aeruginosa* strains when peptide hydrophobicity was high, although at an intermediate optimum hydrophobicity, antimicrobial selectivity was actually maximized (34). Finally, the most hydrophobic analog of two template-based model peptides with different hydrophobicities but identical charges and amphipathicities was found to be more hemolytic and less selective toward Gram-positive and Gram-negative bacteria than the less hydrophobic analog (35).

2.3.3   Amphipathicity

Amphipathicity measures the polarization of hydrophobic and hydrophilic amino acid residues within a peptide. In the case of α-helical peptides, amphipathicity is often quantified by the hydrophobic moment. The hydrophobic moment is calculated as the vectorial sum of individual amino acid hydrophobicity vectors, assuming an ideal α-helix (24).

In the case of antimicrobial peptides, amphipathicity is thought to be an important parameter for their interaction with phospholipid bilayers. A general notion is that hydrophobic peptide domains are buried in the acyl chain region and hydrophilic peptide domains interact with polar and charged phospholipid head groups.

The importance of amphipathicity for microbicidal activity and selectivity has been demonstrated in several *in vitro* experimental investigations. As in the case of the aforementioned investigations on charge and hydrophobicity, also amphipathicity has been found to impact both antimicrobial activity and host cell toxicity. For instance, the importance of amphipathicity was demonstrated in a study in which a scrambled non-amphipathic synthetic model peptide displayed poorer antimicrobial activity but similar hemolytic activity when compared to an amphipathic analog with the same amino acid residue composition (30). In another example, three template-based model peptides, in which the hydrophobic moment was varied while charge and hydrophobicity were kept constant, exhibited increasing antibacterial activity against a large number of Gram-positive and Gram-negative bacteria as a function hydrophobic moment (35). However, these peptides also displayed strongly increasing hemolytic activity as a function of increasing hydrophobic moment, rendering antibacterial selectivity of the most amphipathic model peptides inferior. Accordingly, natural antimicrobial peptides often exhibit an imperfect amphipathic structure (31), and it has been suggested that these imperfect structures might have been chosen by evolution as structures that yields maximal antimicrobial activity and minimal host cell toxicity.

2.4 Popular themes in antimicrobial peptide-lipid membrane interactions

The interactions between antimicrobial peptides and cellular lipid membranes are a topic of uttermost importance. No matter whether a given antimicrobial peptide acts by disrupting the microbial cell membrane or by crossing the membrane to do intracellular damage, it is certainly clear that understanding the antimicrobial peptide-cell membrane interactions is crucial for the overall understanding of peptide activity.

To date, an enormous number of studies on antimicrobial peptide-lipid membrane interactions have been published. These studies are often carried out using synthetic minimal model membranes and various biophysical techniques. Based on these studies, a number of prevailing ideas and models have arisen.

2.4.1 Specific interactions with microbial cell membranes

The cell architecture differs fundamentally between host cells and microbial cells. The literature on antimicrobial peptides often considers these differences to be the reason for the capability of antimicrobial peptides to specifically target infectious microbial pathogens and not the cells of their host organism (28, 36). In particular, the literature on antimicrobial peptides often considers the differences in cell membrane architecture between infectious bacterial cells and mammalian host cells to explain antimicrobial peptide selectivity. An overview of the molecular factors that are thought to contribute to bacterial versus mammalian cell selectivity of antimicrobial peptides is given in Fig. 2.2.

One of the major differences between the cell membrane architectures of bacterial and mammalian membranes is pertaining to charge. To be more specific, bacterial cell envelopes are generally strongly anionic (14). Thus, the lipid A core of lipopolysaccharides on the outer cell membrane of Gram-negative bacteria and teichoic and teichuronic acids on the cell wall of Gram-positive bacteria are negatively charged. Furthermore, bacterial cytoplasmic membranes are generally enriched in the anionic lipids phosphatidylglycerol and cardiolipin. In contrast, mammalian host cell membranes consist primarily of zwitterionic and neutral components, especially in the exoplasmic leaflet. That is, exoplasmic leaflets of mammalian membranes are generally enriched in the zwitterionic phospholipids phosphatidylcholine, phosphatidylethanolamine, and sphingomyelin. Mammalian cell membranes do also contain anionic phospholipids, but they are primarily sequestered in the cytoplasmic leaflet. Thus, antimicrobial peptides, which, as mentioned in Section 2.3.1, generally are cationic, are thought to be electrostatically attracted to bacterial cell envelopes but not to mammalian cell membranes (37, 38).

Charge is not the only proposed modulator of peptide selectivity. For example, as opposed to bacterial membranes, mammalian membranes contain a significant amount of cholesterol (28). Cholesterol alters the packing of lipid membranes, and might, thereby, confer increased resistance on mammalian cells to antimicrobial peptides by preventing the peptides to bind to the mammalian membranes (39–41). The potential protective role of cholesterol is underlined by the fact that the presence of cholesterol in erythrocyte membranes decreases the hemolytic
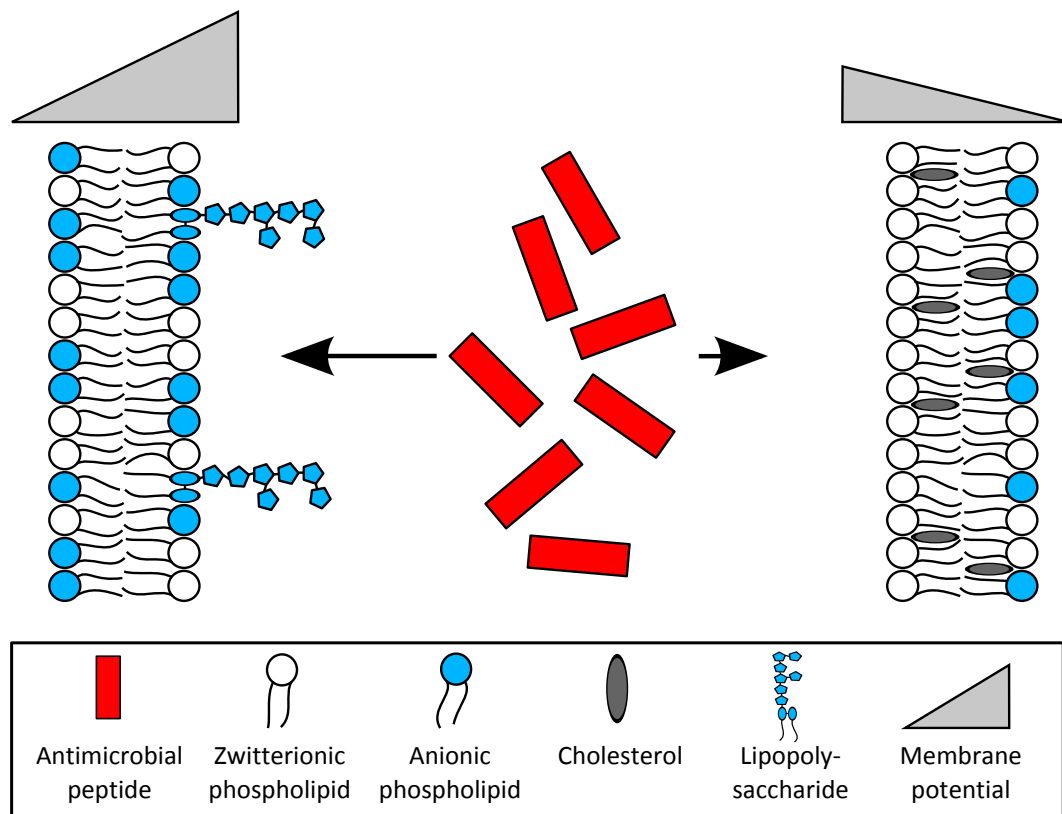
Figure 2.2: Sketch of molecular determinants that have been suggested to promote antimicrobial peptide selectivity to bacterial cell envelopes (*left*) over mammalian cell membranes (*right*). Negative charges on the bacterial cell envelopes, e.g., introduced by anionic phospholipids and lipopolysaccharide, are thought to attract cationic antimicrobial peptides through electrostatic interactions. Other factors, such as cholesterol and membrane potential, might further direct antimicrobial peptide activity.

potency of some antimicrobial peptides, (42). Similar to cholesterol, sphingomyelin is also present in mammalian membranes but not in bacterial membranes. It has been shown that sphingomyelin, together with cholesterol, prevents membrane association of the human antimicrobial peptide LL-37 to synthetic membranes, thereby implying that sphingomyelin might further direct the action of antimicrobial peptides toward bacteria (39).

The transmembrane potential represents another parameter that differs between bacterial cells and mammalian cells. Thus, for bacterial cells in logarithmic growth, the transmembrane potential is -130 to -150 mV, whereas for mammalian cells, the transmembrane potential is -90 to -110 mV (28). This difference might promote activity of antimicrobial peptides in bacterial cells relative to mammalian cell, for example by electrophoretically driving peptide translocation across the cell membrane (42).

It is noteworthy that none of the aforementioned determinants for antimicrobial peptide selectivity are related to any specific molecular targets. Accordingly, even though a few

examples of such specific molecular targets for antimicrobial peptides have been identified (28), the typical notion is that antimicrobial peptides interact with microbial membranes in an unspecific manner and, therefore, that antimicrobial peptide selectivity is determined by general cell surface characteristics, such as those mentioned before. This notion is corroborated by the fact that diastereomers of antimicrobial peptides often retain antimicrobial activity, indicating that antimicrobial peptides do not interact specifically with any molecular receptors on the microbial cell surface (27).

2.4.2 The concept of a threshold concentration

The concept of a threshold concentration is another recurring theme in the literature on antimicrobial peptides. The idea of the concept is that peptides only become active when their membrane-bound concentration increases above a certain threshold. Thus, at low membrane-bound concentrations, peptides typically reside in a planar orientation at the lipid head group level (24), but when the membrane-bound concentration increases above a certain threshold, peptides are thought to be activated (43), for example by inserting into the membrane to form transmembrane pores or by solubilizing the membrane in a detergent-like manner (44).

Typically, threshold concentrations for antimicrobial action in lipid membranes are hypothesized to be in the range of 0.05 to 0.1 peptide-to-lipid molar ratios (43). Since the cross-sectional area of an average antimicrobial peptide containing 20-30 amino acid residues is much larger than the cross-sectional area of a phospholipid, peptides cover one-fifth or even more of the bilayer surface area at these typical threshold concentrations. In other words, typical threshold concentrations represent extremely high membrane-bound concentrations of antimicrobial peptides (43).

2.4.3 Formation of transmembrane pores

It is well-known that antimicrobial peptides can permeabilize lipid bilayers; that is, they can form holes or defects in the bilayers, allowing transmembrane passage of polar solutes that can not cross the unperturbed bilayer (11). For example, as mentioned in Section 2.1.1, microbicidal peptide action is often associated with permeabilization of cellular membranes, entailing leakage of ions or macromolecules. However, there are also ample examples from synthetic model membranes that antimicrobial peptides can induce membrane permeabilization. In fact, most of the structural information on antimicrobial peptide-induced membrane permeabilization has roots in studies on such synthetic model membranes.

For instance, valuable insights into antimicrobial peptide-induced membrane permeabilization have been gained from experiments on synthetic lipid unilamellar vesicles. In typical experiments with such vesicles, an aliquot of a peptide solution is transferred to a solution of lipid vesicles, and leakage of an encapsulated marker from the vesicle lumen is subsequently gauged. A hallmark feature of these vesicle experiments is that peptide-induced membrane permeabilization is only transient; following an initial rapid burst of leakage within the first few minutes after peptide addition, leakage slows down or ceases altogether before all vesicle contents have been released (45–48). A hypothesis that is often suggested to explain this

transience in leakage is that peptides initially only bind to the outer membrane leaflet entailing an asymmetric strain of the membrane. In the process of relieving this asymmetric strain, membrane permeabilization occurs. However, once the peptides are equilibrated across the membrane, the propensity for membrane permeabilization is significantly reduced (45, 49). In agreement with this hypothesis, it has been observed that peptide-induced membrane permeabilization in lipid vesicles is coupled to translocation of peptides across lipid bilayers (50).

A number of other noteworthy observations on antimicrobial peptide-induced membrane permeabilization also come from work done on lipid unilamellar vesicles. For example, membrane permeabilization has been found to be directly coupled to lipid flip-flop (51). Furthermore, leakage kinetics have implied that antimicrobial peptides might self-assemble as part of the membrane permeabilization process (52). Finally, in experiments on peptide-induced leakage of markers from individual giant lipid vesicles, it has been observed that initiation of leakage from individual lipid vesicles occurs at a probabilistic point in time and membrane-bound peptide concentration (47, 48, 53–55). This latter observation implies that nucleation defects in the bilayers are required for peptides to initiate membrane permeabilization (53).

Valuable structural insights into antimicrobial peptide-induced membrane permeabilization also come from experiments conducted on oriented lipid multibilayers. Thus, neutron in-plane scattering experiments on oriented multibilayers have revealed that when the membrane-bound peptide concentration is above a certain threshold, water-filled transmembrane pores are formed (56, 57), in agreement with the ideas of a threshold concentration introduced in Section 2.4.2. Interestingly, oriented circular dichroism experiments on oriented multibilayers have also demonstrated that membrane-bound peptides change orientation when their concentration is above that threshold concentration (58, 59). For α-helical peptides, this corresponds to a change in orientation from their long-axis being parallel to the plane of the membrane surface to their long axis being perpendicular to the plane of the membrane surface. In other words, from these experiments, it seems that the formation of transmembrane pores in oriented multibilayers is directly coupled to peptide insertion into the bilayers (59).

Experiments conducted on oriented lipid multibilayers have also revealed another important feature of antimicrobial peptide-lipid membrane interactions. Thus, X-ray diffraction experiments on oriented multibilayers have shown that peptides, at membrane-bound concentrations below the threshold concentration, entail pronounced stretching and thinning of the bilayers (60), see Fig. 2.3. This bilayer stretching and thinning is thought to occur as a result of peptide preferential embedment in the lipid head group region. That is, the peptides are thought to embed in the head group region and create an empty void in the acyl chain region to be filled by the acyl chains of the adjacent lipids. In order for the bilayer to adapt to this new situation, local stretching and thinning of the bilayer around the surface-associated peptides are required. This stretching and thinning of the membrane is thought to be important for creation of energy-favorable transmembrane pores in the oriented multibilayers; when peptides stretch the membrane area, they will create an internal membrane tension. When this tension is sufficiently high, above a certain threshold, the formation of transmembrane pores is energetically favored (53, 55, 61). It has been suggested that this
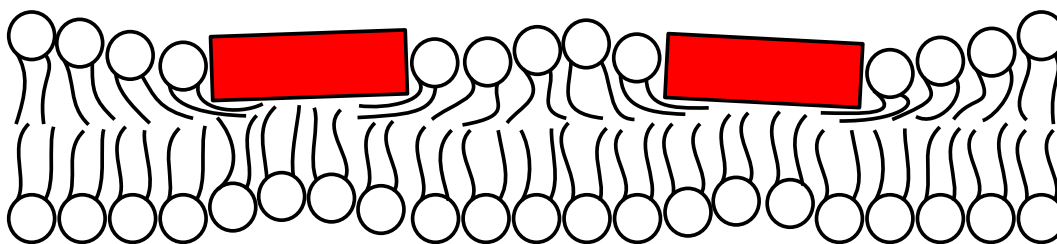
Figure 2.3: Sketch of peptide-induced membrane stretching and thinning. Peptides (schematically drawn as red rectangles) preferentially partition into the lipid head group region creating a gap in the acyl chain region. Acyl chains of adjacent lipids fill this gap causing local membrane stretching and thinning.

internal membrane tension is equivalent to an externally applied membrane tension (61, 62).

Some attempts have been made to bridge the experimental observations from oriented lipid multibilayers to the observations from lipid vesicles. In one example, it was suggested that threshold concentrations for pore formation in oriented multibilayers can be directly correlated to threshold concentrations for peptide-induced membrane permeabilization in giant lipid vesicles simply by observing the peptide-induced bilayer stretching (53, 55). Furthermore, it has been hypothesized that the cooperative formation of transmembrane equilibrium pores observed in oriented lipid multibilayers is also detectable in lipid vesicles by calorimetric techniques (44, 63, 64).

To understand the molecular details of the experimental observations in lipid vesicles and oriented lipid multibilayers, a plethora of different models have been proposed. Two prominent examples of these models, namely the toroidal pore model and the barrel-stave model, involve the formation of explicit water-filled transmembrane pores.

The toroidal pore model

The most influential model to explain the mechanisms underlying antimicrobial peptide pore formation is the toroidal pore model (14). This model is supported by substantial evidence from oriented lipid multibilayers (65–68) and from computer simulations (69, 70). In the toroidal pore model, the two leaflets of a lipid bilayer are connected through a torus-like pore of high local membrane curvature, see Fig. 2.4. The peptides are inserted into the lipid head group region in the toroidal pore in a tilted or perpendicular orientation to stabilize the pore (70, 71), for example, by functioning as fillers in the highly curved head group region (59). Due to the high local membrane curvature of toroidal pores, it has been suggested that bilayers consisting of positive curvature-inducing lipids are much more prone to forming toroidal pores than bilayers consisting of negative curvature-inducing lipids (72). In recent years, this idea has however been challenged in several papers (59, 73), suggesting other factors rather than spontaneous curvature, for example, pertaining to lipid head group hydration, to be the real cause of experimental differences between bilayers.

It has been proposed that antimicrobial peptides promote toroidal pore formation by reducing the line tension of the pore edge. That is, antimicrobial peptides preferentially
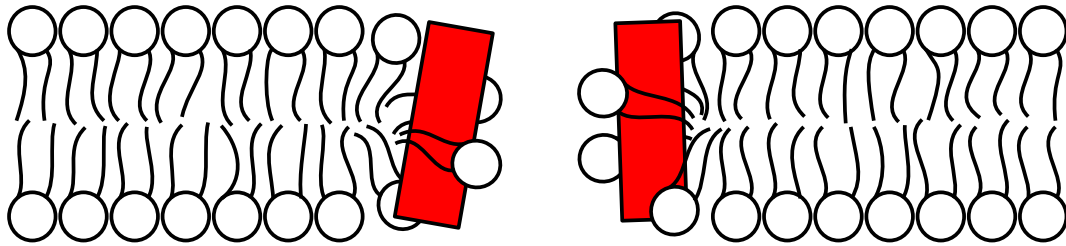
Figure 2.4: Sketch of the toroidal pore model. Peptides (schematically drawn as red rectangles) alter the local curvature of phospholipid bilayers causing formation of toroidal pores lined by peptides and lipids.

associate to the rims of the toroidal pores and stabilize the pores by reducing the line tension (74, 75), similar to the way that also detergents reduce the line tension of pore edges (76). From a physicochemical point of view, antimicrobial peptide pore formation might thus be thought of as a process in which the peptides induce pore formation by simultaneously increasing membrane tension and decreasing pore edge line tension (61).

The barrel-stave pore model

The barrel-stave model represents another model that is quite often cited in the literature. However, in reality, barrel-stave pores are only thought to occur for a few peptides, with alamethicin being the most well-studied example (14, 77, 78). Even so, for completeness, the model is recapitulated in the following lines.

In the barrel-stave model, the peptides insert perpendicularly into the lipid bilayers to line a water-filled pore in a barrel-like manner, see Fig. 2.5. The hydrophilic domains of the peptides preferentially face the pore lumen whereas hydrophobic domains face the bilayer to interact with the hydrophobic acyl chains (14, 79). In this way, a characteristic fingerprint of the barre-stave model is that the orientation of lipid molecules in the bilayer is largely undisturbed (68, 80). This is in contrast to the toroidal pore model in which the local lipid orientation in the vicinity of pores deviates from a lamellar bilayer structure; compare Fig. 2.4 to Fig. 2.5.
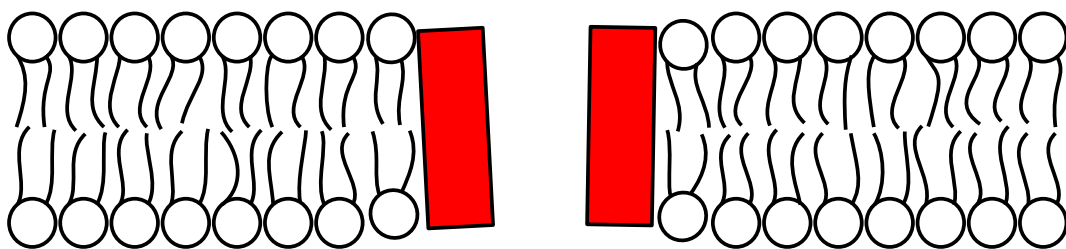
Figure 2.5: Sketch of the barrel stave pore model. Peptides (schematically drawn as red rectangles) line the pore lumen. The hydrophilic peptide domains face the pore lumen, whereas the hydrophobic domains face the hydrophobic acyl chains.
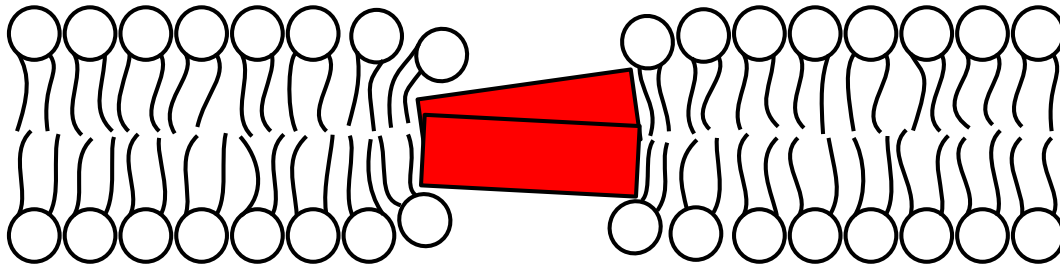
Figure 2.6: Sketch of the sinking raft model. Peptides (schematically drawn as red rectangles) aggregate, in this sketch into a dimer, and sink into the bilayer with their hydrophobic domains facing the acyl chains and their hydrophilic forming an inner cavity.

2.4.4 Non-pore models

Besides the above-mentioned pore models, a number of alternative models have also been suggested, inter alia, to explain how peptide-induced membrane disruption and permeabilization might occur without the formation of explicit water-filled transmembrane pores.

The sinking raft model

Based on a detailed quantitative analysis of vesicle leakage induced by the peptide δ-lysin, the sinking raft model was proposed (81). In the sinking raft model, peptides initially associate to the outer membrane leaflet, creating an asymmetric strain across the bilayer. This process promotes the insertion of small peptide aggregates into the bilayer. Via these small aggregates, peptides translocate across bilayers with their hydrophobic domains facing the lipid acyl chains. In this process, the hydrophilic peptide domains will form an inner cavity through which polar solutes can be transported across the bilayer. Thereby, membrane permeabilization and peptide translocation occur simultaneously, and also lipid flip-flop is expected to occur concomitantly. However, upon peptide equilibration across the lipid bilayer, peptide translocation, and thus also membrane permeabilization and lipid flip-flop, cease (82, 83), in agreement with the observation that peptide-induced leakage from lipid vesicles is a transient process. The sinking raft model is sketched in Fig. 2.6.

One consequence of the sinking raft model is that peptides do not insert perpendicularly into lipid membranes but rather in a planar orientation. This idea matches the observation that α-helical antimicrobial peptides at low peptide-to-lipid ratios are quite often experimentally found in an orientation with their long axis parallel to the bilayers (82). However, even though this observation might support the sinking raft model, it does not directly dismiss the aforementioned toroidal pore model. Thus, it has also been suggested that antimicrobial peptides might associate to toroidal pores while being in a nearly planar orientation, so that tilted or perpendicular peptide insertion is not *per se* a requirement for toroidal pore formation (68, 71).
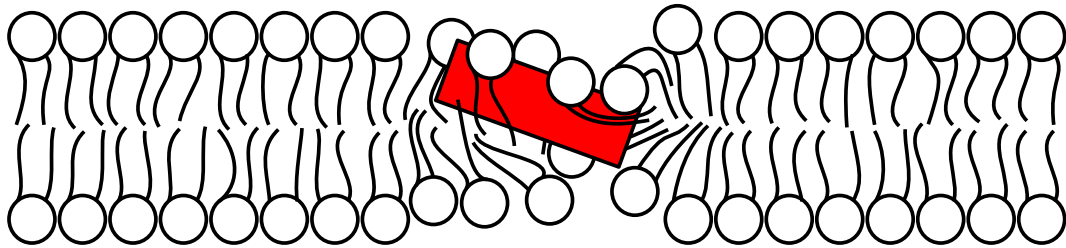
Figure 2.7: Sketch of the interfacial activity model. Imperfect amphipathic peptides (schematically drawn as red rectangles) disrupt the vertical segregation of polar and nonpolar phospholipid moieties. This disruption is associated with peptide and lipid translocation. At high amounts of peptide asymmetrically bound to the bilayer leaflets, transbilayer transport of other polar solutes may also occur.

The interfacial activity model

The interfacial activity model was recently suggested to address the fact that membrane-permeabilizing activity of antimicrobial peptides do not depend on the specific amino acid sequence or peptide structure but rather on the general physicochemical properties of the peptide (84, 85). In addition, the model also addresses the fact that leakage rates across antimicrobial peptide-permeabilized bilayers are often too slow to be explained by the formation of long-lived water-filled transmembrane pores (45).

In the interfacial activity model, the antimicrobial peptides are hypothesized to disrupt the vertical organization of lipid bilayers as a result of imperfect amphipathic peptide structure, see Fig. 2.7. Accordingly, naturally occurring antimicrobial peptides often comprise such imperfect amphipathic structures, in which hydrophobic domains are interrupted by polar or charged amino acid residues. When these imperfect amphipathic peptides insert into lipid bilayers, their hydrophobic domains will naturally insert into the hydrophobic acyl chain core of the bilayer. However, the polar or charged residues adjacent to these hydrophobic domains will preferentially interact with the lipid head groups, promoting the incursion of the lipid head groups deeper into the membrane and, thereby, disruption of vertical bilayer polar-nonpolar segregation. At low concentrations of membrane-bound peptides, the interfacial activity of antimicrobial peptides is thought to lead to concomitant peptide and lipid translocation across the lipid bilayer. At high concentrations of asymmetrically bound peptides, polar solutes may be transported across the lipid bilayer concurrently with peptide and lipid translocation until equilibrium is reached. Thus, the interfacial activity model also provides a possible explanation to the transience of peptide-induced leakage from lipid vesicles (45).

The carpet model

In the carpet model, antimicrobial peptides cover the lipid bilayers in a carpet-like manner (86), see Fig. 2.8. The hydrophilic domains of the peptides interact with the lipid head groups, whereas the hydrophobic domains are oriented towards the acyl chain core of the bilayers. For α-helical antimicrobial peptides, this corresponds to the orientation in which
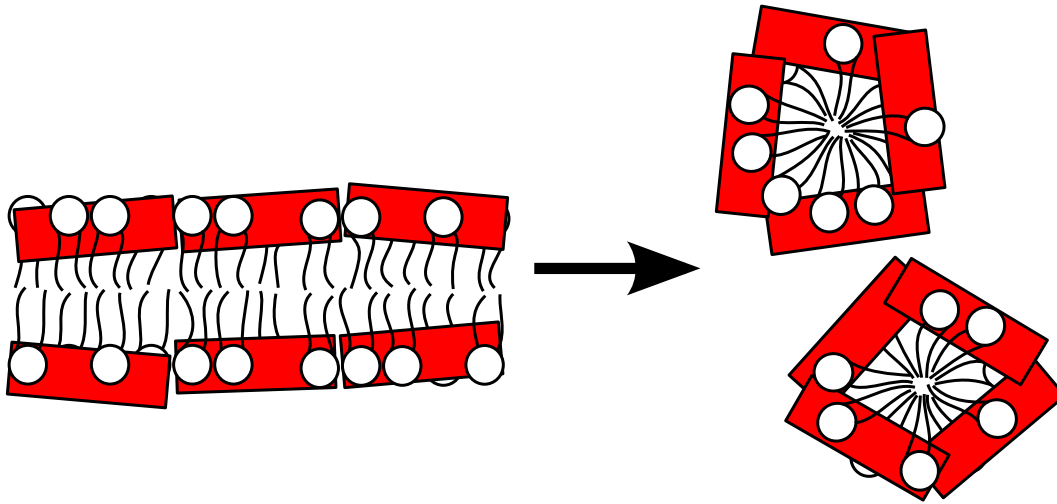
Figure 2.8: Sketch of the carpet model. Peptides (schematically drawn as red rectangles) cover the bilayer like a carpet. At high peptide concentrations, this leads to disruption of lipid packing and disintegration in a detergent-like manner.

their long axis is parallel to the plane of the bilayer. Above a certain threshold concentration, the peptide carpet will entail a global bilayer destabilization thereby leading to a detergent-like disintegration of the bilayer (27, 87). One consequence of the carpet model is that peptide activity does not require any specific peptide structure, explaining why so many different peptides of diverse amino acid sequence and secondary structure display antimicrobial activity (88).

It is worth noting that the carpet model is thought to be compatible with the toroidal pore model (88). Thus, prior to membrane solubilization, the formation of toroidal pores in the membrane might occur. Accordingly, it was observed by calorimetry and electron microscopy that the antimicrobial peptide mastoparan X formed transmembrane pores at low peptide concentrations and globular and worm-like micelles at high peptide concentrations (44).

The lipid clustering model

The lipid clustering model is another proposed scheme for antimicrobial peptide-lipid membrane interactions. In the lipid clustering model, antimicrobial peptides, which, as mentioned in Sections 2.3.1 and 2.4.1, are cationic, will preferentially interact with anionic phospholipids, see Fig. 2.9. In membranes composed of mixtures of zwitterionic and anionic phospholipids, this preferential interaction will lead to the formation of lateral domains enriched in peptides and anionic lipids (89–92). Even in membranes composed solely of anionic phospholipids, lateral segregation might occur (93). Such peptide action might disrupt natural lateral domains existing in microbial membranes, thereby, for example, hampering the function of transmembrane proteins associated to these lateral domains (94). Additionally, peptide-induced lipid clustering might also introduce more boundary effects in the bilayers, facilitating peptide translocation and membrane permeabilization (95, 96).
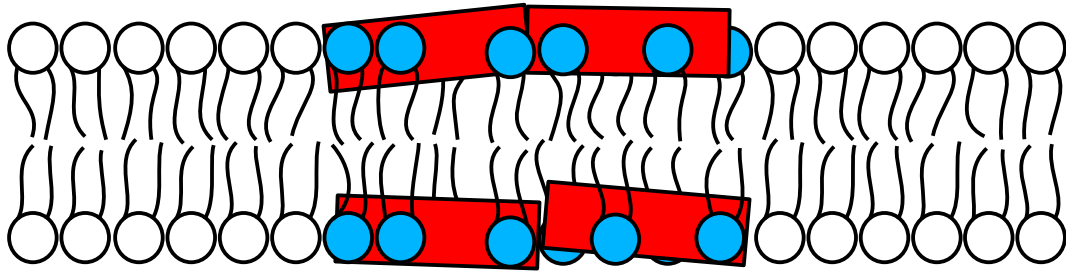
Figure 2.9: Sketch of the lipid clustering model. Peptides (schematically drawn as red rectangles) preferentially interact with anionic phospholipids, thereby causing lateral segregation of anionic phospholipids (drawn with blue head groups) from zwitterionic phospholipids (drawn with white head groups). Clustering of some anionic phospholipids from other anionic phospholipids has also been observed.

2.4.5 A unifying model: phase diagrams and molecular shapes

It has been suggested that many of the aforementioned models represent specific domains in a peptide-lipid phase diagram (97). According to this idea, many of the above models do not contradict each other, but rather they represent different domains in the phase diagram. For example, the formation of toroidal pores might occur in one specific peptide-to-lipid ratio domain in the phase diagram, whereas carpet-induced disintegration of the bilayers into micelles might occur in another specific peptide-to-lipid ratio domain. In that way, the actions of antimicrobial peptides on lipid bilayers are equivalent to the actions of other amphiphiles, such as detergents or phospholipids (98).

An important parameter for these phase diagrams is the molecular shapes of peptides and lipids (99). Thus, certain molecular shapes are ascribed to peptides and lipids, see Fig. 2.10; these molecular shapes then determine the peptide-lipid supramolecular assembly structure, and, thereby, the position of the individual domains in the phase diagrams. For example, phosphatidylcholine is described as a cylinder and form lamellar bilayer structures. In contrast, phosphatidylethanolamine is described as an inverted truncated cone due to its small head group, and, as a result, this lipid tend to aggregate into structures with negative curvature, such as the inverse hexagonal phase. As another example, lysolipids are described as a cone; therefore, they tend to aggregate into structures with positive curvature, such as micelles (98). In continuation of these ideas, antimicrobial peptides, which, as illustrated in Fig. 2.3, typically assume a planar orientation in the lipid head group region, are thought to be similar to a truncated cone, thereby inducing positive curvature strain (98). As a result of this positive curvature strain, antimicrobial peptides might, for instance, promote the formation of toroidal pores (72). According to these ideas, peptide-induced toroidal pore formation would, therefore, be promoted in bilayers with positive-curvature-inducing phospholipids. However, as also mentioned before, it should again be mentioned that the idea of molecular shape to explain the propensity of antimicrobial peptides to induce toroidal pores has been challenged in recent years (59, 73).

| Phospholipid with cylinder shape | Phospholipid with inverted truncated cone shape | Phospholipid with cone shape | Peptide with truncated cone shape |
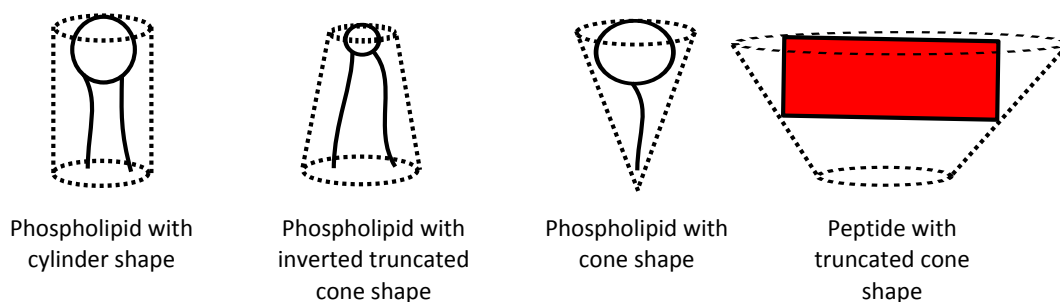
Figure 2.10: Examples of lipids and peptides with different molecular shapes. The molecular shape of lipids and peptides are thought to determine the structure of their resulting supramolecular assembly.

2.5 What questions remain unanswered about antimicrobial peptide activity?

From the above sections, it is clear that much is known about antimicrobial peptides. However, even so, a number of questions about antimicrobial peptides still remain to be answered.

2.5.1 Structure-activity relationship

One topic that still remains unclear, in spite of years of intense research efforts, is the relationship between the physicochemical structure and the microbicidal activity of antimicrobial peptides. While it is clear that physicochemical parameters such as charge, hydrophobicity, and amphipathicity all affect antimicrobial activity and selectivity, it is also clear that peptide optimization is not just a simple linear process in which each of these parameters independently can be optimized. Rather, antimicrobial activity and selectivity depend on an intricate interplay between many parameters (100). Thus, even subtle changes in the amino acid sequence of a given peptide might confer great changes on the properties of that peptide (84, 85, 101). In addition, peptide microbicidal activity also depends on the properties of the microbial membrane, including the lipid composition (102). This further complicates the understanding of the factors contributing to antimicrobial peptide activity.

However, advanced computational methods might hold future promise to reveal these delicate structure-activity relationships of antimicrobial peptides. For example, computational methods in conjunction with high-throughput activity data have been used to identify molecular descriptors that correlate to antimicrobial activity and, thereby, design novel synthetic antimicrobial peptides with high potency (103). Also, molecular dynamics simulations might provide insight into the molecular mechanisms of antimicrobial peptide action; indeed, there are already examples of synthetic antimicrobial peptides being designed on the basis of molecular dynamics simulations (104).

2.5.2 Antimicrobial peptide-lipid membrane interactions

As mentioned previously, it is evident that antimicrobial peptides must interact with the cell membrane to kill a given cell; as a result, antimicrobial peptide-lipid membrane interactions

have been studied extensively. However, a number of open questions still remain about these interactions (10).

A central question to be answered is related to the actual role of the microbial cell membrane in antimicrobial peptide action (10). To be more specific, it is not known how interactions between antimicrobial peptides and microbial cell membranes lead to cell death. As mentioned before in Section 2.1.1, there are indications that lethal action of antimicrobial peptides is related to membrane disruption, but there are also indications that lethal action of antimicrobial peptides is related to translocation across the cell membrane to inhibit vital intracellular metabolic processes. As these two routes to cell death are not mutually exclusive, it is unclear whether cell killing always proceeds via one or the other of these routes, or whether peptides follows both routes simultaneously. Certainly, rational optimization of antimicrobial peptides for anti-infective therapeutic purposes would be a lot easier if it was known for which route exactly that the peptides were optimized.

Another central question on antimicrobial peptide-lipid membrane interactions is related to the mechanisms of peptide-induced membrane permeabilization. Even though much is known about antimicrobial peptide-induced membrane permeabilization and many models have been proposed, the molecular details underlying this membrane permeabilization is still unraveled. For instance, the reasons that permeabilization of model membranes in lipid vesicles is a transient phenomenon remain elusive (10). It seems that some sort of structural reorganization in the membrane brings leakage to a halt, possibly due to complete peptide equilibration across the lipid membrane, but the details of this process is not entirely understood. As an extension of this question, it is also still an open question how exactly that peptide and lipid translocation across the bilayer is coupled with permeabilization of membranes in lipid vesicles.

Another important question about peptide-induced membrane permeabilization is pertaining to the correlation between the transient permeabilization that have been identified in lipid vesicles and the equilibrium pores that have been identified in oriented lipid multibilayers. Even though elegant experimental designs have been applied to study permeabilization under equilibrium conditions in free-standing lipid bilayers (46, 105, 106), no direct correlation between permeabilization in lipid vesicles and pore formation in oriented multibilayers has so far been established. Without such a correlation, the structural insights gained from experiments on oriented multibilayers are not easily transferrable to the free-standing membranes in lipid vesicles and, thereby, also not easily transferable to cellular membranes[1].

Yet another pivotal question is about whether all of the many models that have been suggested to explain antimicrobial peptide-lipid membrane interactions represent distinct mechanisms, or whether many of them are manifestations of one single grand mechanism (10). As mentioned in Section 2.4.5, it was suggested that many of the individual models could be unified into a single model by considering phase diagrams and molecular shapes of phospholipids and peptides, but a definite validation of this approach is still lacking.

Finally, it would of course be highly desirable if the mode of interaction of antimicrobial peptides with phospholipid bilayers could be understood and predicted based on the physic-

---

[1]Considerations on the correlation between transient permeabilization in lipid vesicles and equilibrium pores in oriented multibilayers represent personal views of the author of this thesis.

Peptide name	Sequence length	Charge (pH 7.4)	Hydrophobic residues	One-letter sequence
Mastoparan X	14	+4	43 %	INWKGIAAMAKKLL-NH$_2$
Melittin	26	+6	31 %	GIGAVLKVLTTGLPALISW-IKRKRQQ-NH$_2$
Magainin 2	23	+3	30 %	GIGKFLHSAKKFGKAFVG-EIMNS

Table 2.1: Summary of the amino acid sequence characteristics of the three antimicrobial peptides studied in this thesis. To estimate the net peptide charge at pH 7.4, it was assumed that lysines and arginines are completely protonated and that histidines are completely deprotonated. Furthermore, estimates of the net charge also took into account that mastoparan X and melittin each gain an extra charge due to C-terminal amidation. To calculate the percentage of hydrophobic residues, the Wimley-White interfacial hydrophobicity scale was considered (114). Thus, a given residue was defined to be hydrophobic if it according to the Wimley-White interfacial hydrophobicity scale preferentially partitions into the lipid bilayer interface. According to this definition, tryptophan, phenylalanine, tyrosine, leucine, isoleucine, cysteine, and methionine are defined as hydrophobic.

ochemical characteristics of the peptides, for example, through quantification of molecular shapes (45). However, models to explain antimicrobial peptide-lipid membrane interactions are generally qualitative, and data aiming at quantitative correlations between peptide physicochemical properties and behavior in lipid bilayers is scarce. In a series of noteworthy papers, antimicrobial peptide free energies of binding and insertion in lipid bilayers were attempted correlated to peptide behavior in membranes (107–109) but no certain conclusions were reached. However, it is clear that successful completion of such attempts to quantitatively correlate peptide physicochemical characteristics to their behavior in lipid bilayers would represent a great scientific advance in the understanding of antimicrobial peptide-lipid membrane interactions (10).

2.6   Antimicrobial peptides studied in this thesis

In this thesis, three representative peptides with antimicrobial activity are studied (110–112): mastoparan X, melittin, and magainin 2. Each of these peptides originate from natural sources; mastoparan X was isolated from the venom of the hornet *Vespa xanthoptera* (113), melittin was isolated from the venom of the honeybee *Apis mellifera* (27), and magainin 2 was isolated from the skin of the frog *Xenopus laevis* (52). The amino acid sequences of these three peptides are archetypal to that of antimicrobial peptides; the sequences are short and enriched in cationic and hydrophobic residues. A summary of the amino acid sequence characteristics of mastoparan X, melittin and magainin 2 is given in Table 2.1.

In addition to their archetypal amino acid sequences, mastoparan X, melittin, and magainin 2 are also characterized by a number of other typical structural and functional features of antimicrobial peptides. Thus, similar to many other antimicrobial peptides, all three peptides are often reported to be in random coil or partially folded states in aqueous solution (111, 113, 115–117), albeit high peptide concentration, high ionic strength, and high pH
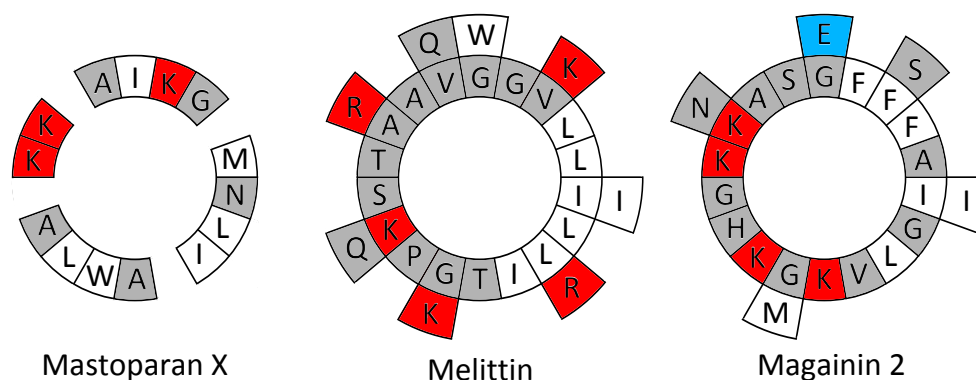
Figure 2.11: Helical wheel projection of the three antimicrobial peptides studied in this thesis: mastoparan X, melittin and magainin 2. Cationic residues are red, anionic residues are blue, hydrophobic residues are white, and the remaining residues are grey. Hydrophobic residues are defined as residues that according to the Wimley-White interfacial hydrophobicity scale preferentially partition into the bilayer interface (114). Histidine is assumed to be deprotonated at pH 7.4 and is, therefore, not represented as a cationic residue.

might induce peptide structuring and/or aggregation (111, 112, 118, 119). Upon association to lipid bilayers, all three peptides fold into α-helical structures (111, 117, 120–123): for mastoparan X, it has been suggested that residues Trp^3-Leu^{14} form a stable helix, whereas Ile^1-Asn^2 are unstructured (120, 121); for melittin, it has been suggested that about 20 amino acid residues take part in a stable helix and that the cationic residues at the C-terminal are unstructured (111); and for magainin 2, it has been suggested that at least residues Ile^2-Ile^{20} take part in a stable helix (112, 117). The helical wheel projections, shown in Fig. 2.11, predict that hydrophobic residues in these helical structures tend to cluster on one side of the helix and polar and charged residues tend to cluster on the opposite side, thereby creating an amphipathic structure as is also commonly observed in many other antimicrobial peptides (28). However, it should be noted that the helical wheel projections, drawn in Fig. 2.11, are primarily meant for illustrative purposes; they do not provide a completely accurate representation of the actual membrane-bound structure. For instance, the Ile^1 residue in mastoparan X is not necessarily located at the hydrophilic face as it has been predicted to not take part in the helical segment of the peptide (120, 121). Likewise, the C-terminal cationic resides in melittin are probably not distributed as predicted by the helical wheel projection as they also have been predicted not to take part in the helical segment of the peptide (111). Even so, in spite of these limitations of the helical wheel projection, it should still be clear that mastoparan X, melittin, and magainin 2 to some extent all fold into amphipathic structures upon association to phospholipid membranes.

The amphipathic features of mastoparan X, melittin, and magainin 2 allow them to interact with phospholipid bilayers in a manner similar to other antimicrobial peptides. Due to their amphipathic nature, they are thus often found in a planar orientation with their long axis parallel to the plane of the bilayer (111, 117, 122, 124). In this orientation, their hydrophobic faces are turning towards the acyl chain core of the bilayers, whereas their

hydrophilic faces are turning towards the lipid head groups of the bilayers, just as the typical orientation of many other α-helical antimicrobial peptides. However, there are certainly also examples that the all three peptides might insert perpendicularly into oriented multibilayers or lipid bicelles, and it has been hypothesized that this perpendicular insertion is coupled to the formation of transmembrane toroidal pores (56, 59, 66, 124). For all three peptides, it is not clear whether they generally are monomeric (111, 125, 126) or aggregated (64, 122, 127) when partitioned into phospholipid membranes.

The three peptides also display other archetypal features of antimicrobial peptides. Thus, in agreement with their net cationic charge, their partition coefficient is typically higher for partitioning into anionic phospholipid vesicles than for partitioning into zwitterionic phospholipid vesicles (110, 112, 128, 129). Furthermore, they have all been found to induce partial transient leakage from lipid vesicles (50, 52, 55, 56, 66, 128, 130–133). However, whereas mastoparan X and magainin 2 have been found to lyse anionic lipid vesicles more effectively than zwitterionic lipid vesicles (51, 112, 128), melittin has interestingly been found to lyse zwitterionic lipid vesicles more effectively than anionic lipid vesicles (42, 111), possibly because anionic lipid head groups immobilize melittin at the head group region (134).

2.7 Thesis scope revisited

In Section 1.2, it was stated that the thesis scope is to quantitatively study interactions between antimicrobial peptides and phospholipid membranes. To elaborate on that statement, a brief introduction to each of the manuscripts in Chapters 3, 4, and 5 is now given.

The manuscript in Chapter 3 is concerned with the adsorption of mastoparan X, melittin, and magainin 2 to solid surfaces of glass and plastic. This adsorption is examined by analytical HPLC. In that way, the manuscript is not *per se* concerned with quantitative studies of antimicrobial peptide-lipid membranes interactions. Rather, the manuscript is concerned with an effect that might have immense experimental implications for anyone who wants to perform quantitative studies of antimicrobial peptide-lipid membranes interactions. Thus, these adsorptive interactions might lead to poor control of the actual experimental concentration of peptides. Without accurate control of the experimental peptide concentration, it is impossible to conduct any quantitative studies on antimicrobial peptide-lipid membranes interactions.

The manuscript in Chapter 4 is concerned with using fluorescence correlation spectroscopy (FCS) as a method for quantitative studies of antimicrobial peptide-induced leakage of fluorescent markers from lipid vesicles. The goal of the manuscript is first and foremost to develop the technique for the purpose of quantifying leakage from lipid vesicles in solution; that is, the goal of the manuscript is not to apply the technique for any systematic investigations of antimicrobial peptide-induced membrane permeabilization; only mastoparan X is considered to show the applicability of FCS.

The manuscript in Chapter 5 is concerned with using fluorescently-labeled surface-tethered vesicles to quantitatively study antimicrobial peptide-induced leakage of fluorescent markers on the single-vesicle level. Specifically, confocal imaging of surface-tethered vesicles are combined with FCS to quantitatively study leakage induced by mastoparan X, melittin, and

magainin 2. In other words, the scope of the manuscript is both to introduce a novel approach for quantitative studies of antimicrobial peptide-induced leakage on the single-vesicle level and to use this approach, together with FCS, to quantitatively study leakage induced by mastoparan X, melittin, and magainin 2

It should be mentioned that in the first and third manuscript, the peptides are called "cationic membrane-active peptides" instead of "antimicrobial peptides"; this is due to the fact that the angles of the three manuscripts differ slightly. However, the reader of this thesis should keep in mind that the term "cationic membrane-active peptides" is basically just a synonym for the antimicrobial peptides that were discussed in the present chapter.

It should also be mentioned that the three manuscripts do not contain any discussion about how their contents might specifically be used to answer some of the questions posed in Section 2.5.2. However, for completeness, Chapter 6 contains a brief discussion about the future perspectives of the work presented in the three manuscripts, and, thereby, also a discussion about how the work presented in the manuscripts might be used for answering some of the questions posed in Section 2.5.2.

Finally, a comment should be made concerning the choice of synthetic lipid vesicles used in this thesis. Thus, it should be mentioned that several type of lipid vesicles with different sizes prepared by different methods are used in the literature to study antimicrobial peptide-phospholipid membrane interactions: Small unilamellar vesicles (SUVs) with a typical diameter of approximately 30 nm, prepared by ultrasonic irradiation (132); large unilamellar vesicles (LUVs) with a typical diameter of approximately 100 nm, prepared by extrusion (51, 110); and giant unilamellar vesicles (GUVs) with a typical diameter of approximately 5-100 μm, prepared by electroformation or spontaneous swelling (47, 135, 136). In terms of experimental design, both possibilities and limitations are associated with each type of lipid vesicles, and it can not be said that one type of lipid vesicle is better than the other. That being said, the work presented in this thesis is based on LUVs as they provide a model membrane system with multiple desirable attributes. In particular, solutions of LUVs represent a collection of size-homogenous vesicles with low membrane curvature. In addition, the lipid concentration of these solutions can, within a broad concentration range, be fine-tuned to the exact needs of a given experiment. In the following chapters, the usefulness of these attributes will be clearly demonstrated.

Adsorption of antimicrobial peptides to glass and plastic surfaces

The following chapter contains a manuscript in preparation. The manuscript is entitled "Adsorption of cationic membrane-active peptides to glass and plastic surfaces".

3.1 Abstract

Cationic membrane-active peptides have been studied for years in the hope of developing them into novel types of therapeutics. In this article, we report on an effect that might have immense experimental implications for investigators who wish to study these peptides, namely, that the peptides adsorb to solid surfaces of glass and plastic. Specifically, we used analytical HPLC to systematically study the influence of parameters like surface-to-volume ratio and ionic strength on the adsorption of the three α-helical cationic membrane-active peptides mastoparan X, melittin, and magainin 2 to the walls of disposable plastic and glass containers. The results show that at typical experimental concentrations, $90\ \%$ or more of the peptides might be lost due to rapid surface adsorption. Consequently, we conclude that investigators should keep these adsorptive effects in mind when designing and interpreting experiments on cationic membrane-active peptides.

3.2 Introduction

Cationic membrane-active peptides with antimicrobial (5, 14) and/or cell-penetrating properties (137, 138) have been studied intensely for years with the goal of developing these peptides into new types of therapeutics; for example, cationic membrane-active peptides have been suggested to hold promise for becoming a novel class of antibiotics (8). In the endeavor of studying and understanding these cationic membrane-active peptides, numerous advanced experimental and theoretical methods have been employed, resulting in a wealth of informative scientific articles. In these many articles, however, a quite important piece of

information is often put in a side note; cationic membrane-active peptides adsorb to solid surfaces, such as surfaces of glass or plastic. In spite of its immense experimental implications, this effect is seldom considered in its own right, except in a small handful of papers that clearly demonstrate the seriousness of this issue (139–143).

The goal of the present article is, therefore, to provide a systematic investigation of the adsorption of cationic membrane-active peptides to solid surfaces. Specifically, the goal is to systematically investigate the adsorption of the three α-helical cationic membrane-active peptides mastoparan X, melittin, and magainin 2 to the walls of disposable glass and plastic containers. Each of these three peptides have previously been extensively studied, especially, to reveal the mechanisms by which they interact with phospholipid bilayers (50, 52, 110–112, 128–132). For the purpose of studying the surface adsorption of these three peptides, we used analytical HPLC. Our results clearly show that interactions between cationic membrane-active peptides and solid surfaces of glass and plastic is an effect that should not be taken lightly upon by experimental investigators.

3.3 Materials and methods

3.3.1 Materials

1-palmitoyl-2-oleoyl-*sn*-glycero-3-phosphocholine (POPC) and 1-palmitoyl-2-oleoyl-*sn*-glycero-3-[phospho-rac-(1-glycerol)], sodium salt (POPG) were purchased from Avanti Polar Lipids (Alabaster, AL, USA). N-(2-hydroxyethyl)piperazine-N'-(2-ethanesulfonic acid) (HEPES) and the corresponding sodium salt (HEPES-Na), acetonitrile (MeCN), trifluoroacetic acid (TFA), and NaCl were purchased from Sigma-Aldrich (Brøndby, Denmark). Melittin was purchased from Peptide 2.0 (Chantilly, VA, USA), and mastoparan X and magainin 2 were purchased from GL Biochem (Shanghai, China). Mastoparan X was further purified by semi-preparative HPLC (Waters semi-preparative HPLC equipped with a Waters 600 pump & controller and a Waters 2489 UV/vis detector, Waters, Milford, MA, USA). The purity of all three peptides was checked by analytical HPLC (Shimadzu LC-2010C analytical HPLC equipped with a UV/vis detector, Shimadzu, Kyoto, Japan, or Gilson analytical HPLC equipped with a Gilson 321 HPLC pump and a Gilson 155 UV/vis detector, Gilson, Middleton, MI, USA) and the identity of the peptides was confirmed by MALDI-TOF (Bruker Reflex IV MALDI-TOF spectrometer, Bruker, Billerica, MA, USA).

Glass vials (borosilicate glass sample vials, 2 mL, diameter 12 mm) were purchased from Brown Chromatography Supplies (VWR - Bie & Berntsen, Herlev, Denmark), plastic tubes (polypropylene Safe-Lock tubes, 2 mL, inner diameter 9.2 mm) and LoBind tubes (Protein LoBind tubes, 2 mL, inner diameter 9.2 mm) were purchased from Eppendorf (VWR - Bie & Berntsen). Quartz glass cuvette (Suprasil, inner dimensions 4×10 mm) was purchased from Hellma (Müllheim, Germany). PTFE-coated magnetic stirring bar was purchased from VWR (VWR - Bie & Berntsen).

3.3.2   LUV preparation and characterization

POPC/POPG (3:1) solutions were prepared in chloroform/methanol (9:1). The organic solvent was removed under a gentle stream of nitrogen. The samples were subsequently kept in vacuum overnight to remove the residual solvent. The lipid films were hydrated in 10 mM HEPES, 100 mM NaCl, pH 7.4 buffer with vigorous vortexing every 5 min for a period of 30 min. The hydrated lipid suspensions were then subject to 5 freeze-thaw cycles by alternately placing the sample vials in an isopropanol/dry ice bath and a warm water bath. Next, the lipid suspensions were extruded 21 times through a 100 nm polycarbonate filter (Whatman, Maidstone, UK) using a mini-extruder (Avanti Polar Lipids) to form LUVs. The size of the LUVs was checked by dynamic light scattering (ZetaPALS, Brookhaven Instruments, Holtsville, NY, USA). Phosphorous concentrations of the LUV solutions were determined using the method of Rouser et al. (144), albeit with slightly modified reagent concentrations.

3.3.3   Peptide stock solutions

Peptide stock solutions were prepared in 10 mM HEPES, 100 mM NaCl, pH 7.4 buffer. To prevent loss of peptides due to adsorption to tube walls and/or pipette tips, the peptide stock solutions were handled in LoBind tubes at a high concentration of at least 100 µM. To determine the concentration of peptide stock solutions, the extinction coefficients of peptides at 220 nm were calculated to be 40100 cm^{-1}M^{-1} for mastoparan X, 46700 cm^{-1}M^{-1} for melittin, and 23900 cm^{-1}M^{-1} for magainin 2 by correlating the peptide concentrations determined by an Antek 8060 chemiluminescent nitrogen detector (PAC, Houston, TX, USA) to the absorbance of the same peptide samples, determined by a NanoDrop 2000c spectrophotometer (NanoDrop Products, Wilmington, DE, USA). Given these extinction coefficients, peptide concentrations of stock solutions were then always determined by recording the absorbance at 220 nm using the NanoDrop 2000c spectrophotometer.

3.3.4   Preparation of samples for analytical HPLC

The general procedure for preparation of samples for analytical HPLC, to be described in detail in the following lines, was that peptide solutions were incubated in glass or plastic containers before they were transferred to HPLC autosampler vials containing inserts (conical inserts, borosilicate glass, 300 µL, diameter 6 mm, Brown Chromatography Supplies, Mikrolab Aarhus, Højbjerg, Denmark). After transfer of solutions to the inserts, POPC/POPG (3:1) LUVs were added to the inserts to prevent surface adsorption of peptides to the walls of the inserts. The solutions in the inserts were then subject to HPLC analysis to quantify the amount of peptide in the inserts and, thereby, also the amount of peptide that had been lost to surface adsorption in the glass and plastic containers in which the peptide solutions had been incubated before they were transferred to the inserts.

In the following, all samples were prepared in 10 mM HEPES, 100 mM NaCl, pH 7.4 buffer, except where otherwise noted.

Concentration standard curves

Peptide solutions of varying concentrations were prepared directly in the inserts in the autosampler vials. Specifically, varying volumes of 100 μM peptide stock solutions were added to varying volumes of buffer in the inserts to a final solution volume of 200 μL. After peptide addition, the autosampler vials were vortexed for a few seconds. Next, 50 μL of 5 mM POPC/POPG (3:1) LUV was added to each of the inserts to a final LUV concentration of 1 mM and a final volume of 250 μL. The autosampler vials were again vortexed for a few seconds. Finally, the samples in the inserts were subject to HPLC analysis.

Peptide loss in glass and plastic containers

Peptide solutions of 1, 2, 5, 10, or 20 μM were prepared by adding varying volumes of 100 μM peptide stock solutions to varying volumes of buffer in glass vials, plastic tubes, or LoBind tubes to a final solution volume of 220 μL. After peptide addition, solutions were vortexed for a few seconds and then incubated for 1 h. Next, 200 μL of each solution was transferred by pipette to the inserts in the autosampler vials. The autosampler vials were then vortexed for a few seconds. Subsequently, 50 μL of 5 mM POPC/POPG (3:1) LUV was added to each of the inserts to a final LUV concentration of 1 mM and a final volume of 250 μL. Autosampler vials were again vortexed for a few seconds. Subsequently, samples in the inserts were subject to HPLC analysis.

Loss in peptide solutions of larger volumes were also considered. Specifically, 2 mL solutions of 2 μM peptide were prepared in glass vials, plastic tubes, LoBind tubes, or quartz glass cuvettes by adding 40 μL of 100 μM peptide stock solutions to 1960 μL buffer. The solutions in the glass vials, plastic tubes, and LoBind tubes were then vortexed for a few seconds and incubated for 1 h before 200 μL of each solution was transferred by pipette to the inserts in the autosampler vials. The solutions in the quartz glass cuvettes were constantly stirred for 1 h by a magnetic bar before 200 μL of each solution was transferred by pipette to the inserts in the autosampler vials. For all samples, upon transfer to the inserts, the protocol was then identical to that described before; the autosampler vials were vortexed for a few seconds, 50 μL of 5 mM POPC/POPG (3:1) LUV was added to each of the inserts to a final LUV concentration of 1 mM, the autosampler vials were again vortexed for a few seconds, and, finally, samples in the vial inserts were subject to HPLC analysis.

Peptide loss during successive transfers between containers

Peptide solutions in four identical containers (glass vials, plastic tubes, or LoBind tubes) were prepared by adding 12.5 μL of 100 μM peptide stock solution to 237.5 μL buffer in each of the containers to a final peptide concentration of 5 μM and a final solution volume of 250 μL. Following peptide addition, each of four the containers were vortexed for a few seconds. The solution in the first container was then incubated for 1 h before 200 μL of the solution was transferred by pipette to an insert in an autosampler vial. The solution in the second container was transferred by pipette into an empty container of the same kind. This new container was then vortexed for a few seconds. After 1 h incubation, 200 μL of

the solution in this new container was transferred by pipette to an insert in an autosampler vial. The solution in the third container was successively transferred by pipette into two empty containers of the same kind. After each transfer step, the solution was vortexed for a few seconds. Upon transfer to the last empty container, the solution was incubated for 1 h before 200 μL of the solution was transferred by pipette to an insert in an autosampler vial. The solution in the fourth container was successively transferred by pipette into three empty containers of the same kind. After each transfer step, the solution was vortexed for a few seconds. Upon transfer to the last empty container, the solution was incubated for 1 h before 200 μL of the solution was transferred by pipette to an insert in an autosampler vial. Once in the inserts in the autosampler vials, each of the four solutions were treated as described before; the autosampler vials were vortexed for a few seconds, 50 μL of 5 mM POPC/POPG (3:1) LUV was added to each of the inserts to a final LUV concentration of 1 mM, the autosampler vials were again vortexed for a few seconds, and, at last, the samples in the inserts were subject to HPLC analysis.

Peptide loss as a function of NaCl concentration

Peptide solutions of 2 μM were prepared in glass vials, plastic tubes, or LoBind tubes. The solutions were prepared by adding 4.4 μL of 100 μM peptide stock solution (in 10 mM HEPES, 100 mM NaCl, pH 7.4 buffer) to 215.6 μL buffer (10 mM HEPES, pH 7.4 with either 0 mM NaCl or 150 mM NaCl) to a final volume of 220 μL and final NaCl concentrations of 2 mM or 149 mM, respectively. In that way, solutions with different NaCl concentrations were prepared. The rest of the protocol was then identical to that described before; solutions were vortexed for a few seconds, incubated for 1 h before 200 μL of each solution was transferred by pipette to inserts in autosampler vials. Then, the autosampler vials were vortexed for a few seconds, 50 μL of 5 mM POPC/POPG (3:1) LUV (in 10 mM HEPES, 100 mM NaCl, pH 7.4 buffer) was added to each of the inserts to a final LUV concentration of 1 mM, the autosampler vials were again vortexed for a few seconds, and, finally, samples in the inserts were subject to HPLC analysis.

To confirm that peptide concentrations could still be quantified by the HPLC method upon changing the NaCl concentration, we prepared 2 μM peptide solutions directly in the inserts in the autosampler vials by adding 4 μL of 100 μM peptide stock solution (in 10 mM HEPES, 100 mM NaCl, pH 7.4 buffer) to 196 μL buffer (10 mM HEPES, pH 7.4 with either 0 mM NaCl or 150 mM NaCl) to a final volume of 200 μL. Autosampler vials were vortexed for a few seconds. Next, 50 μL of 5 mM POPC/POPG (3:1) LUV (in 10 mM HEPES, 100 mM NaCl, pH 7.4 buffer) was added to each of the inserts to a final LUV concentration of 1 mM. The autosampler vials were again vortexed for a few seconds, and, at last, the contents of the vial inserts were subject to HPLC analysis.

Surface pre-saturation and LUV-induced desorption

Peptide solutions of 2 μM were prepared in glass vials, plastic tubes, or LoBind tubes by adding 4.4 μL of 100 μM peptide stock solution to 215.6 μL buffer to a final volume of 220 μL. The solutions were vortexed for a few seconds and then incubated for 1 h. Following

this incubation time, 200 μL of each solution was aspirated into a pipette tip and discarded. Next, 196 μL buffer and then 4 μL of 100 μM peptide stock solution were added to the each of the containers to a final volume of 220 μL (20 μL had remained in the containers after discarding 200 μL). The solutions were vortexed for a few seconds and incubated for 1 h. Subsequently, the solutions were treated in the same manner as described before; 200 μL of each of the solutions were transferred by pipette to inserts in autosampler vials, the autosampler vials were vortexed for a few seconds, 50 μL of 5 mM POPC/POPG (3:1) LUV was added to each of the inserts to a final LUV concentration of 1 mM, the autosampler vials were again vortexed for a few seconds, and, at last, the samples in the inserts were subject to HPLC analysis.

In connection with these pre-saturation experiments, we also investigated the effect of POPC/POPG (3:1) LUVs to entail desorption of peptides from the walls of the glass vials, plastic tubes, and LoBind tubes. Specifically, we considered the effect of POPC/POPG (3:1) LUVs to induce desorption in both containers that had not been pre-saturated with peptide and containers that had been pre-saturated with peptide. In the experiments with non-saturated containers, peptide solutions were prepared in glass vials, plastic tubes, or LoBind tubes by adding 4.4 μL of 100 μM peptide stock solution to 205.6 μL buffer. Solutions were vortexed for a few seconds and then 10 μL of 22 mM POPC/POPG (3:1) LUV was added to each of the solutions to a final peptide concentration of 2 μM, a final LUV concentration of 1 mM, and a final volume of 220 μL. Solutions were again vortexed for a few seconds, and then incubated for 1 h. Next, 200 μL of each of the solutions were transferred by pipette to the inserts in the autosampler vials. The autosampler vials were vortexed for a few seconds and 50 μL of 1 mM POPC/POPG (3:1) LUV was added to each of the inserts to a final LUV concentration of 1 mM. The autosampler vials were again vortexed and the samples in the inserts were subject to HPLC analysis.

In the experiments with pre-saturated containers, peptide solutions were prepared in glass vials, plastic tubes, or LoBind tubes by adding 4.4 μL of 100 μM peptide stock solution to 215.6 μL buffer to a final peptide concentration of 2 μM and a final volume of 220 μL. Solutions were vortexed for a few seconds and, subsequently, incubated for 1 h. After this incubation time, 200 μL of each of the solutions was aspirated into a pipette tip and discarded. Next, 186 μL buffer and then 4 μL of 100 μM peptide stock solutions were added to each container. The solutions were vortexed for a few seconds and then 10 μL of 22 mM POPC/POPG (3:1) LUV was added to each of the solutions to a final peptide concentration of 2 μM, a final LUV concentration of 1 mM, and a final volume of 220 μL. The containers were again vortexed and incubated for 1 h. Then the samples were treated in a manner identical to before; 200 μL of each of the solutions were transferred by pipette to inserts in autosampler vials, the autosampler vials were vortexed for a few seconds, 50 μL of 1 mM POPC/POPG (3:1) LUV was added to the inserts to a final LUV concentration of 1 mM, the autosampler vials were again vortexed, and, finally, the samples in the inserts were subject to HPLC analysis.

Adsorption and desorption kinetics

To investigate the adsorption kinetics of peptides, we considered only mastoparan X. Specifically, a number of samples with 2 μM mastoparan X were prepared by adding 4.4 μL of 100 μM mastoparan X stock solution to 215.6 μL buffer in glass vials, plastic tubes, or LoBind tubes to a final volume of 220 μL. The solutions were vortexed for a few seconds and then incubated for 10 s, 1 h, or 24 h. After these incubation times, solutions were handled as also described before; 200 μL of the solutions were transferred by pipette to inserts in autosampler vials, the autosampler vials were vortexed for a few seconds, 50 μL of 5 mM POPC/POPG (3:1) LUV was added to each of the inserts to a final LUV concentration of 1 mM, the autosampler vials were again vortexed, and, finally, the samples in the inserts were subject to HPLC.

3.3.5   Analytical HPLC measurements

Analytical HPLC was performed on a Shimadzu LC-2010C integrated HPLC system equipped with a UV/vis detector (Shimadzu, Kyoto, Japan). For samples of mastoparan X together with 1 mM POPC/POPG (3:1) LUV, 80 μL was loaded onto the system. For samples of melittin or magainin 2 together with 1 mM POPC/POPG (3:1) LUV, 50 μL was loaded onto the system. We found that when larger volumes were injected, peptide peak areas were no longer linear to peptide concentrations. The flow rate of the system was 1 mL/min. Mobile phases were (A) water with 5 % MeCN and 0.1 % TFA and (B) MeCN with 0.1 % TFA. Gradients were linear from 85 % A to 0 % A over 12 min. Peptides and lipids were separated on a XTerra RP8 (5 μm, 4.6×150 mm) column (Waters). UV absorbances were recorded at 220 nm. Peptide peak areas were determined by using the LC Postrun Analysis software.

3.4   Results

3.4.1   Concentration standard curves

To confirm that the HPLC method is applicable to quantify peptide concentrations, we prepared a number of 200 μL concentration standard solutions of varying mastoparan X, melittin, or magainin 2 concentrations directly in inserts in HPLC autosampler vials. To each of these standard solutions, 50 μL of 5 mM POPC/POPG (3:1) LUV solution was added to a final LUV concentration of 1 mM to prevent adsorption of peptides to the walls of the inserts. Samples were then subject to HPLC analysis. Fig. 3.1 shows a typical HPLC chromatogram of a 200 μL standard solution of 5 μM mastoparan X to which 50 μL of 5 mM POPC/POPG (3:1) LUV solution had been added. The peptide peak and the lipid peak are clearly separated. For melittin and magainin 2, we also found that the peptide and lipid peaks were well separated in chromatograms (examples not shown). Fig. 3.2, *A*, *C*, and *E*, shows the peptide peak area as a function of the mastoparan X, melittin, and magainin 2 concentration of the 200 μL standard solutions, respectively. (That is, the concentrations in Fig. 3.2 are the concentration of the standard solutions before 50 μL LUV solutions were added). A linear correlation between the peptide peak area and the peptide concentration was
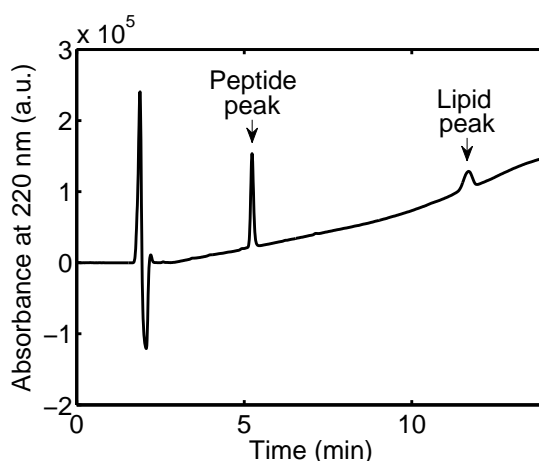
Figure 3.1: Example of HPLC chromatogram for a sample in which 200 µL of 5 µM mastoparan X had been mixed with 50 µL of 5 mM POPC/POPG (3:1) LUV directly in inserts in HPLC autosampler vials. The peptide peak and the lipid peak was found to be clearly separated.

observed for all three peptides, albeit at concentrations ≤ 200 nM, significant uncertainties in the peak area was observed for mastoparan X and magainin 2, see Fig. 3.2, *A* and *E*, respectively. Nevertheless, the linear standard curves lead to the conclusion that HPLC is suitable to quantify peptide concentrations across the entire investigated concentration range.

In order to further assess the accuracy of the HPLC method to quantify peptide concentrations, the percentage of recovered peptide was calculated by the equation

$$\text{Recovered peptide} = 100 \times \frac{\text{Peak area}}{\text{Slope} \times \text{Concentration}} \tag{3.1}$$

using the peak areas, the slopes and the concentrations from Fig. 3.2, *A*, *C*, and *E*. In order for HPLC to be applicable for accurately quantifying the peptide concentration across the entire concentration range, the percentage of recovered peptide should be close to 100 % for all of the concentration standard solutions. Fig. 3.2, *B*, *D*, and *F*, confirms that this is indeed the case for all three peptides, underlining the conclusion from Fig. 3.2, *A*, *C*, and *E*, that the HPLC method is an accurate method for quantifying peptide concentrations across the entire investigated concentration range. However, it should be noted that Fig. 3.2, *B* and *F*, also underlines the conclusion from Fig. 3.2, *A*, and *E*, that measurements of mastoparan X and magainin 2 concentration ≤ 200 nM are subject to large relative uncertainties.

In the following, we present the results of a number of experiments in which peptide solutions were incubated in different types of sample containers before 200 µL of the solutions were transferred by pipette to inserts in HPLC autosampler vials together with 50 µL of 5 mM POPC/POPG (3:1) LUV for HPLC analysis. The acquired peptide peak areas are always recalculated to percentages of recovered peptide using Eq. 3.1. In this recalculation, we always use the slopes from the standard curves in Fig. 3.2, *A*, *C*, and *E*. If the percentages of recovered peptides are found to be < 100 %, that must mean that some peptide have
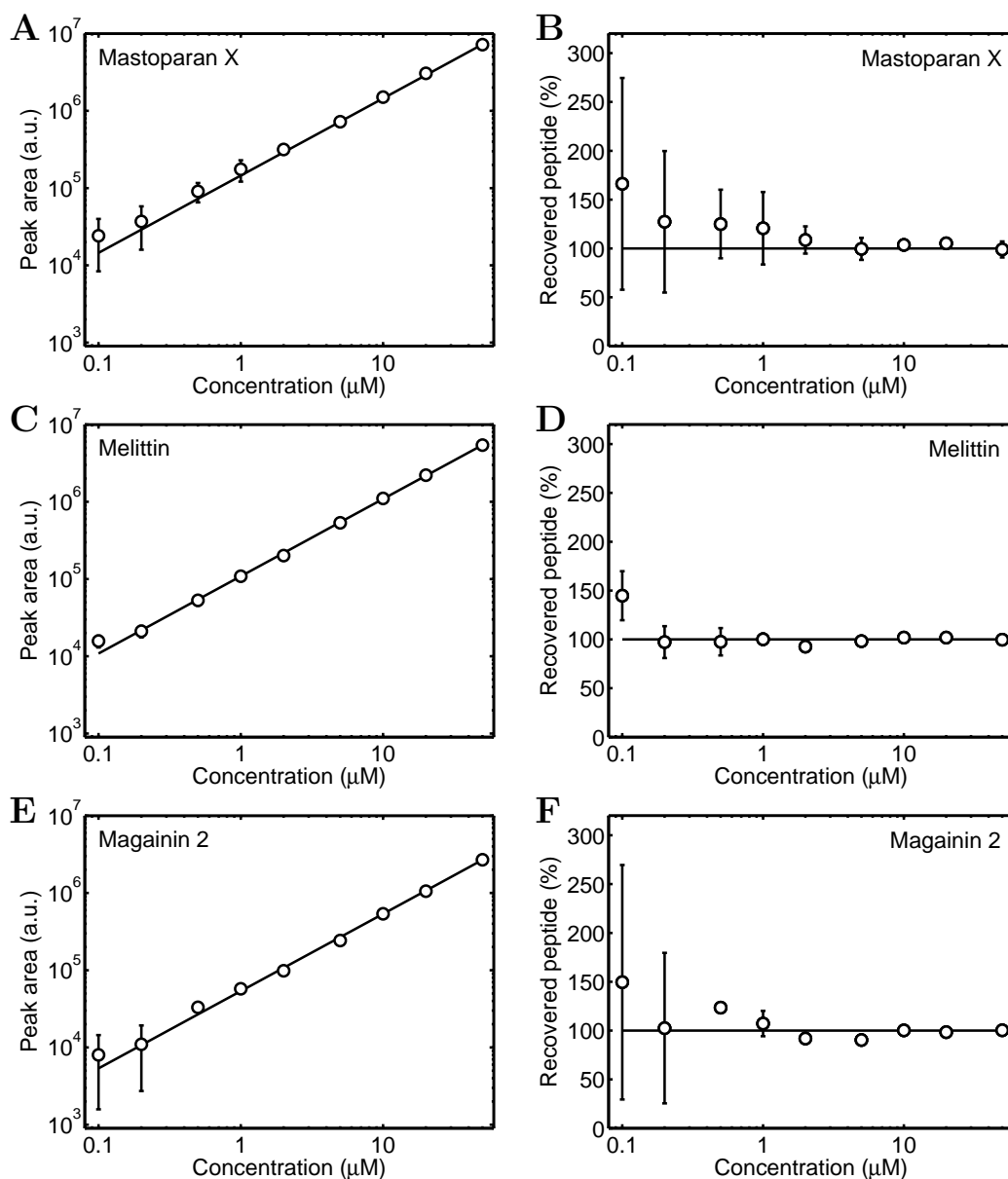
Figure 3.2: Peptide concentration standard curves. Samples were prepared by mixing 200 μL peptide standard solutions of varying peptide concentration with 50 μL of 5 mM POPC/POPG (3:1) LUV directly in inserts in HPLC autosampler vials. The concentrations in the figure are the concentrations of the 200 μL peptide standard solutions. (*A, C, E*) Peak area vs concentration of mastoparan X, melittin, and magainin 2 standard solutions, respectively. The straight lines are the best least squares fits to the data. (*B, D, F*) Percentage of recovered peptide, as calculated from Eq. 3.1, vs concentration of mastoparan X, melittin, and magainin 2 standard solutions. In all panels, the data are the average of three separate experiments. The error bars show the standard deviations. The error bars are not shown when they are smaller than the symbols. The data demonstrate that the HPLC method is applicable to quantify the peptide concentration across the entire investigated concentration range.
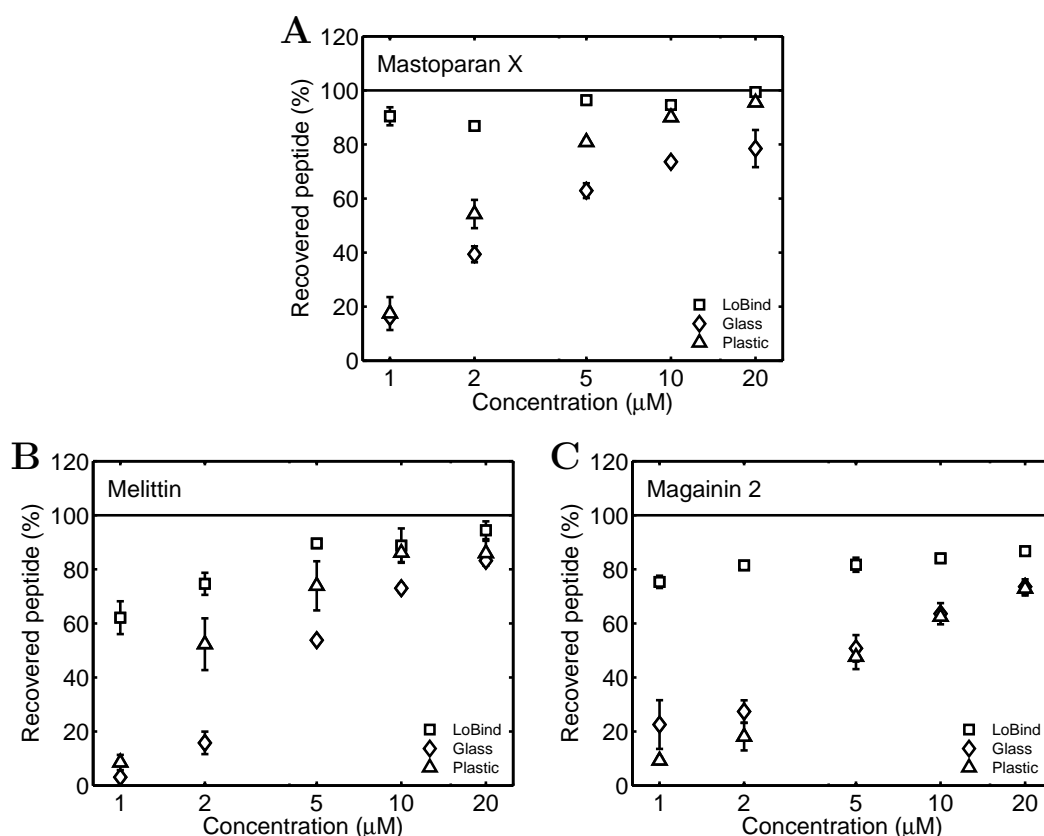
Figure 3.3: Loss of mastoparan X (*A*), melittin (*B*), and magainin 2 (*C*) in 220 µL peptide solutions incubated in glass vials, or plastic or LoBind tubes as a function of the peptide concentration. In all panels, the data are the average of two separate experiments. The error bars show the standard deviations. The error bars are not shown when they are smaller than the symbols. The data demonstrate that all three peptides tend to adsorb to glass and plastic surfaces, especially at low peptide concentration where only $10 - 20$ % of the expected peptide contents are recovered. In contrast, peptides do not absorb to LoBind tubes to the same extent.

been lost in the experimental process; either because peptides adsorb onto the walls of the samples containers, or because peptides adsorb on pipette tips during the transfer from solutions from the sample containers to the inserts. The latter explanation was ruled out by a control experiment, see Fig. 3.9 in the Supporting material. Thereby, the loss of peptide reported in the following experiments is ascribed to adsorption of peptide onto the walls of the disposable glass and plastic containers.

3.4.2 Peptide loss in glass and plastic containers

To study the adsorption of mastoparan X, melittin, and magainin 2 to the walls of disposable glass and plastic containers, we prepared a number of 220 µL peptide solutions of 1, 2, 5, 10, or 20 µM peptide in glass vials or plastic tubes. For comparison, we also prepared a number
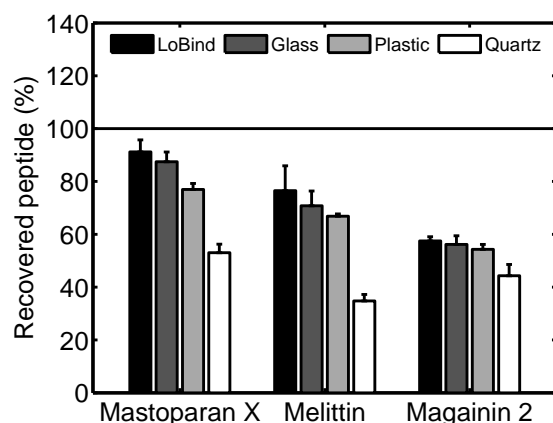
Figure 3.4: Loss of mastoparan X, melittin, and magainin 2 in 2 mL, 2 µM peptide solutions incubated in glass vials, plastic tubes, LoBind tubes, or quartz glass cuvettes. The data are the average of two separate experiments. The error bars show the standard deviations. The data demonstrate that peptide surface-adsorption is not just a phenomenon that occurs at high container surface-to-solution volume ratios.

of 220 µL peptide solutions of 1, 2, 5, 10, or 20 µM peptide in LoBind tubes, designed to reduce the surface adsorption of proteins and peptides. After a few seconds of vortexing and 1 h incubation, 200 µL of each of the solutions was transferred to inserts in the autosampler vials together with 50 µL of 5 mM POPC/POPG (3:1) LUV and subject to HPLC analysis. Fig. 3.3 shows the percentage of peptide thus recovered from the 220 µL peptide solutions as a function of the peptide concentration. A number of common observation were done for all three peptides. First, for 1 µM peptide solutions incubated in glass vials or plastic tubes, only $10 - 20$ % of the peptides were recovered, meaning that most of the peptide adsorbed to the walls of these containers at this concentration. Second, for peptide solutions in glass vials or plastic tubes, an increasing percentage of peptide was recovered as a function of the peptide concentration, indicating that the walls became saturated with peptide. Third, for peptide solutions incubated in LoBind tubes, peptides were not lost to the same extent as in the glass vials and plastic tubes, albeit loss of peptide did in some cases still occur, see, for example, melittin at 1 µM in Fig. 3.3 *B*.

To investigate whether surface adsorption also occurred at lower container surface-to-solution volume ratios, at which the surfaces would more easily be saturated with peptides, we prepared a number of 2 mL, 2 µM mastoparan X, melittin, or magainin 2 solutions in glass vials, plastic tubes, and LoBind tubes. In addition, in these experiments, we also prepared 2 mL, 2 µM mastoparan X, melittin, or magainin 2 solutions in quartz glass cuvettes. After a few seconds of vortexing and 1 h incubation, 200 µL of each solution was transferred to inserts in the autosampler vials together with 50 µL of 5 mM POPC/POPG (3:1) LUV, and the samples were analyzed by HPLC. Fig. 3.4 shows the percentage of peptide recovered from the 2 mL solutions. The data in the figure shows that reducing the container surface-to-solution volume ratio entails an increase in the percentage of recovered peptide (compare
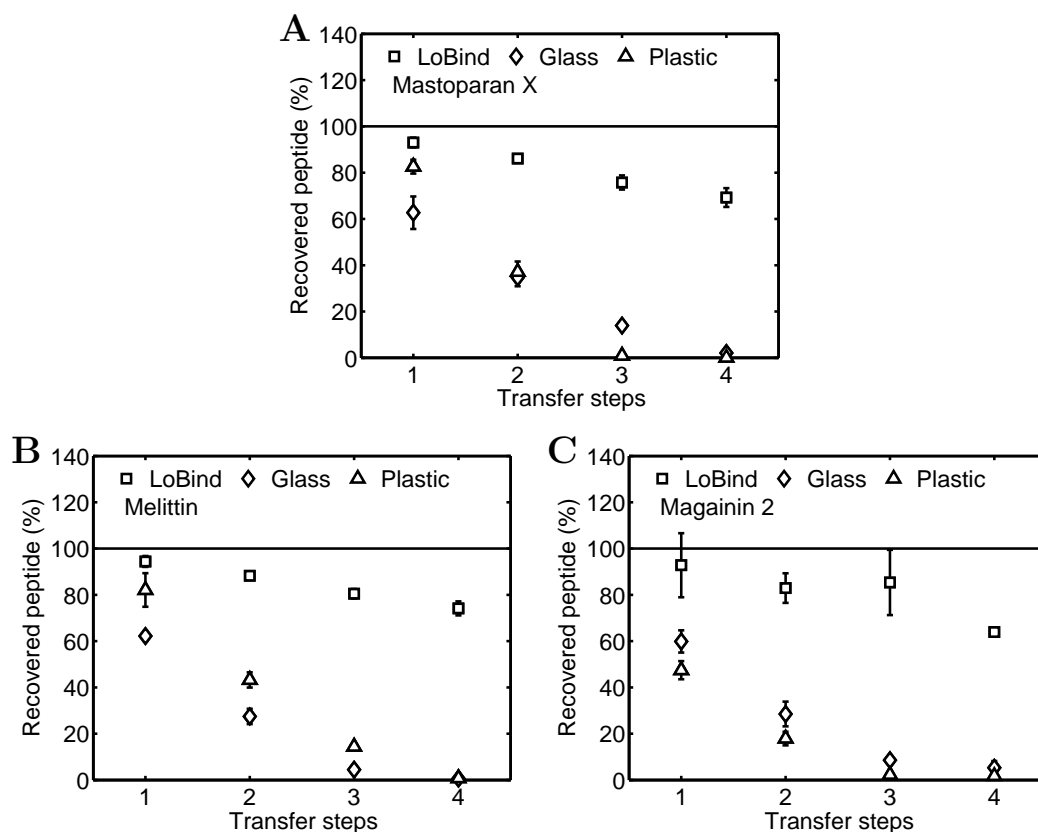
Figure 3.5: Loss of mastoparan X (*A*), melittin (*B*), and magainin 2 (*C*) during successive transfers of 250 µL, 5 µM peptide solutions between glass vials, plastic tubes, and LoBind tubes. In all panels, the data are the average of two separate experiments. The error bars show the standard deviations. The error bars are not shown when they are smaller than the symbols. The data highlights the strong interaction between peptides and the walls of glass vials and plastic tubes; after four transfer steps in glass vials or plastic tubes, all three peptides were below the detection limit of the HPLC method.

Fig. 3.3 to 3.4), albeit the data also shows that surface adsorption of mastoparan X, melittin, and magainin 2 is a phenomenon that not only occurs at high container surface-to-solution volume ratios. An interesting observation from Fig. 3.4 is that mastoparan X, melittin, and magainin 2 adsorb rather effectively to quartz glass cuvettes; the percentage of recovered peptide in the quartz glass cuvettes was generally ≤ 50 % for all peptides. Another peculiar observation from Fig. 3.4 is that peptides, within the experimental uncertainty, adsorb to the same extent to the walls of LoBind tubes on the one hand and to the walls of glass vials and plastic tubes on the other hand. This is in marked contrast to the observations in Fig. 3.3, in which peptides were found to adsorb much more effectively to glass vials and plastic tubes than to LoBind tubes.

3.4.3   Peptide loss during successive transfers between containers

We also investigated the effect of successively transferring 250 µL, 5 µM mastoparan X, melittin, and magainin 2 solutions between glass vials, plastic tubes, and LoBind tubes; specifically, peptides were transferred between 1 to 4 containers with vortexing of solutions between each transfer step. After 1 h incubation in the last container, 200 µL of each of the solutions was transferred to inserts in the autosampler vials together with 50 µL of 5 mM POPC/POPG (3:1) LUV, and the samples were subject to HPLC analysis. Fig. 3.5 shows the percentage of recovered peptide as a function of the number of transfer steps. The data confirms the observations from Figs. 3.3 and 3.4; peptides adsorb to the walls of the containers. In particular, the data in Fig. 3.5 highlights the strong interaction between peptides and the walls of glass vials and plastic tubes; in no cases after four transfer steps were any peptide recovered in neither the glass vials nor the plastic tubes.

3.4.4   Peptide loss as a function of NaCl concentration

Up until now, presented experiments were carried out in 10 mM HEPES, 100 mM NaCl, pH 7.4 buffer. To investigate whether the NaCl concentration impacted the adsorption process of mastoparan X, melittin, and magainin 2, we prepared a number of 220 µL, 2 µM peptide solutions in glass vials, plastic tubes, or LoBind tubes using buffers of varying NaCl concentrations. Specifically, the solutions were prepared in 10 mM HEPES, pH 7.4 with 2 mM NaCl, 100 mM NaCl, or 149 mM NaCl. After a few seconds of vortexing and 1 h incubation in the containers, 200 µL of each of the solutions was transferred to inserts in the autosampler vials together with 50 µL of 5 mM POPC/POPG (3:1) LUV, and the samples were subject to HPLC. In addition, samples with 200 µL, 2 µM mastoparan X, melittin, or magainin 2 solutions with different NaCl concentration were prepared directly in the inserts, similar to the way that also the solutions for the concentration standard curves in Fig. 3.2 were prepared directly in inserts. Fig. 3.6 *A* shows that in the samples mixed directly in the inserts, approximately 100 % peptide is recovered for all peptides, independent on the NaCl concentration, demonstrating that the applicability of the HPLC method is not dependent upon the NaCl concentration of the solutions. Fig. 3.6, *B*, *C*, and *D*, shows that the percentage of recovered mastoparan X, melittin, or magainin 2 as a function of NaCl concentration. We found that, within the experimental uncertainty, the percentage of surface-adsorbed peptide was not influenced by the concentration of NaCl.

3.4.5   Surface pre-saturation and LUV-induced desorption

We investigated the effect of pre-saturating containers with peptide. More specifically, glass vials, plastic tubes, and LoBind tubes were pre-saturated with 220 µL, 2 µM peptide solution before fresh 220 µL, 2 µM peptide solutions were transferred to each of the containers. After a few seconds of vortexing and 1 h incubation, 200 µL of each of the solutions were transferred to inserts in autosampler vials together with 50 µL of 5 mM POPC/POPG (3:1) LUV. Solutions were then subject to HPLC analysis. Fig. 3.7 shows the effect of pre-saturation on the peptide content in the different containers; pre-treating glass vials and
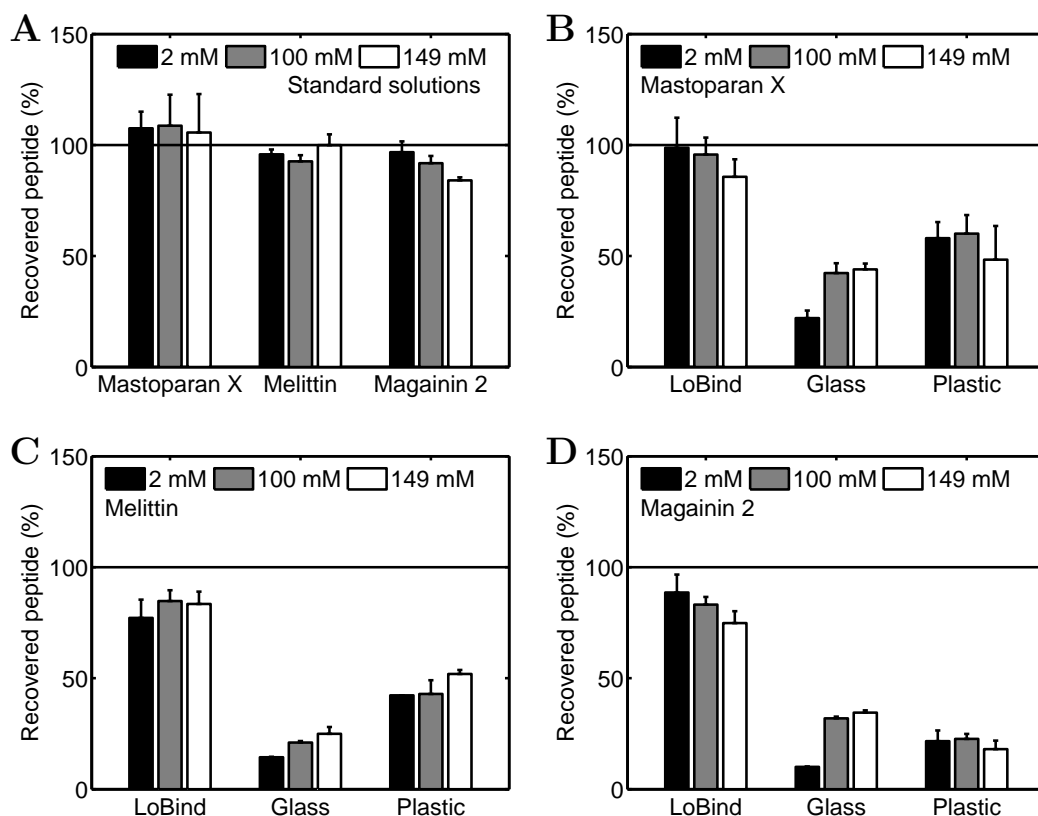
Figure 3.6: Percentage of recovered peptide as a function of NaCl concentration for 220 μL, 2 μM mastoparan X (*B*), melittin (*C*), and magainin 2 (*D*) solutions in glass vials, plastic vials, or LoBind tubes. (*A*) The percentage of recovered peptide in control solutions prepared directly in the inserts of the autosampler vials. The data are the average of two separate experiments, expect in (*A*) in which three experiments were averaged. The error bars show the standard deviations. Within the experimental uncertainties of the HPLC method, the NaCl concentration was not found to impact the surface adsorption of any of the three peptides.

plastic tubes with peptide solutions does entail a small increase in the peptide content, but the percentages of recovered peptide are generally still well below 100 %.

In connection with these experiments on the effect of pre-saturation of containers with peptide solutions, we also investigated the effect of LUVs to entail desorption of peptide from the walls of glass vials, plastic tubes, and LoBind tubes; both containers that had not been pre-saturated with peptide solution and containers that had been pre-saturated with 220 μL, 2 μM peptide solution were considered. To both the non-saturated and in the pre-saturated containers, 210 μL, 2.1 μM peptide solutions were added and, following vortexing, 10 μL of 22 mM POPC/POPG (3:1) LUV was added to a final peptide concentration of 2 μM and a final LUV concentration of 1 mM. After 1 h incubation, samples were then transferred to inserts in the autosampler vials together with 50 μL of 1 mM POPC/POPG (3:1) LUV for HPLC analysis. Fig. 3.7 shows the capability of LUVs to entail desorption
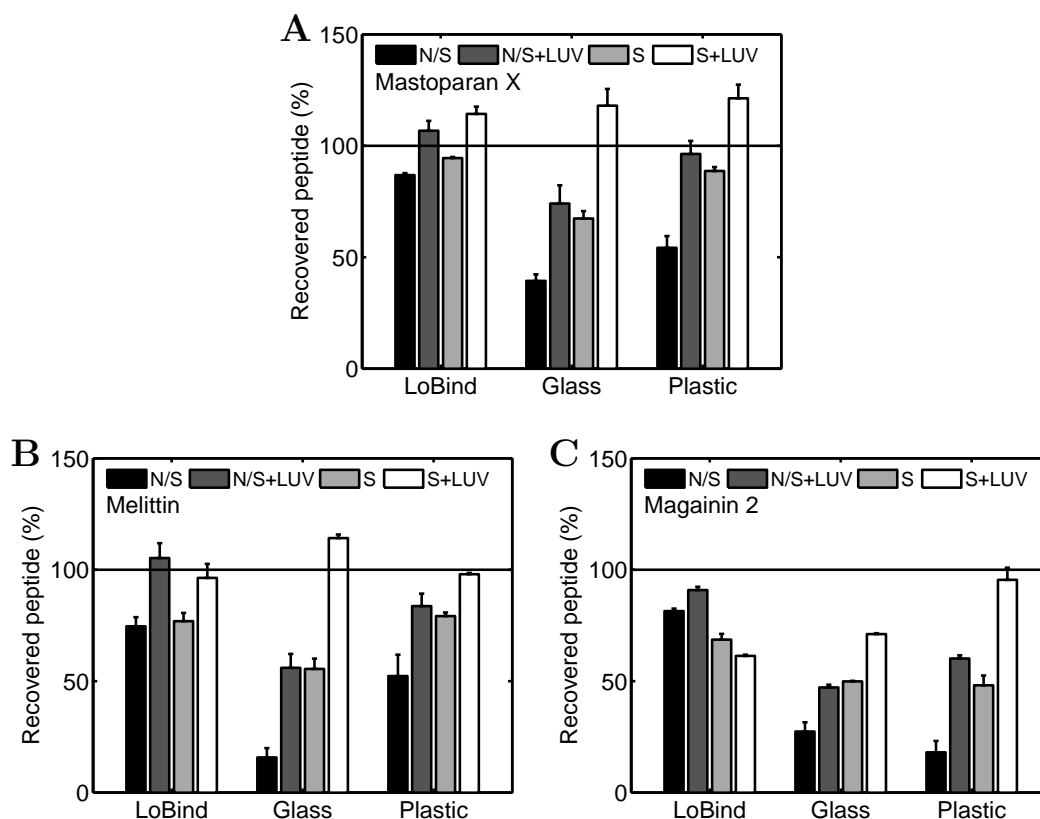
Figure 3.7: Effect of pre-saturation of glass vials, plastic tubes, and LoBind tubes with peptide solutions, and the capability of 1 mM POPC/POPG (3:1) LUV to induce desorption in non-saturated and pre-saturated containers. (*A*) Mastoparan X. (*B*) Melittin. (*C*) Magainin 2. N/S: 220 µL, 2 µM peptide solutions in vials that were not pre-saturated. N/S+LUV: 10 µL of 22 mM POPC/POPG (3:1) LUV was added to 210 µL, 2.1 µM peptide solutions in vials that were not pre-saturated. S: 220 µL, 2 µM peptide solutions in vials that had been pre-saturated. S+LUV: 10 µL of 22 mM POPC/POPG (3:1) LUV was added to 210 µL, 2.1 µM peptide solutions in vials that had been pre-saturated. The data are the average of two separate experiments. The error bars show the standard deviations. The N/S-samples together with S-samples demonstrate that pre-saturation of surfaces with peptide does not necessarily ensure complete recovery of peptide. The N/S+LUV-samples demonstrate that LUVs induce partly desorption of peptide from the walls of the glass and plastic containers. The S+LUV-samples demonstrate that LUVs also induce desorption from pre-saturated samples, and in many cases, more than 100 % peptide was recovered.

from both non-saturated and pre-saturated containers. For the non-saturated containers, LUV induced some desorption, especially from the glass vials and plastic tubes. However, in many cases, LUVs were not found to induce complete desorption. For the pre-saturated containers, LUVs were also found to induce desorption, and in many cases, more than 100 % peptide was recovered. A peculiarly observation from Fig. 3.7 *C* is that for magainin 2 in LoBind tubes, the percentage of recovered peptide was lowest for samples in which LUVs were added to pre-saturated tubes; no good explanation to this observation was found.
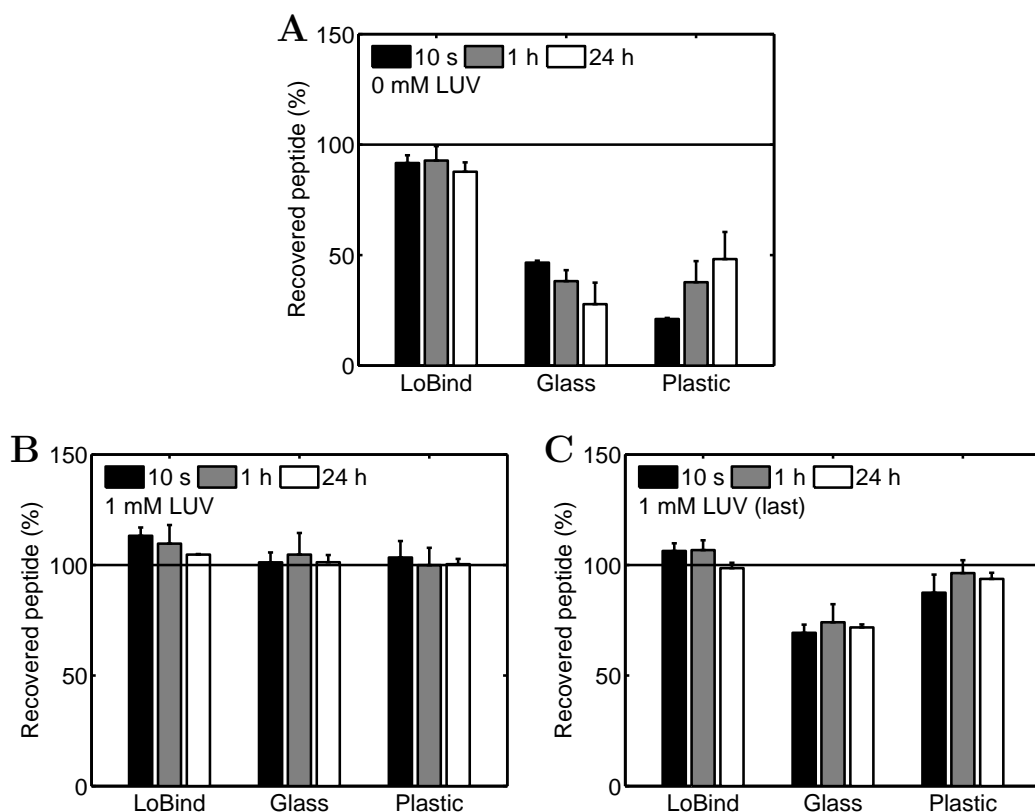
Figure 3.8: Kinetics of mastoparan X adsorption and desorption in glass vials, plastic tubes, and LoBind tubes. (*A*) Kinetics of adsorption in 2 μM, 220 μL mastoparan X solutions. (*B*) Kinetics of adsorption in 2 μM, 220 μL mastoparan X solutions with 1 mM POPC/POPG (3:1) LUV. (*C*) Kinetics of desorption in 2 μM, 220 μL mastoparan X solutions induced by 1 mM POPC/POPG (3:1) LUV. The data are the average of two separate experiments. The error bars show the standard deviations. Generally, adsorption and desorption are fast processes that takes place within a few seconds. The data indicate that mastoparan X adsorption to glass surfaces is partly irreversible.

3.4.6 Adsorption and desorption kinetics

We studied the kinetics of mastoparan X adsorption onto the walls of the glass vials, plastic tubes, and LoBind tubes. To do that, volumes of mastoparan X stock solutions were added to volumes buffer in glass vials, plastic tubes, and LoBind tubes to a final concentration of 2 μM mastoparan X and a final volume of 220 μL. After a few seconds of vortexing, the solutions were incubated for 10 s, 1 h, or 24 h and, thereafter, 200 μL of each solution was transferred to the inserts in the autosampler vials together with 50 μL of 5 mM POPC/POPG (3:1) LUV for analysis by HPLC. Fig. 3.8 *A* shows the recovered percentage of mastoparan X for the three different incubation times. Within the experimental uncertainty, the percentage of recovered peptide is independent on incubation time, showing that adsorption of mastoparan X to surfaces of glass and plastic is a fast process that occurs during the vortexing within the first few seconds after peptide addition to the solutions.

We also studied the adsorption kinetics of mastoparan X in the presence of 1 mM POPC/POPG (3:1) LUV in glass vials, plastic tubes, and LoBind tubes. In order to do that, volumes of mastoparan X stock solutions were added to volumes of LUV solutions in glass vials, plastic tubes, and LoBind tubes to a final concentration of 2 µM mastoparan X, a final LUV concentration of 1 mM, and a final volume of 220 µL. After a few seconds of vortexing, the solutions were incubated for 10 s, 1 h, or 24 h and, thereafter, 200 µL of each solution was transferred to inserts in the autosampler vials together with 50 µL of 1 mM POPC/POPG (3:1) LUV and, subsequently, analyzed by HPLC. Fig. 3.8 *B* shows the percentage of recovered peptide as a function of the incubation time. For all incubation times in all sample containers, the presence of 1 mM POPC/POPG (3:1) LUV prevented surface adsorption of mastoparan X, meaning that mastoparan X partitioned rapidly onto the LUVs.

Finally, we also studied the desorption kinetics of mastoparan X. In order to do that, we prepared solutions with 210 µL, 2.1 µM mastoparan X in glass vials, plastic tubes, and LoBind tubes. After vortexing, 10 µL of 22 mM POPC/POPG (3:1) LUV was added to each of these solutions. After vortexing, the solutions were incubated for 10 s, 1 h, or 24 h, and, thereafter, 200 µL of each solution was transferred to inserts in the autosampler vials together with 50 µL of 1 mM POPC/POPG (3:1) LUV for analysis by HPLC. Fig. 3.8 *C* shows the percentage of recovered peptide as a function of the incubation time. The percentage of recovered peptide was found to be independent on the incubation time; thereby, similarly to the adsorption process, we found that the desorption process was a fast process that happened during the vortexing within the first few seconds after LUV addition. In the case of the glass vials, as also shown in Fig. 3.7 *A*, the LUVs did not induce complete desorption of mastoparan X. In additional experiments, we found that vortexing for longer periods did not induce additional desorption from the glass surfaces (data not shown).

3.5   Discussion

In this article, we confirm previous studies demonstrating the applicability of analytical HPLC to study surface adsorption of peptides (145), and we confirm previous observations that proteins and peptides in general (146, 147) and cationic membrane-active peptides in specific (139–142) adsorb to different types of solid surfaces. Specifically, we considered the three archetypal α-helical cationic membrane-active peptides mastoparan X, melittin, and magainin 2, which previously have been suggested to adsorb to solid surfaces of glass and plastic (130, 148, 149). In this article, we confirm that all three peptides readily adsorb to negatively charged surfaces (borosilicate and quartz glass) as well as hydrophobic surfaces (polypropylene), see Figs. 3.3 to 3.5. Importantly, we show that this surface adsorption is significant at commonly chosen experimental peptide concentrations. That is, at peptide concentrations of 1 to 2 µM, 90 % percent or even more of the peptides might be adsorbed to the walls of the glass and plastic containers, see Fig. 3.3. It is needless to say that ignoring this phenomenon might lead to inaccurate experimental conclusions, for example, in *in vitro* assays evaluating the antimicrobial and hemolytic potencies of cationic membrane-active peptides.

Our experiments also revealed a few other details about the adsorption of mastoparan

X, melittin, and magainin 2 to surfaces of glass and plastic. For example, our experiments revealed that the adsorption is not dependent on the NaCl concentration of the buffer, at least within the experimental uncertainty of the HPLC method, see Fig. 3.6. Not even for negative glass surfaces where interactions are electrostatically driven (141) did we notice a significant screening effect of NaCl. This is in contrast to previous observations on the cationic peptide salmon calcitonin, for which it was found that the ionic strength affected the adsorption of the peptide to both surfaces of borosilicate glass and polypropylene (141).

Using mastoparan X as a model peptide, our experiments also revealed that the adsorption process is a fast process, see Fig. 3.8; during vortexing of the solutions in the glass or plastic containers, mastoparan X adsorbed to the walls of the containers within a few seconds. In addition, experiments on mastoparan X show that also desorption from glass and plastic surfaces induced by LUVs is a rapid process occurring within a few seconds during vortexing. However, the fact LUVs did not always induce complete desorption of neither mastoparan X from glass surfaces (Figs. 3.7 and 3.8) nor of melittin and magainin 2 from both glass and plastic surfaces (Fig. 3.7), not even during longer periods of vortexing (data not shown), could indicate that part of the peptides were irreversibly bound: However, further experiments are required to confirm or dismiss that notion.

In order to reduce the problem of surface adsorption of cationic membrane-active peptides, several strategies have previously been pursued. One strategy has been to modify the surfaces. For example, adsorbing the cationic polymer poly(ethylenimine) to the walls of quartz glass cuvettes was found to effectively prevent the surface adsorption of the peptide penetratin (139). Another strategy has been to pre-saturate the surfaces with peptide. However, due to the, at least partly, reversible nature of the adsorption process, this strategy might in some cases be dangerous. Thus, as demonstrated in Fig. 3.7, in experiments where volumes of LUV solutions are added to glass or plastic containers with peptide solutions, the walls of the containers might provide a reservoir of peptides that, upon addition of LUVs, desorb from the walls and instead partition onto the LUVs. These peptide reservoirs will persist even after pre-saturation of container walls with peptide solution; thus, the pre-saturation strategy will not always be an effective strategy for controlling the experimental peptide concentration.

Our results lead to a few other recommendations on how to alleviate the problem of surface adsorption of cationic membrane-active peptides. The first recommendation comes from the observation that relatively more peptide adsorbs to surfaces of glass and plastic at low peptide concentrations, see Fig. 3.3. This observation leads to the recommendation that peptide concentrations should be kept as high as possible during handling. The second observation comes from the observation that some sample tubes lead to more surface adsorption than other sample tubes. To be more specific, we observe that surface adsorption of peptides is more dominant in sample tubes consisting of borosilicate or polypropylene than in the commercially available LoBind tubes, see Figs. 3.3 to 3.5. These observations lead to the recommendation that also the choice of sample containers should be subject to careful considerations. Finally, the most important recommendation following from our data is that experimental investigators at all times should be aware of the critical impact that the adsorptive interactions can have on the outcome of their experiments.
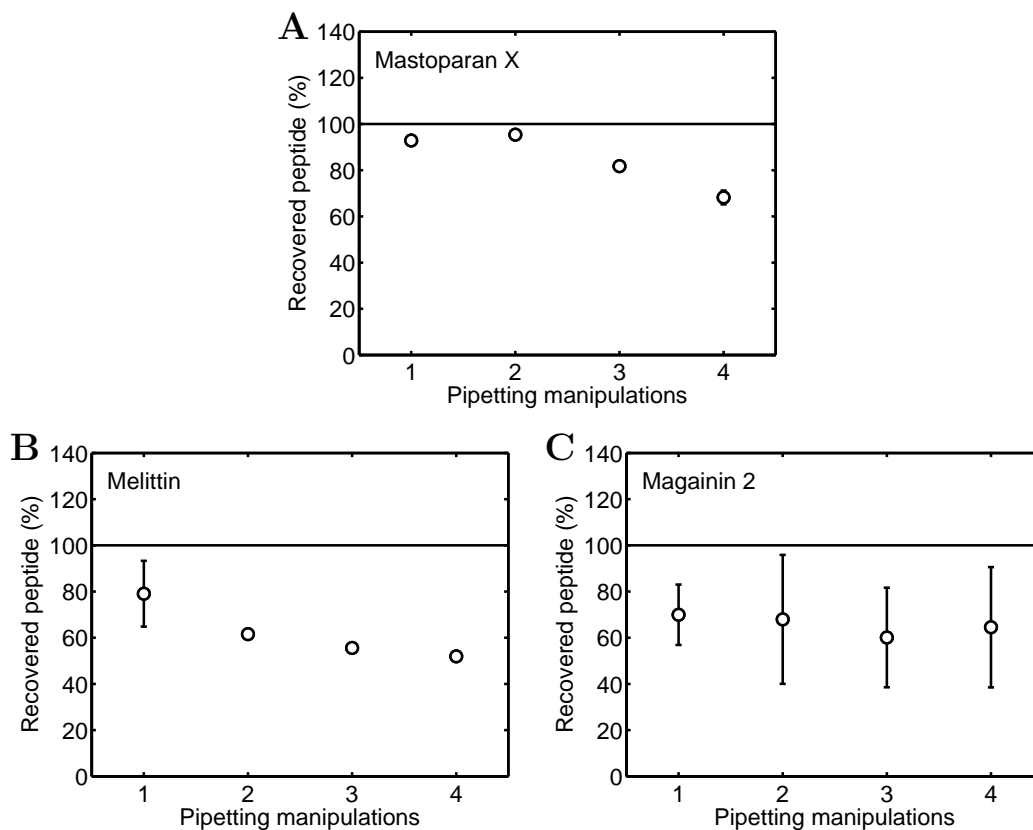
Figure 3.9: Adsorption loss during pipetting of 200 μL of 1 μM mastoparan X (*A*), melittin (*B*), or magainin 2 (*C*) solutions. Solutions were subject to 1-4 pipetting manipulations. The data are the average of two separate experiments. The error bars show the standard deviations. The error bars are not shown when they are smaller than the symbols. Only a small loss, if any, is observed during pipetting.

3.6 Supporting material

3.6.1 Adsorption on pipette tips

Method

Four identical peptide solutions of 1 μM were prepared in LoBind tubes by adding 2.2 μL of 100 μM peptide stock solution to 217.8 μL buffer to a final volume of 220 μL. The solutions were vortexed for a few seconds and then incubated for 1 h. After this incubation time, 200 μL of each of the solutions were aspirated into a pipette tip and allowed to adsorb to the pipette tip for ~ 5 s before being deposited back into the same tube from which they were aspirated. This manipulation was repeated 1-4 times using new pipette tips for each manipulation. After the last manipulation, solutions were not deposited back into the LoBind tubes but instead into the inserts in the HPLC autosampler vials. The autosampler

vials were then vortexed for a few seconds. Subsequently, 50 μL of 5 mM POPC/POPG (3:1) LUV was added to each of the inserts to a final LUV concentration of 1 mM and a final volume of 250 μL. Autosampler vials were again vortexed, and, subsequently, samples in the inserts were subject to HPLC analysis.

Results

Fig. 3.9 shows that the percentage of recovered peptide does not change much as a function of the number of pipetting manipulations. Thus, we conclude that aspiration of 200 μL, 1 μM peptide solutions into the pipette tips does not entail a dramatic loss of peptide due to adsorption on the pipette tips. Thereby, the loss of peptide presented in the main document must be due to the adsorption of peptide to the walls of the glass vials, plastic tubes, LoBind tubes, and quartz glass cuvettes.

Quantification of antimicrobial peptide-induced leakage by FCS

The following chapter contains a manuscript in preparation. The manuscript is entitled "Quantification of antimicrobial peptide-induced leakage from large unilamellar vesicles by FCS".

4.1   Abstract

The mechanisms by which antimicrobial peptides permeabilize lipid bilayers have been subject to extensive scientific interest for years. In this article, we evaluate the potential of the technique fluorescence correlation spectroscopy (FCS) to study these membrane-permeabilizing activities. Specifically, we derive the mathematical framework needed for using FCS to study peptide-induced leakage from large unilamellar vesicles, and we highlight a number of experimental artifacts that might compromise the accuracy of the FCS-determined leakage values. We show that if all of these pitfalls are avoided, then FCS can be used to quantify leakage of fluorescent markers from the lumen of the lipid vesicles, including leakage of fluorescent markers of different sizes. To demonstrate the applicability of FCS to study antimicrobial peptide-induced leakage, we consider the antimicrobial peptide mastoparan X, and we show that the peptide forms transmembrane pores to induce size-dependent leakage of markers from POPC/POPG (3:1) vesicles.

4.2   Introduction

Antimicrobial peptides with broad-spectrum microbicidal activity have been identified in organisms across the entire evolutionary spectrum, including bacteria, fungi, plants, fishes, amphibians, birds, and mammals (5, 14). Due to the natural capabilities of these peptides to kill a wide range of infectious pathogens, including multi-drug resistant bacteria, they have attracted significant scientific attention as candidates to become a novel class of anti-infective

therapeutics (8). However, despite this attention, the mechanisms by which antimicrobial peptides kill pathogenic microbes are still not fully elucidated.

As a group, antimicrobial peptides represent a large variety of different primary amino acid sequences. Despite this diversity, antimicrobial peptides are, however, still described by a number of common characteristics. More specifically, antimicrobial peptides are typically small and enriched in cationic and hydrophobic amino acid residues. Furthermore, antimicrobial peptides typically form amphipathic secondary structures that allow different modes of interaction with cellular membranes (28). The central role of these peptide-membrane interactions are emphasized by the fact that antimicrobial peptides always interact with the cell membrane to kill a given cell; either the antimicrobial peptides disrupt the structural integrity of the cell membrane, or they translocate across the cell membrane to target an intracellular metabolic process, such as DNA, RNA, or protein synthesis (12). Accordingly, it is widely believed that a detailed understanding of these antimicrobial peptide-cell membrane interactions is key to unraveling the mechanisms of antimicrobial peptide activity (10).

In order to study these peptide-membrane interactions, synthetic lipid vesicles are often used as minimal models of cellular membranes. In particular, size-homogenous unilamellar lipid vesicles with a diameter of 100 nm, commonly termed large unilamellar vesicles (LUVs), are often employed. Typically, these LUVs are incubated with antimicrobial peptides to induce leakage of entrapped fluorescent markers from the LUVs. Leakage is then commonly observed as an increase in emission intensity as a result of fluorescence dequenching (52, 150); that is, the fluorescent molecules are initially entrapped at high self-quenching concentrations or together with a quencher, but upon leakage, their local concentration decreases entailing a dramatic increase in fluorescent emission intensity. This approach has yielded valuable insights into the mechanisms underlying antimicrobial peptide-induced membrane permeabilization, for example, revealing that peptide-induced leakage from lipid vesicles is a transient process in which leakage, following an initial rapid burst over the course of a few minutes, slows down or ceases altogether before all LUVs are empty of fluorescent markers (45). In addition to the dequenching-based detection approach, other elaborate schemes have also been employed to detect leakage from LUVs, for example, to study leakage of fluorescent markers of different sizes, thereby providing information on the size of transmembrane pores formed by antimicrobial peptide (151, 152).

Another spectroscopic technique that has been used to study antimicrobial peptide-induced leakage from LUVs is fluorescence correlation spectroscopy (FCS) (153–155). In FCS, fluctuations in emission intensity from fluorescent molecules diffusing across a small excitation volume are statistically analyzed via an autocorrelation function to yield information about concentrations, diffusion properties, triplet state kinetics, and other things of the fluorescent molecules (156, 157). Thus, FCS can be used to detect leakage of fluorescent molecules from LUVs as the diffusion coefficient of entrapped fluorescent molecules differ from that of released fluorescent molecules; entrapped fluorescent molecules are restricted to diffuse together with the LUVs, thereby having the same diffusion coefficient as the LUVs, whereas released fluorescent molecules diffuse freely with a much higher diffusion coefficient than the LUVs and thereby the entrapped fluorescent molecules. In addition, by labeling the lipid membranes of the LUVs with a lipid-anchored fluorescent probe, FCS can also be

used to evaluate the release mechanism (158). If leakage is due to formation of transmembrane pores, the LUVs will remain intact, and the diffusion coefficient of the lipid-anchored fluorophores will not change during leakage. In contrast, if leakage is due to membrane solubilization, the diffusion coefficient of the lipid-anchored fluorophores will decrease as the fluorophores are incorporated into mixed peptide-lipid micelles. The diffusion time of the lipid-anchored fluorophores will also reveal if vesicle aggregation and/or fusion occurs during leakage as that would entail an increase in the diffusion coefficient of the lipid-anchored fluorophores.

In this article, we evaluate the requirements for using FCS to quantify antimicrobial peptide-induced leakage from LUVs. In particular, we derive the necessary mathematical framework to quantify leakage, and we highlight the experimental pitfalls. We show that, if all of these pitfalls are avoided, FCS can be used to accurately quantify leakage of fluorescent markers from LUVs, including leakage of fluorescent markers of different sizes.

To demonstrate the potential of FCS as a method to study antimicrobial peptide-induced leakage, we consider the natural peptide mastoparan X (MPX), isolated from the venom of the hornet *Vespa xanthoptera* (159). MPX displays many archetypal features of antimicrobial peptides, including a short sequence of 14 amino acid residues, a strong net charge of $+4$ and an amphipathic α-helical secondary membrane-bound structure (120, 121). It has previously been shown that MPX entails leakage of contents from LUVs, including size-dependent leakage of entrapped markers (51, 128, 130, 160, 161). Here, we confirm these observations as we show that MPX-induced leakage from POPC/POPG (3:1) LUVs is due to the formation of transmembrane pores and that the size of these pores leads to size-selective leakage of fluorescent probes ranging in size from ~ 500 Da to ~ 10 kDa. Thereby, we show that FCS as a method to study antimicrobial peptide-induced leakage from LUVs display a number of advantages over other existing methods to study leakage.

4.3 Theory

Upon transfer of leakage-inducing antimicrobial peptides to a solution of LUVs entrapping fluorescent molecules, a certain fraction of the initially entrapped fluorescent molecules will leak out of the LUVs. This fraction L must be given by the equation

$$L = \frac{C_{\mathrm{f}} - C_{\mathrm{f0}}}{C_{\mathrm{f100}} - C_{\mathrm{f0}}} \tag{4.1}$$

where C_{f0} is the concentration of unentrapped fluorescent molecules before peptide addition, C_{f} is the concentration of unentrapped fluorescent molecules after peptide addition, and C_{f100} is the concentration of unentrapped fluorescent molecules at complete leakage. In the following section, we derive an analytical expression relating leakage L, as defined in Eq. 4.1, to the output parameters of FCS. This derivation begins with the fundamental equations of FCS.

For a single species of fluorescent molecules diffusing freely into and out of a three-dimensional Gaussian excitation volume, the autocorrelation function, $G(\tau)$, with triplet

state contribution is given by (156, 162)

$$G(\tau) = \frac{1}{N}g(\tau) = \frac{1}{N}\left(1 + \frac{T}{1-T}\mathrm{e}^{-\tau/\tau_{\mathrm{T}}}\right)\left(1 + \frac{\tau}{\tau_{\mathrm{D}}}\right)^{-1}\left(1 + \frac{\tau}{S^2\tau_{\mathrm{D}}}\right)^{-\frac{1}{2}} \tag{4.2}$$

where τ is the lag time, N is the average number of fluorescent molecules in the excitation volume, T is the fraction of fluorescent molecules in the triplet state, τ_{T} is the characteristic triplet state lifetime, S is the ratio of the radial to axial dimensions of the excitation volume, and τ_{D} is the characteristic translational diffusion time of the fluorescent molecules. In case there are multiple diffusing species of fluorescent molecules, the autocorrelation function is a weighted sum of the autocorrelation functions of the individual species (156, 162):

$$G(\tau) = \sum_{i=1}^{n} B_i^2 N_i^2 G_i(\tau) \bigg/ \left(\sum_{i=1}^{n} B_i N_i\right)^2$$

$$= \sum_{i=1}^{n} B_i^2 N_i g_i(\tau) \bigg/ \left(\sum_{i=1}^{n} B_i N_i\right)^2 = \sum_{i=1}^{n} A_i g_{\mathrm{i}}(\tau) \tag{4.3}$$

where B_i is the brightness (photon count rate per molecule) of the molecules of the ith species, N_i is the mean number of molecules of the ith species in the excitation volume, and A_i is the amplitude of the ith species. The sum in the denominator corresponds to the total photon count rate of the system, B_{tot}:

$$\sum_{i=1}^{n} B_i N_i = B_{\mathrm{tot}}. \tag{4.4}$$

For leaky LUVs in solution, there are two distinct diffusing species: LUVs entrapping fluorescent molecules (index v) and unentrapped fluorescent molecules (index f). The autocorrelation function must then be given by

$$G(\tau) = \frac{B_{\mathrm{f}}^2 N_{\mathrm{f}} g_{\mathrm{f}}(\tau) + B_{\mathrm{v}}^2 N_{\mathrm{v}} g_{\mathrm{v}}(\tau)}{B_{\mathrm{tot}}^2} = A_{\mathrm{f}} g_{\mathrm{f}}(\tau) + A_{\mathrm{v}} g_{\mathrm{v}}(\tau). \tag{4.5}$$

The mean number of unentrapped molecules in the excitation volume N_{f} must be linearly proportional to the concentration of the unentrapped molecules C_{f} through the relation $C_{\mathrm{f}} = N_{\mathrm{f}}/(N_{\mathrm{A}} V_{\mathrm{eff}})$ where N_{A} is Avogadro's number and V_{eff} is the effective excitation volume (163). Consequently, Eq. 4.1 can be rewritten to contain N_{f}-values instead of C_{f}-values:

$$L = \frac{N_{\mathrm{f}} - N_{\mathrm{f}0}}{N_{\mathrm{f}100} - N_{\mathrm{f}0}}. \tag{4.6}$$

According to Eq. 4.5, N_{f} is related to A_{f} by the equation

$$A_{\mathrm{f}} = \frac{B_{\mathrm{f}}^2 N_{\mathrm{f}}}{B_{\mathrm{tot}}^2}. \tag{4.7}$$

The total photon count rate B_{tot} in the denominator of this equation is a function of leakage, L:

$$B_{\text{tot}} = B_{\text{f}} \left(N_{\text{f100}} - N_{\text{f0}}\right) L + kB_{\text{f}} \left(N_{\text{f100}} - N_{\text{f0}}\right) (1 - L) + B_{\text{f}} N_{\text{f0}} + B_{\text{b}} \qquad (4.8)$$

where B_{b} is an uncorrelated background contribution, B_{f} is the brightness of unentrapped molecules, and k is the brightness ratio between entrapped and unentrapped molecules, defined by $k = B_{\text{e}}/B_{\text{f}}$ where B_{e} is the brightness of entrapped molecules. Setting $N_{\text{f0}} = 0$ in Eq. 4.8, we then get that

$$B_{\text{tot}} = B_{\text{f}} N_{\text{f100}} L + kB_{\text{f}} N_{\text{f100}}(1 - L) + B_{\text{b}}. \qquad (4.9)$$

By inserting Eqs. 4.7 and 4.9 into Eq. 4.6, a quadratic equation in L is finally obtained:

$$L = \frac{A_{\text{f}} \left(B_{\text{f}} N_{\text{f100}} L + kB_{\text{f}} N_{\text{f100}}(1 - L) + B_{\text{b}}\right)^2 - A_{\text{f0}} \left(kB_{\text{f}} N_{\text{f100}} + B_{\text{b}}\right)^2}{A_{\text{f100}} \left(B_{\text{f}} N_{\text{f100}} + B_{\text{b}}\right)^2 - A_{\text{f0}} \left(kB_{\text{f}} N_{\text{f100}} + B_{\text{b}}\right)^2}. \qquad (4.10)$$

The details on how to experimentally determine each of the parameters in Eq. 4.10 in order to calculate L are given in the Materials and Methods section. However, before proceeding to this section, a number of comments should be made regarding the derivation of Eq. 4.10. Firstly, in the above derivation, it was implicitly assumed that all unentrapped fluorescent molecules have the same brightness. However, this assumption might not always be true. For example, in the case of fluorescently-labeled dextrans, individual dextran molecules are labeled with variable numbers of fluorophores. However, as long as the probability of a given dextran molecule being released is not dependent on the number of fluorescent-labels on that dextran molecule, then the above theoretical framework is still applicable, albeit with the modification that N_{f} and B_{f} only represent apparent values for the unentrapped dextran molecules. Additional mathematical derivations to gain a more elaborate understanding on the interpretation of such apparent N and B-values are presented in the Supporting material.

Secondly, even though they are not included in the Eq. 4.10, the N_{v} and B_{v}-parameters also deserve some attention. In the limit where the mean number of entrapped fluorescent molecules per LUV is much smaller than 1, i.e., in the limit where the number of LUVs with more than 1 fluorescent molecule entrapped is negligibly small, then N_{v} and B_{v} represent the B and N-values of the entrapped fluorescent molecules, i.e., in this limit $N_{\text{v}} = \left(N_{\text{f100}} - N_{\text{f0}}\right) (1 - L)$ and $B_{\text{v}} = kB_{\text{f}}$. In the opposite limit where the concentration of encapsulated fluorescent molecules is so high that the relative variations in the number of entrapped fluorescent molecules among LUVs is very small, then N_{v} and B_{v} correspond to the mean number of LUVs in the excitation volume and the average brightness of the LUVs, respectively, i.e., $N_{\text{v}} = N_{\text{LUV}}$ where N_{LUV} is the mean number of LUVs in the excitation volume, and $B_{\text{v}} = kB_{\text{f}}\tilde{B}$ where $\tilde{B}$ is the mean number of fluorescent molecules entrapped per LUV. However, in order for this limit to apply, it is required that all LUVs have the same lumen volume and that the encapsulation process itself does not entail variations in the numbers of entrapped fluorescent molecules among individual LUVs; therefore, it is questionable whether this limit is at all experimentally feasible. For any experimental system in between the two limiting cases, the interpretation of the apparent N_{v} and B_{v}-values is not trivial and requires specific information about the brightness distribution of the LUVs.

Thirdly, different assumptions about N_{f0} were made in Eqs. 4.6, and 4.9. Thus, in Eq. 4.6, N_{f0} was included, leading to the inclusion of A_{f0} in Eq. 4.10. The inclusion of this A_{f0}-value in Eq. 4.10 is important, even in cases where all unentrapped fluorescent molecules are completely removed from the LUVs during the preparation process. Thus, when Eq. 4.5 is fitted to autocorrelation curves recorded in sample only containing LUVs, then an artificial non-zero value of A_f is often obtained, typically of a few percent of the entire amplitude of the autocorrelation curve. Thus, removing A_{f0} from Eq. 4.10 would bias the calculated L-values toward higher values, and especially small values of L would be subject to significant bias. In contrast, omitting N_{f0} in Eq. 4.9 does not lead to the same bias of the calculated values of leakage, provided that unentrapped fluorescent molecules are efficiently removed from the LUVs during the preparation process.

Fourthly, when setting $A_{f0} = 0$, $k = 1$, and $B_b = 0$ kHz in Eq. 4.10, an expression completely analogous to previously derived expressions to determine the LUV-bound fractions of fluorescently-labeled proteins by FCS is obtained (162, 164). However, in the present study, this simplified expression will not be used as (i) setting $A_{f0} = 0$ will bias calculated values of L toward higher values as mentioned above, (ii) $k \neq 1$ in our experimental system, and (iii) B_b is included to calculate L as precise as possible.

Finally, as B_{tot} is a direct output parameter of any FCS experiment, N_f, N_{f0}, and N_{f100} can all be estimated from individual experiments, using Eq. 4.7, provided that B_f is determined in a control experiment. In that way, the N_f-values can be directly inserted into Eq. 4.6 to calculate leakage, L. This approach would definitely be simpler than solving the quadratic equation in Eq. 4.10. However, in our experience, due to variations in B_{tot} between individual experiments, this approach would entail large uncertainties in the determination of L. In contrast, Eq. 4.10 provides a more robust and accurate approach to calculate leakage. In particular, the brightness ratio parameter k can be determined by averaging multiple experiments. In that way, Eq. 4.10 is based on more precise estimates of the relative changes of B_{tot}-values as a function of leakage, L, than what is attainable by actually recording B_{tot} in each individual experiment.

4.4 Materials and methods

4.4.1 Materials

1-palmitoyl-2-oleoyl-*sn*-glycero-3-phosphocholine (POPC), 1-palmitoyl-2-oleoyl-*sn*-glycero-3-[phospho-rac-(1-glycerol)], sodium salt (POPG), and 1-palmitoyl-2-[11-(dipyrrometheneboron difluoride)undecanoyl]-*sn*-glycero-3-phosphocholine (TopFluor PC) were purchased from Avanti Polar Lipids (Alabaster, AL, USA). 4-(1,1,3,3-tetramethylbutyl)phenyl-polyethylene glycol (Triton X-100), N-(2-hydroxyethyl)piperazine-N'-(2-ethanesulfonic acid) (HEPES) and the corresponding sodium salt (HEPES-Na), and NaCl were purchased from Sigma-Aldrich (Brøndby, Denmark). Rhodamine 6G chloride (Rh6G), Alexa Fluor 488 hydrazide, sodium salt (Alexa488), Alexa Fluor 488 dextran, 3000 MW, anionic (Alexa488-3kMW), and Alexa Fluor 488 dextran, 10000 MW, anionic, fixable (Alexa488-10kMW) were purchased from Life Technologies (Nærum, Denmark). Mastoparan X (MPX) was purchased from GL Biochem

(Shanghai, China) and further purified by semi-preparative HPLC (Waters semi-preparative HPLC equipped with a Waters 600 pump & controller and a Waters 2489 UV/vis detector, Waters, Milford, MA, USA). The purity of the purified peptide was assessed to be $> 99\%$ by analytical HPLC (Gilson analytical HPLC equipped with a Gilson 321 HPLC pump and a Gilson 155 UV/vis detector, Gilson, Middleton, MI, USA). Furthermore, the peptide identity was confirmed by MALDI-TOF (Bruker Reflex IV MALDI-TOF spectrometer, Bruker, Billerica, MA, USA).

4.4.2 Sample preparation

LUV preparation and characterization

Lipid solutions were prepared in chloroform/methanol (9:1). The organic solvent was removed under a gentle stream of nitrogen. The samples were subsequently kept in vacuum overnight to remove the residual solvent. The lipid films were hydrated in HEPES buffer (10 mM HEPES, 100 mM NaCl, pH 7.4) with vigorous vortexing every 5 min for a period of 30 min. The hydrated lipid suspensions were then subject to 5 freeze-thaw cycles by alternately placing the sample vials in an isopropanol/dry ice bath and a warm water bath. Next, the lipid suspensions were extruded 21 times through a 100 nm polycarbonate filter (Whatman, Maidstone, UK) using a mini-extruder (Avanti Polar Lipids) to form LUVs. The size of the LUVs was checked by dynamic light scattering (ZetaPALS, Brookhaven Instruments, Holtsville, NY, USA). Phosphorous concentrations of the LUV solutions were determined using the method of Rouser et al. (144), albeit with slightly modified reagent concentrations.

To prepare LUVs labeled with TopFluor PC, POPC/POPG (3:1) with 0.1 mol% TopFluor PC was dissolved in the initial chloroform/methanol (9:1) solution. The rest of the preparation protocol was then completely identical to the above protocol for preparation of unlabeled LUVs.

To prepare LUVs entrapping fluorescent molecules, the HEPES buffer used to hydrate the POPC/POPG (3:1) lipid films was prepared with 4 or 30 μM Alexa488, 5 μM Alexa488-3kMW, or 2.5 μM Alexa488-10kMW. Concentrations of these fluorescent molecules were determined from the absorbance, recorded by a NanoDrop 2000c spectrophotometer (NanoDrop Products, Wilmington, DE, USA), assuming that (i) the extinction coefficient of Alexa488 at maximum absorption at ca. 495 nm is 71000 $cm^{-1}M^{-1}$ and (ii) that the degree of labeling of Alexa488-3kMW and Alexa488-10kMW is 1 and 2, respectively, as stated by the manufacturer. The rest of the preparation protocol was again completely identical to the above protocol for unlabeled LUVs, except that before the determination of phosphorous concentrations, LUV solutions were run on a size exclusion chromatography column (Sepharose CL-4B, GE Healthcare, VWR - Bie & Berntsen, Herlev, Denmark) to remove the unentrapped fluorescent molecules from the LUV solution.

MPX stock solutions

MPX stock solutions were prepared in HEPES buffer. To prevent loss of MPX due to adsorption to vial surfaces, MPX stock solutions were generally handled in Protein LoBind tubes

(Eppendorf, VWR - Bie & Berntsen) and at high concentrations of at least 100 μM. To calculate the concentration of MPX stock solutions, the extinction coefficient of MPX at 220 nm was calculated to be 40100 cm^{-1}M^{-1} by correlating the MPX concentration determined by an Antek 8060 chemiluminescent nitrogen detector (PAC, Houston, TX, USA) to the absorbance of the same MPX sample, determined by a NanoDrop 2000c spectrophotometer. Given this extinction coefficient, MPX concentrations of stock solutions were then always determined by recording the absorbance at 220 nm using the NanoDrop 2000c spectrophotometer.

4.4.3 FCS experiments

Experimental setup

FCS measurements were performed using a DCS-120 confocal scanning FLIM system (Becker & Hickl, Berlin, Germany) connected to a Zeiss Axio Observer Z1 inverted microscope equipped with a C-Apochromat 40x/1.2 W Corr UV-VIS-IR water immersion objective (Carl Zeiss, Jena, Germany). The excitation source for the system was a 473 nm picosecond diode laser (BDL-473-SMC, Becker & Hickl) operated at a pulse repetition rate of 50 MHz. The incident excitation power at the objective rear aperture was measured by a PM100D optical power meter (Thorlabs, Goteborg, Sweden). After passing through a 485 nm long-pass filter (HQ485LP, Becker & Hickl) and a confocal pinhole, the fluorescence emission was detected with a HPM-100-40 hybrid detector connected to a SPC-150 module (Becker & Hickl). Lifetime-gating was used to partially suppress background noise. SPCM software (Becker & Hickl) was used to calculate the experimental autocorrelation curves. The curves were subsequently exported to be fitted by MATLAB (The MathWorks, Natick, MA). All samples were measured in uncoated μ-slide 8 wells (ibidi, DFA Instruments, Glostrup, Denmark) by positioning the laser focus $\sim$ 50 μm above the top of the cover glass. The acquisition time for all experiments was 300 s. By calibration with Alexa488, the effective excitation volume was determined to be 1.0 fL (163). From the same calibration experiments, the S-parameter was determined to be 7.4 by weighted least squares fitting of the experimental autocorrelation curves to the single-component autocorrelation function given in Eq. 4.2 (165). The S-parameter was always fixed to this value when fitting all other experimental autocorrelation curves. Except for the experiments determining the S-parameter, all autocorrelation curves in this article were analyzed using unweighted least squares fitting. Autocorrelation curves dominated by single bright events were discarded in the data analysis.

Protocol to determine leakage from FCS data

Values of τ_T and T were determined in separate experiments; these values were then kept fixed when fitting the autocorrelation curves from the leakage experiments. For a given leakage experiment, a number of samples with unknown values of leakage, L, were prepared. In addition, two samples with 0% and 100% leakage, respectively, were also prepared. The vesicle diffusion time τ_Dv was obtained by fitting Eq. 4.2 to the autocorrelation curve of the sample with 0% leakage. The diffusion time of free molecules τ_Df was obtained by fitting Eq.

4.2 to the autocorrelation curve of the sample with $100\,\%$ leakage. From this fit, we also obtained a average number of molecules in the excitation volume, N_{m100}. Correcting N_{m100} for an uncorrelated background contribution yields the true average number of molecules in the excitation volume, N_{f100} (163, 166):

$$N_{\mathrm{f100}} = \frac{N_{\mathrm{m100}}\left(B_{100} - B_{\mathrm{b}}\right)^2}{B_{100}^2} \tag{4.11}$$

where B_{100} is the photon count rate of the sample with $100\,\%$ leakage. The uncorrelated background count rate B_{b} was determined by a measurement in buffer. In principle, Eq. 4.11 is only valid for molecules with negligible triplet contribution, but since we already know T and since this value of T is generally small, below 0.05, the equation is also valid to fit our autocorrelation data. Complete leakage of initially entrapped molecules from the LUVs was confirmed by comparing τ_{Df} with a control experiment on free molecules in solution. Given N_{f100}, the brightness of unentrapped molecules B_{f} was then obtained by

$$B_{\mathrm{f}} = \frac{B_{100} - B_{\mathrm{b}}}{N_{\mathrm{f100}}}. \tag{4.12}$$

Next, keeping τ_{Dv} and τ_{Df} fixed, Eq. 4.5 was fitted to all autocorrelation curves of the given leakage experiment to obtain the A_{f}-values required in Eq. 4.10. In particular, A_{f0} and A_{f100} were obtained from the samples with 0% leakage to $100\,\%$ leakage, respectively, and A_{f} was obtained from the samples with unknown leakage, L. Finally, in order to solve Eq. 4.10, the ratio between the brightness of entrapped to unentrapped molecules k was determined using the equation

$$k = \frac{B_0 - B_{\mathrm{b}}}{B_{100} - B_{\mathrm{b}}} \tag{4.13}$$

where B_0 is recorded from samples with $0\,\%$ leakage. Across all individual experiments studying leakage of a given type of fluorescent molecule at a given excitation power, the same value of k, as determined by averaging six individual experiments, was used to solve Eq. 4.10. Thus, for an excitation power of 10.9 µW, we found that $k = 0.85$ for Alexa488, $k = 0.96$ for Alexa488-3kMW, and $k = 0.95$ for Alexa488-10kMW. In addition, for an excitation power of 43.2 µW, we found that $k = 0.59$ for Alexa488. Given the parameters determined via the above protocol, Eq. 4.10 was then solved using Maple (Maplesoft, Waterloo, Ontario, Canada) to determine the unknown values of L.

Test experiments

We prepared a series of samples in which variable percentages ($0\,\%$ to $100\,\%$) of Alexa488, Alexa488-3kMW, or Alexa488-10kMW were entrapped in POPC/POPG (3:1) LUVs. These samples were prepared by mixing variable volumes of (i) a stock sample with 1 mM POPC/PO-PG (3:1) LUVs entrapping 4 µM Alexa488, 5 µM Alexa488-3kMW, or 2.5 µM Alexa488-10kMW with (ii) a stock sample with free Alexa488, Alexa488-3kMW, or Alexa488-10kMW in buffer. The molar concentrations of the stock samples with free Alexa488, Alexa488-3kMW, or Alexa488-10kMW were identical to those of samples in which $0.1\,\%$ Triton X-100 had induced complete release from 1 mM POPC/POPG (3:1) LUVs entrapping 4 µM

Alexa488, 5 μM Alexa488-3kMW, or 2.5 μM Alexa488-10kMW, respectively. The mixed samples were vigorously vortexed before being transferred to the μ-slide 8 wells for examination by FCS. Experiments were conducted with an excitation power of 10.9 μW. Percentages of unentrapped molecules were calculated using Eq. 4.10.

Experimental artifacts

To investigate the effect of the number of fluorescent molecules per LUVs, samples with variable percentages of entrapped Alexa488 were, again, prepared. However, in these samples, Alexa488 was entrapped in LUVs at a local concentration of 30 μM instead of the concentration of 4 μM used in the above test experiments. FCS experiments were then conducted with an excitation power of 10.9 μW.

To investigate the effect of the brightness ratio parameter k, we reused the samples of the test experiments in which LUVs entrapping 4 μM Alexa488 were mixed with free Alexa488. However, FCS experiments were conducted with an excitation power of 43.2 μW instead of the excitation power of 10.9 μW used in the test experiments.

To investigate interactions of Alexa488, Alexa488-3kMW, Alexa488-10kMW, and Rh6G with POPC/POPG (3:1) LUVs, we prepared samples with 40 nM of Alexa488, Alexa488-3kMW, Alexa488-10kMW or Rh6G in (i) buffer, (ii) 1 mM unlabeled POPC/POPG LUVs (3:1) or (iii) 1 mM unlabeled POPC/POPG (3:1) LUVs with 50 μM MPX. All samples were mixed in Protein LoBind tubes, and vigorously vortexed for a few seconds before transfer to the μ-slide 8 wells for examination by FCS. Experiments were conducted with an excitation power of 10.9 μW.

Interaction of MPX with LUVs

To investigate MPX-induced leakage from POPC/POPG (3:1) LUVs, variable volumes of MPX stock solutions were transferred to Protein LoBind tubes containing POPC/POPG (3:1) LUVs entrapping 4 μM Alexa488, 5 μM Alexa488-3kMW, or 2.5 μM Alexa488-10kMW. The final LUV concentrations of these samples were always 1 mM. Immediately after addition of MPX, each sample was vigorously vortexed for a few seconds and subsequently incubated at room temperature. After 1 hour incubation, the samples were transferred to the μ-slide 8 wells for examination by FCS. Experiments were conducted with an excitation power of 10.9 μW. Leakage values were calculated using Eq. 4.10.

To investigate whether MPX-induced leakage is due to membrane solubilization, MPX stock solutions were transferred to Protein LoBind tubes containing POPC/POPG (3:1) LUVs labeled with TopFluor PC. The final LUV concentrations of these samples were always 1 mM. After vigorous vortexing, the samples were incubated for 1 h before transfer to the μ-slide 8 wells for examination by FCS. The excitation power of these experiments was 2.6 μW.
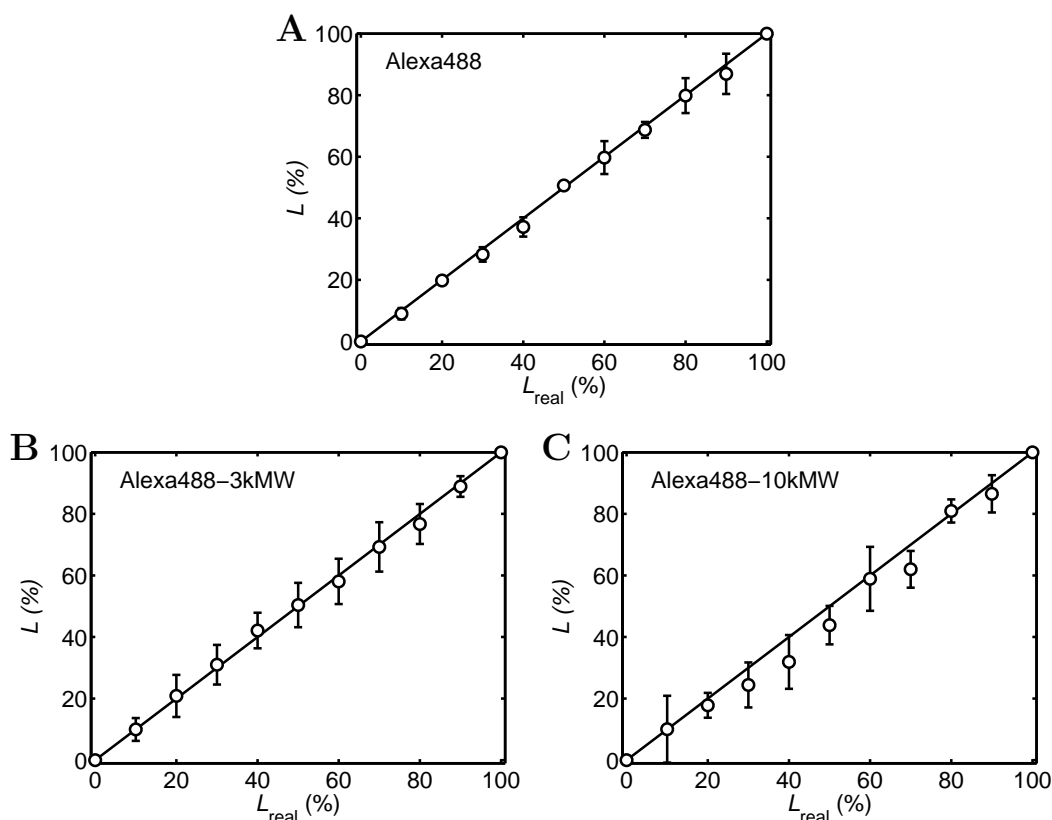
Figure 4.1: Calculated percentage of unentrapped fluorescent molecules, L, vs actual percentage of unentrapped fluorescent molecules, L_{real}, for samples with variable percentages of fluorescent molecules entrapped in POPC/POPG (3:1) LUVs. (*A*) Samples of free Alexa488 and POPC/POPG (3:1) LUVs entrapping 4 μM Alexa488. (*B*) Samples of free Alexa488-3kMW and POPC/POPG (3:1) LUVs entrapping 5 μM Alexa488-3kMW. (*C*) Samples of free Alexa488-10kMW and POPC/POPG (3:1) LUVs entrapping 2.5 μM Alexa488-10kMW. In all panels, the data are the average of three separate experiments. The error bars show the standard deviations. The L-values at $L_{\text{real}} = 0$ % and $L_{\text{real}} = 100$ % are, by definition, always set to 0 % and 100 %, respectively. The data confirms that FCS can be used to accurately quantify leakage of fluorescent molecules of different sizes from LUVs.

4.5   Results and discussion

4.5.1   Test experiments

The simple experimental situation of only one type of diffusing species is considered in Figs. 4.7 and 4.8 in the Supporting material. From these experiments, we found that the typical diffusion times are ~ 46 μs, ~ 110 μs, ~ 220 μs, and ~ 4800 μs for Alexa488, Alexa488-3kMW, Alexa488-10kMW, and POPC/POPG (3:1) LUVs, respectively, corresponding to hydrodynamic radii of ~ 0.5 nm, ~ 1.3 nm, ~ 2.6 nm, and ~ 56 nm, respectively.

Next, we prepared a series of samples in which one percentage (between 0 % to 100 %)

of Alexa488, Alexa488-3kMW, or Alexa488-10kMW were entrapped in POPC/POPG (3:1) LUVs and the remaining percentage of Alexa488, Alexa488-3kMW, or Alexa488-10kMW, respectively, was free in solution. In these samples, the local concentrations inside the LUVs were 4 μM for Alexa488, 5 μM for Alexa488-3kMW, or 2.5 μM for Alexa488-10kMW. In the samples with 100 % of the molecules being entrapped, the lipid concentrations were 1 mM. In that way, these series of samples mimicked a perfect all-or-none leakage process from 1 mM POPC/POPG (3:1) LUVs entrapping 4 μM Alexa488, 5 μM Alexa488-3kMW, or 2.5 μM Alexa488-10kMW. Fig. 4.9 in the Supporting material shows some examples of autocorrelation curves obtained from these samples. Fig. 4.1 shows the calculated percentages of unentrapped fluorescent molecules, L, as obtained by solving Eq. 4.10, vs the actual percentages of unentrapped fluorescent molecules, L_{real}. The good agreement between the calculated and actual values confirm that FCS is indeed applicable to accurately calculate the percentage of unentrapped fluorescent molecules and thereby also applicable for quantitative studies on leakage from LUVs.

4.5.2 Experimental pitfalls

In order for FCS to correctly quantify leakage from LUVs, a number of experimental pitfalls should be avoided. In the following sections, we highlight three of the most prominent examples of such pitfalls.

Number of fluorescent molecules per LUV, $\tilde{B}$

In a multicomponent autocorrelation function, written in a generalized form in Eq. 4.3, the amplitude of the ith component, A_i, scales with the square of the brightness of that component B_i^2. Consequently, molecules with very high brightness will dominate such multicomponent autocorrelation functions. In cases where fluorophore concentrations inside the LUVs are high, this effect might significantly compromise the capability of FCS to quantify leakage from LUVs (158). In order to understand this effect in detail, we prepared two series of samples in which variable percentages of Alexa488 were entrapped inside POPC/POPG (3:1) LUVs at local concentrations of 4 μM or 30 μM, respectively. Autocorrelation curves recorded from these samples were fitted using Eq. 4.5 with fixed values of τ_{Df} and τ_{Dv}. Fig. 4.2 shows fractional amplitudes of unentrapped Alexa488, $f_{\text{f}} = A_{\text{f}}/(A_{\text{f}} + A_{\text{v}})$, as determined from the data fitting vs the percentage of unentrapped Alexa488, L. From Fig. 4.2, it is clear that the fractional amplitude, f_{f}, is generally less sensitive to changes in L in the case of 30 μM Alexa488 inside the vesicles than in the case of 4 μM Alexa488 inside the vesicles, especially at low values of L; thus, when using LUVs entrapping 30 μM Alexa488 inside the LUVs, it will be more difficult to distinguish low values of leakage, L, than when using LUVs entrapping 4 μM Alexa488.

To further elucidate the impact of the number of molecules per LUV on the capability of FCS to calculate leakage, we also included four theoretical curves in Fig. 4.2. These curves were calculated using the equation
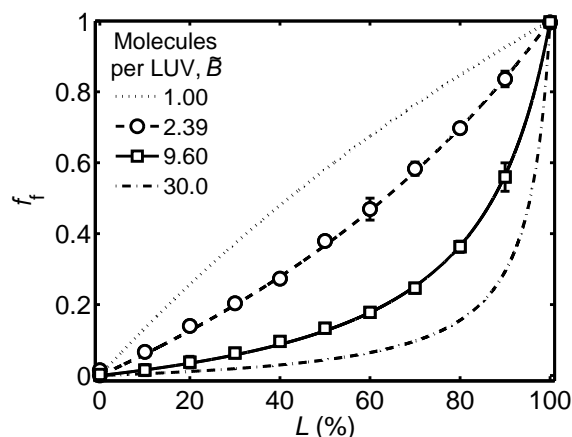
Figure 4.2: Fractional amplitude of unentrapped fluorescent molecules in the autocorrelation function, $f_f = A_f/(A_f + A_v)$, vs the percentage of unentrapped molecules, L, for different numbers of fluorescent molecules per LUV, $\tilde{B}$. Data points are recorded from samples in which variable percentages of Alexa488 molecules are entrapped in POPC/POPG (3:1) LUVs at local concentrations of $4\ \mu M$ or $30\ \mu M$, corresponding 2.39 or 9.60 Alexa488 molecules per apparent LUV, respectively. The data are the average of three separate experiments. The error bars show the standard deviations. The error bars are not shown if they are smaller than the symbols. Lines are theoretically calculated using Eq. 4.14 by assuming that the apparent number of fluorescent molecules per LUV is 1, 2.39, 9.60 and 30, respectively. The results demonstrate that in order to calculate leakage from LUVs, the concentration fluorescent molecules inside the LUVs should be kept as low as possible.

$$f_f = \frac{A_f}{A_f + A_v} = \frac{L}{L + k^2 \tilde{B}\,(1 - L)} \tag{4.14}$$

where $\tilde{B} = N_{f100}/N_{v0}$ is the apparent number of fluorescent molecules per LUV and N_{v0} is the apparent number of LUVs recorded in a sample with $0\ \%$ leakage. The derivation of Eq. 4.14 is given in the Supporting material. To calculate the four theoretical curves, we assumed that $k = 0.85$ and $\tilde{B} = 1;\ 2.39;\ 9.60;\ \text{or}\ 30$, respectively. The value of $k = 0.85$ was used because it corresponds to the experimental value of k. Likewise, the values of $\tilde{B} = 2.39$ and $\tilde{B} = 9.60$ were used because they correspond to the apparent values of $\tilde{B}$ for POPC/POPG (3:1) LUVs containing $4\ \mu M$ or $30\ \mu M$ Alexa488, respectively. Accordingly, the theoretical curves for $\tilde{B} = 2.39$ and $\tilde{B} = 9.60$ should agree with the experimental data points. Indeed, Fig. 4.2 demonstrate a very good agreement between the experimental results and the theoretical curves, confirming the validity of Eq. 4.14.

Thus, the theoretical curves supplement the experimental data, and thereby they can be used to further emphasize the problematic consequences of encapsulating high numbers of fluorescent molecules per LUV. More specifically, for the theoretical curve calculated using $\tilde{B} = 30$, we find that $f_f < 0.02$ for $L < 30\ \%$. This mean that the value of f_f for $L < 30\ \%$ is essentially indistinguishable from the artificial non-zero value of f_f that is usually obtained from samples only containing LUVs and no free fluorophores. Thus, in a system where

$\tilde{B} = 30$, it would be impossible to use FCS to study leakage when $L < 30$ %. Along these lines, it can then be concluded that the concentration of fluorescent molecules inside the LUVs should, in principle, be kept as low as possible to obtain maximal sensitivity of A_f to leakage. On the other hand, a lower limit to the number of fluorescent molecules per LUV is dictated by the fact that a certain experimental photon count rate significantly above the background level is also required. Accordingly, optimal experimental designs to accurately calculate leakage by FCS should balance the requirement for low numbers of fluorescent molecules per LUV and high photon count rates.

Brightness ratio between entrapped and unentrapped molecules, k

In order for the number of fluorescent molecules per LUV to be kept low, a high photon count rate per molecule is required. One way to increase the photon count rate per molecule is to increase the intensity of the excitation source. However, as shown in Fig. 4.3 in the Supporting material, increasing the excitation intensity might significantly affect the ratio between the brightness of entrapped and unentrapped fluorescent molecules k. To understand the effect of k, we considered a number of samples with variable percentages of Alexa488 entrapped in POPC/POPG (3:1) LUVs. The local concentration of Alexa488 inside the LUVs was 4 μM. Two different laser intensities, corresponding to $k = 0.59$ and $k = 0.85$, respectively, were employed to conduct FCS on the samples. Autocorrelation curves were fitted using Eq. 4.5 with fixed values of τ_Df and τ_Dv. Fig. 4.3 shows A_f vs the percentage of unentrapped molecules, L. For both laser intensities, we observed that A_f is a monotonic function of L, albeit for $k = 0.59$, we observe that A_f levels off at high values of L, indicating that for this value of k, it might be difficult to precisely calculate leakage at high values of leakage.

To gain further insight into the effect of k, we also plotted four theoretical curves for $k = 0.40$; 0.59; 0.85; or 1.00, respectively, using the equation

$$A_\text{f} = \frac{B_\text{f}^2 N_\text{f100} L}{\left(L N_\text{f100} B_\text{f} + (1 - L) N_\text{f100} k B_\text{f} + B_\text{b}\right)^2}. \tag{4.15}$$

This equation is derived by inserting Eq. 4.9 into Eq. 4.7 and assuming that $N_\text{f} = N_\text{f100} L$. The theoretical curves for $k = 0.40$ and $k = 0.59$ are based on the B_f, B_b and N_f100-values from the experiments in which $k = 0.59$, whereas the theoretical curves for $k = 0.85$ and $k = 1.00$ are based on the B_f, B_b and N_f100-values from the experiments in which $k = 0.85$. Fig. 4.3 shows that a very good agreement between the experimental results and theoretical curves is achieved, confirming the validity of Eq. 4.15. Thus, we can use the theoretical curves to further understand the effect of k. In particular, we observe that A_f will become a completely linear function of L when $k = 1$. However, for $k = 0.40$, we observe that A_f will display a single maximum at $L \approx 68$ %. That is, A_f will not be a monotonic function of L for low values of k, and it will, therefore, be impossible to use Eq. 4.10 to calculate leakage in this case. Thus, from both the experimental data and the theoretical curves, we can conclude that the value of k should be kept close to 1 in order for Eq. 4.10 to be used to calculate leakage. Please note that as k is dependent on the excitation intensity, it is not sufficient to determine k from experiments with a conventional fluorometer.
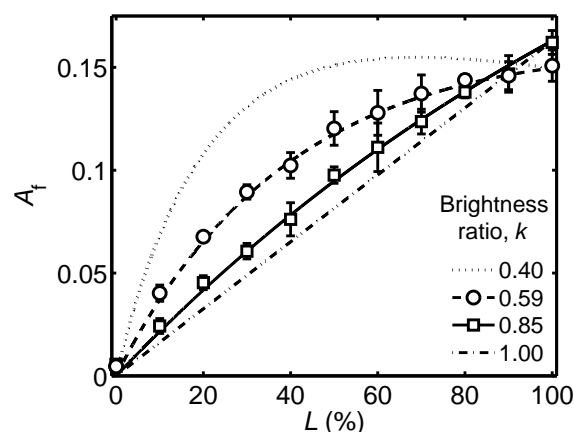
Figure 4.3: The amplitude of the unentrapped molecules, A_f, vs the percentage of unentrapped molecules, L, for different brightness ratios between entrapped and unentrapped fluorescent molecules, k. Data points were recorded from samples in which variable percentages of Alexa488 molecules were entrapped in POPC/POPG (3:1) LUVs at a local concentration of 4 µM. To record the data points, two different excitation powers were employed, corresponding to $k = 0.59$ and $k = 0.85$, respectively. The data are the average of three separate experiments. The error bars show the standard deviations. The error bars are not shown if they are smaller than the symbols. Theoretical curves were calculated using Eq. 4.15 and assuming that $k = 0.40$; 0.59; 0.85; or 1.00. Both the experimental data and the theoretical lines demonstrate that k should be kept close to 1 in order for Eq. 4.10 to be applicable for calculating leakage.

Interaction of fluorescent molecules with LUVs

Another important part of the experimental design is the choice of fluorescent molecules to be entrapped inside the LUVs. In the present article, we used the hydrophilic anionic dye Alexa488, unconjugated or conjugated to dextran molecules, However, another popular choice of dye for leakage studies by FCS is the cationic dye Rh6G. To investigate the suitability of each of these dyes for leakage experiments by FCS, we prepared a series of samples in which 40 nM Alexa488, Alexa488-3kMW, Alexa488-10kMW, or Rh6G was mixed with (i) buffer, (ii) 1 mM unlabeled POPC/POPG (3:1) LUV, or (iii) 1 mM POPC/POPG (3:1) LUV and 50 µM MPX. Fig. 4.4 shows the fractional amplitude of the unbound molecules, $f_f = A_f/(A_f + A_v)$, for each of these samples as obtained by fitting the data with Eq. 4.5 with τ_{Df} fixed at diffusion times recorded in buffer and τ_{Dv} fixed at 4800 µs, a typical diffusion time for LUVs. For Alexa488, Alexa488-3kMW, and Alexa488-10kMW, f_f was always found to be close to 1, indicating that none of these fluorescent molecules bound to the POPC/POPG (3:1) LUVs. In contrast, when Rh6G was mixed with 1 mM POPC/POPG (3:1) LUV, then $f_f \approx 0.14$, indicating that a large fraction of the cationic Rh6G molecules bound to the anionic LUV surfaces. Interestingly, if MPX was present together with the LUVs, then f_f increased to ~ 0.48. Thus, binding of MPX to the LUVs will entail unbinding of Rh6G, probably due to charge neutralization of the lipid membrane. Such peptide-induced unbinding of Rh6G from the LUVs might easily be mistaken for peptide-induced leakage from
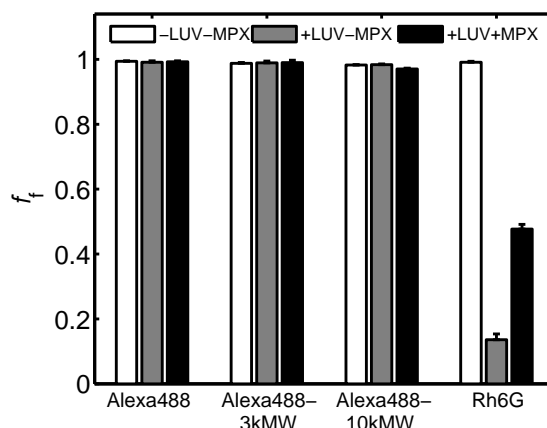
Figure 4.4: Fractional amplitude of the free molecules, $f_f = A_f/(A_f + A_v)$, for samples with 40 nM Alexa488, Alexa488-3kMW, Alexa488-10kMW, or Rh6G in (i) buffer, (ii) 1 mM unlabeled POPC/POPG (3:1) LUV, or (iii) 1 mM POPC/POPG (3:1) LUV and 50 µM MPX. The data are the average of three separate experiments. Error bars show the standard deviations. The data shows that Alexa488, Alexa488-3kMW, and Alexa488-10kMW do not interact with the LUVs. In contrast, Rh6G clearly interacts with the LUVs. Upon addition of MPX, a significant fraction of the membrane-bound Rh6G molecules dissociates from the membrane. This peptide-induced unbinding might easily be confused with peptide-induced leakage from LUVs.

the LUVs. Therefore, great caution should be taken when using Rh6G as the fluorescent marker in leakage experiments.

4.5.3   Leakage induced by MPX

In order to demonstrate the potential of our FCS-based protocol to study antimicrobial peptide-induced leakage, we considered the peptide MPX. Fig. 4.5 shows MPX-induced leakage, L, vs the peptide-to-lipid ratio, [P]/[L] ratio as determined by FCS after 1 h incubation of variable concentrations of MPX with 1 mM POPC/POPG (3:1) LUVs entrapping 4 µM Alexa488, 5 µM Alexa488-3kMW, or 2.5 µM Alexa488-10kMW. It is clear that MPX-induced leakage from POPC/POPG (3:1) LUVs is dependent on the size of the entrapped fluorescent molecules; for example, Alexa488 (570 Da) was completely released at [P]/[L] = 0.025, whereas only ~ 55 % and ~ 24 % of Alexa488-3kMW and Alexa488-10kMW, respectively, were released at the same [P]/[L] ratio. However, at higher [P]/[L] ratios, Alexa488-3kMW and Alexa488-10kMW were also completely released. Such size-dependent leakage have also previously been reported for MPX (51). Fig. 4.11 in the Supporting material shows leakage at selected [P]/[L] ratios recorded after 10 min, 20 min, 1 h, and ~ 18 h incubation of MPX with LUVs. These data confirm that leakage of all three fluorescent markers is a transient process, in which a rapid burst of leakage within the first few minutes is followed by a dramatic slowing down or complete cessation of marker efflux. Such biphasic leakage kinetics have also previously been reported for MPX (128, 130) as well as for many other antimicrobial peptides (45). In that way, the leakage values recorded from samples
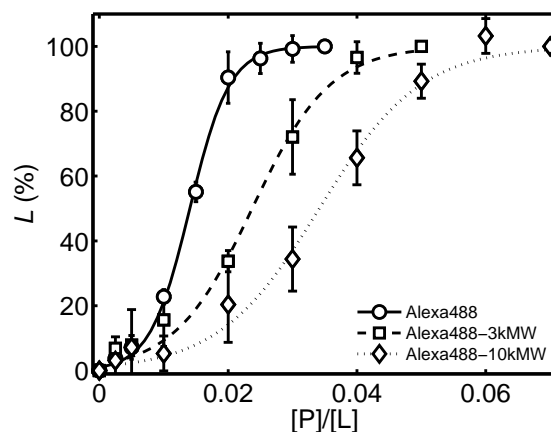
Figure 4.5: MPX-induced leakage, L, vs [P]/[L] ratio. Leakage was calculated after 1 h incubation of MPX together with 1 mM POPC/POPG (3:1) LUVs entrapping 4 µM Alexa488, 5 µM Alexa488-3kMW, or 2.5 µM Alexa488-10kMW. The data are the average of three separate experiments. The error bars show the standard deviations. The leakage values at the lowest and highest peptide-to-lipid ratios correspond to no leakage and complete leakage, respectively, and, therefore, they are, by definition, always set to 0 % and 100 %, respectively. Trendlines are added to guide the line. Smaller fluorescent probes were more effectively released than larger fluorescent probes.

incubated for 1 h are, by and large, representative of the leakage occurring within the first few minutes after addition of peptide to the LUVs.

To investigate whether MPX-induced leakage is due to the formation of transmembrane pores, we incubated MPX together with 1 mM of POPC/POPG (3:1) LUVs labeled with 0.1 % TopFluor PC. Experimental autocorrelation data was fitted with the single-component autocorrelation function (Eq. 4.2) to obtain the apparent mean number of LUVs in the excitation volume, N_{app}, and the LUV diffusion time, τ_{D}. Fig. 4.6 shows the obtained values of N_{app} and τ_{D} vs the [P]/[L] ratio. From the figure, it is clear that both N_{app} and τ_{D} are largely unaffected by MPX. This observation strongly implies that the LUVs remain intact and therefore release of entrapped markers is due to the formation of transmembrane pores and not due to membrane solubilization. This is in accordance with previously published data that shows that MPX only solubilizes POPC/POPG (3:1) LUVs at higher [P]/[L] ratios than what we consider in this article (44).

In the Theory section, we pointed out that Eq. 4.10 is fully applicable to study leakage of fluorescently-labeled dextrans as long as the probability of a given dextran molecule being released is not dependent on the number of fluorescent labels bound to that dextran molecule. A control experiment, based on equilibrium dialysis, is presented in Fig. 4.12 in the Supporting material to demonstrate that this is a reasonable assumption for Alexa488-labeled dextrans. From the release profiles of the Alexa488 and the Alexa488-labeled dextrans in Fig, 4.5, we can then get an estimate of the pore size. Thus, at low [P]/[L] ratios, Alexa488, with a hydrodynamic radius of ~ 0.5 nm, was more effectively released than were Alexa488-3kMW, with a hydrodynamic radius of ~ 1.3 nm, and Alexa488-10kMW, with a hydrodynamic radius
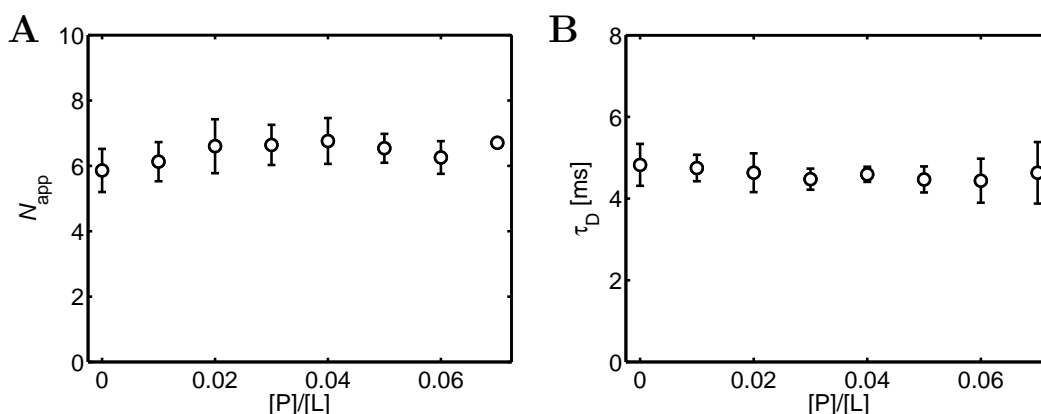
Figure 4.6: Interaction of MPX with TopFluor PC-labeled LUVs.(*A*) The apparent mean number of LUVs in the excitation volume, N_{app}, vs [P]/[L] ratio. (*B*) the LUV diffusion time, τ_{D}, vs the [P]/[L] ratio. Data was recorded after 1 h incubation of MPX with 1 mM LUVs. The data are the average of three separate experiments. The error bars show the standard deviations. Error bars are not shown when they are smaller than the symbols. The fact that N_{app} and τ_{D} are largely independent on the [P]/[L] ratio indicate that leakage is due to the formation of transmembrane pores and not due to membrane solubilization.

of ~ 2.6 nm. This observation suggests that the typical pore radius at low [P]/[L] ratios is between ~ 0.5 nm and ~ 2.6 nm. At higher [P]/[L] ratios, the Alexa488-labeled dextrans were completely released, suggesting that the pore radius at higher [P]/[L] ratio increases to above ~ 2.6 nm. However, please note that the pore radii estimated from the hydrodynamic radii of the dextran molecules should be regarded with caution. Thus, the dextran molecules are not perfect spheres with a well-defined radius. Rather, dextran molecules are modeled as prolate ellipsoids with a short axis and a long axis, complicating attempts to relate their hydrodynamic radius to pore sizes (167). In addition, it has been suggested that the dextran molecules might pass through the peptide-induced pores by reptation, further complicating the interpretation of dextran leakage data (151). Therefore, other types of fluorescently-labeled macromolecules might represent more appropriate choices for accurately estimating the size of transmembrane pores. Nevertheless, in this article, we chose to use dextrans as that is also the common choice in most other articles in the literature.

Under all circumstances, it is clear that FCS can be used to rapidly determine peptide-induced leakage of probes of different sizes. Therefore, FCS can be used as a medium-throughput technique to answer questions that, as of today, are unanswered about antimicrobial peptides. For example, FCS can be used to compare the pore size for different peptides, providing information about the dependence of the pore size on the amino acid residue sequence. Another interesting question that FCS could address pertains to the dependence of the pore size on the lipid composition. For instance, for the bee venom peptide melittin, size-dependent leakage was observed from POPC LUVs, whereas size-independent leakage was observed from POPG LUVs (151, 168). This observation strongly implies that the size of the pores formed by melittin is dependent on the lipid composition. FCS could

be used as a method to expand on these observations by probing pore size of melittin, and other antimicrobial peptides, in many different lipid compositions.

Another interesting attribute of FCS is, as demonstrated by the results in Fig. 4.6, that it reveals whether leakage is due to the formation of transmembrane pores or due to detergent-like solubilization of the lipid membrane. This information could, for example, be used to understand whether the above-mentioned size-independent leakage, as observed for melittin in POPG LUVs, is indeed due the formation of large transmembrane pores or, in reality, just due to peptide-induced solubilization of the LUVs.

Yet another advantageous feature of FCS is that it only requires very low concentrations of fluorescent molecules inside the LUVs. More specifically, in a typical FCS leakage experiment, only a few fluorescent molecules are encapsulated in each vesicle. Consequently, when studying leakage by FCS, investigators are free to systematically vary the osmolarity and ionic strengths of the buffers inside and outside the vesicles. In contrast, the experimental designs in the conventional quenching-based leakage experiments are restricted by the fact that fluorophore concentrations inside the LUVs have to be in the millimolar range to obtain self-quenching (52, 150).

Finally, an important advantage of FCS is that calculation of leakage is independent on the leakage mode of the fluorescent molecules. More specifically, as there are no contributions from A_v in Eq. 4.10, calculation of leakage by FCS is independent on whether leakage proceeds by a graded process, in which all vesicles release part of their contents, or an all-or-none process, in which part of the vesicles release all of their contents and part of the vesicles release no contents. This is a great advantage of FCS as compared to the conventional quenching-based leakage assays, in which the self-quenching factor of entrapped fluorescent molecules is highly dependent on the nature of the leakage process (52, 150).

4.6 Concluding remarks

In this work, we considered FCS as a technique to study antimicrobial peptide-induced leakage from large unilamellar vesicles (LUVs). To this endeavor, we derived the necessary theoretical framework, and we highlighted the experimental pitfalls that might lead to inaccurate and/or false conclusions. To avoid these pitfalls, we showed that (i) the number of fluorescent molecules per LUV should be low, (ii) the brightness ratio between entrapped and unentrapped molecules should be close to 1, and (iii) control experiments should ensure that the fluorescent probe does not interact with the LUVs. FCS was then used to investigate leakage induced by the antimicrobial peptide mastoparan X (MPX). From the leakage data of MPX, we concluded that FCS displays a number of advantages when compared to other existing methods to study leakage: (i) FCS provides a fast method for sizing of transmembrane pores, whereas this is often more laborious with other existing methods; (ii) FCS requires a much lower concentration of entrapped fluorescent molecules per LUV than does other existing methods, allowing investigators to more freely vary the experimental conditions; (iii) FCS reveals whether leakage is due to the formation of transmembrane pores or membrane solubilization; and (iv) calculation of leakage by FCS is independent on whether the leakage process is an all-or-none process or a graded process, whereas calculation of leakage by the

conventional quenching-based methods requires that the leakage process is taken explicitly into account.

4.7 Supporting material

4.7.1 Additional theory

Interpretation of apparent B and N-values

Consider a solution with multiple diffusing species. If this solution contains a subset of particles (index r) with variable values of B but constant values of τ_{T}, T, and τ_{D}, then the multicomponent autocorrelation function in Eq. 4.3 can be written as

$$G(\tau) = \frac{\sum\limits_{j=1}^{m} B_{\mathrm{r}j}^2 N_{\mathrm{r}j} g_{\mathrm{r}}(\tau) + \sum\limits_{i=1}^{n} B_i^2 N_i g_i(\tau)}{\left(\left(\sum\limits_{j=1}^{m} B_{\mathrm{r}j} N_{\mathrm{r}j}\right) + \left(\sum\limits_{i=1}^{n} B_i N_i\right)\right)^2} \tag{4.16}$$

where $N_{\mathrm{r}j}$ is the average number of particles within the subset with brightness $B_{\mathrm{r}j}$. The total number of particles within the subset, N_{r}, is related to $N_{\mathrm{r}j}$ by

$$N_{\mathrm{r}j} = p_j N_{\mathrm{r}} \tag{4.17}$$

where p_j is the probability for a given particle within the subset to have brightness $B_{\mathrm{r}j}$. By definition:

$$\sum_{i=j}^{m} p_j = 1. \tag{4.18}$$

Using Eqs. 4.17 and 4.18, then Eq. 4.16 can be rewritten to

$$\begin{aligned} G(\tau) &= \frac{N_{\mathrm{r}} \sum\limits_{j=1}^{m} p_j B_{\mathrm{r}j}^2 g_{\mathrm{r}}(\tau) + \sum\limits_{i=1}^{n} B_i^2 N_i g_i(\tau)}{\left(\left(N_{\mathrm{r}} \sum\limits_{j=1}^{m} p_j B_{\mathrm{r}j}\right) + \left(\sum\limits_{i=1}^{n} B_i N_i\right)\right)^2} \\ &= \frac{\left\langle B_{\mathrm{r}}^2 \right\rangle N_{\mathrm{r}} g_{\mathrm{r}}(\tau) + \sum\limits_{i=1}^{n} B_i^2 N_i g_i(\tau)}{\left(\left\langle B_{\mathrm{r}} \right\rangle N_{\mathrm{r}} + \sum\limits_{i=1}^{n} B_i N_i\right)^2} \end{aligned} \tag{4.19}$$

where $\left\langle B_{\mathrm{r}} \right\rangle$ is the mean brightness of the particles within the subset and $\left\langle B_{\mathrm{r}}^2 \right\rangle$ is the mean square brightness of the particles within the subset. If we want to represent the particles

within the subset by apparent B and N-values, then we would write Eq. 4.16 on the form

$$G(\tau) = \frac{B_{\mathrm{ra}}^2 N_{\mathrm{ra}} g_{\mathrm{r}}(\tau) + \sum\limits_{i=1}^{n} B_i^2 N_i g_i(\tau)}{\left(B_{\mathrm{ra}} N_{\mathrm{ra}} + \left(\sum\limits_{i=1}^{n} B_i N_i\right)\right)^2} \tag{4.20}$$

where B_{ra} is the apparent brightness value for the particles within the subset and N_{ra} is the apparent average number of particles in the excitation volume within the subset. By comparing Eqs. 4.19 and 4.20, it follows that

$$N_{\mathrm{ra}} = \frac{\langle B_{\mathrm{r}} \rangle^2}{\langle B_{\mathrm{r}}^2 \rangle} N_{\mathrm{r}} \tag{4.21}$$

and that

$$B_{\mathrm{ra}} = \frac{\langle B_{\mathrm{r}}^2 \rangle}{\langle B_{\mathrm{r}} \rangle}. \tag{4.22}$$

Thus, the apparent particle number, N_{ra}, is linearly proportional to the real particle number, N_{r}, and B_{ra} is a constant number that depends on the brightness distribution of the particles within the subset.

Derivation of Eq. 4.14

To derive Eq. 4.14 from the main document, we use that

$$A_{\mathrm{f}} = \frac{B_{\mathrm{f}}^2 N_{\mathrm{f}}}{B_{\mathrm{tot}}^2} \tag{4.23}$$

and

$$A_{\mathrm{v}} = \frac{B_{\mathrm{v}}^2 N_{\mathrm{v}}}{B_{\mathrm{tot}}^2}. \tag{4.24}$$

Then we get that the fractional amplitude, f_{f}, is given by

$$f_{\mathrm{f}} = \frac{A_{\mathrm{f}}}{A_{\mathrm{f}} + A_{\mathrm{v}}} = \frac{B_{\mathrm{f}}^2 N_{\mathrm{f}}}{B_{\mathrm{f}}^2 N_{\mathrm{f}} + B_{\mathrm{v}}^2 N_{\mathrm{v}}}. \tag{4.25}$$

Assuming that $N_{\mathrm{f}0} = 0$, then the apparent number of molecules per LUV, $\tilde{B}$, is be given by

$$\tilde{B} = \frac{N_{\mathrm{f}100}}{N_{\mathrm{v}0}} = \frac{B_{\mathrm{v}}}{k B_{\mathrm{f}}}, \tag{4.26}$$

and the values of N_{f} and N_{v} are given by

$$N_{\mathrm{f}} = L N_{\mathrm{f}100} \tag{4.27}$$

$$N_{\mathrm{v}} = (1 - L) N_{\mathrm{v}0}. \tag{4.28}$$

Note that Eq. 4.28 is only valid for a situation of perfect all-or-none leakage, which fortunately is exactly the type of process that we mimick in our experiments. Finally, by inserting Eqs. 4.26, 4.27, and 4.28 into Eq. 4.25 we retrieve Eq. 4.14 from the article:

$$f_{\mathrm{f}} = \frac{A_{\mathrm{f}}}{A_{\mathrm{f}} + A_{\mathrm{v}}} = \frac{L}{L + k^2 \tilde{B} (1 - L)}. \tag{4.29}$$

4.7.2   Concentration standard curves

Method

A number of samples with varying concentrations of Alexa488, Alexa488-3kMW, or Alexa488-10kMW in HEPES buffer solution were prepared. The samples were transferred to the μ-slide 8 wells for examination by FCS. Experiments were conducted with an excitation power of 10.9 μW, expect for samples with concentrations above ∼100 nM, in which the excitation power had to be reduced to avoid overloading the detector. Recorded autocorrelation curves were fitted using Eq. 4.2. Additionally, we also prepared a number of samples with varying concentrations of POPC/POPG (3:1) LUVs either labeled with 0.1 % TopFluor PC or loaded with 4 μM Alexa488, 5 μM Alexa488-3kMW, or 2.5 μM Alexa488-10kMW. These samples were also transferred to the μ-slide 8 wells for examination by FCS. Again, experiments were conducted with an excitation power of 10.9 μW, expect for the experiments on the TopFluor PC-labeled LUVs, which were excited with 2.6 μW. Recorded autocorrelation curves were again fitted using Eq. 4.2.

Results

Fig. 4.7, *A*, *C*, and *E*, shows the mean number of Alexa488, Alexa488-3kMW, or Alexa488-10kMW molecules in the excitation volume, N, vs the molar molecule concentration, C. In the case of Alexa488-3kMW and Alexa488-10kMW, the mean number of molecules in the excitation volume is an apparent number, N_{app}, due to the variable brightness of the dextran molecules. Both uncorrected and background-corrected mean molecules numbers are shown in Fig. 4.7. The background-corrected mean molecule numbers, N_{cor}, are calculated using the equation

$$N_{\mathrm{cor}} = \frac{(B_{\mathrm{exp}} - B_{\mathrm{b}})^2}{B_{\mathrm{exp}}^2} N_{\mathrm{meas}} \tag{4.30}$$

where N_{meas} is the measured (uncorrected) mean molecule number, B_{exp} is the measured photon count rate, and B_{b} is the uncorrelated background photon count rate as measured in pure buffer. (Note that Eq. 4.30 is same formula as Eq. 4.11, just with different symbols.) After correcting for the uncorrelated background, we achieve a linear relationship between N or N_{app} vs C as is also theoretically expected. From the slope of the line in Fig. 4.7 *A*, we calculated the effective excitation volume to be 1.0 fL using the relation $V_{\mathrm{eff}} = N_{\mathrm{f}}/(N_{\mathrm{A}} C_{\mathrm{f}})$. Fig. 4.7, *B*, *D*, and *F*, shows the diffusion time of the fluorescent molecules as a function of molar concentration. The diffusion times are essentially constant throughout the entire concentration range, indicating the absence of intermolecular interactions. Typical diffusion times were ~ 46 μs, ~ 110 μs, ~ 220 μs for Alexa488, Alexa488-3kMW, and Alexa488-10kMW, respectively, corresponding to hydrodynamic radii of ~ 0.5 nm, ~ 1.3 nm, and ~ 2.6 nm.

   Fig. 4.8, *A*, *C*, *E*, and *G*, shows apparent average number of LUVs in the excitation volume, N_{app}, as a function of the molar lipid concentrations of POPC/POPG (3:1) LUVs labeled with 0.1 % TopFluor PC, or loaded 4 μM Alexa488, 5 μM Alexa488-3kMW, or 2.5 μM Alexa488-10kMW. Both uncorrected and background-corrected LUV numbers are included
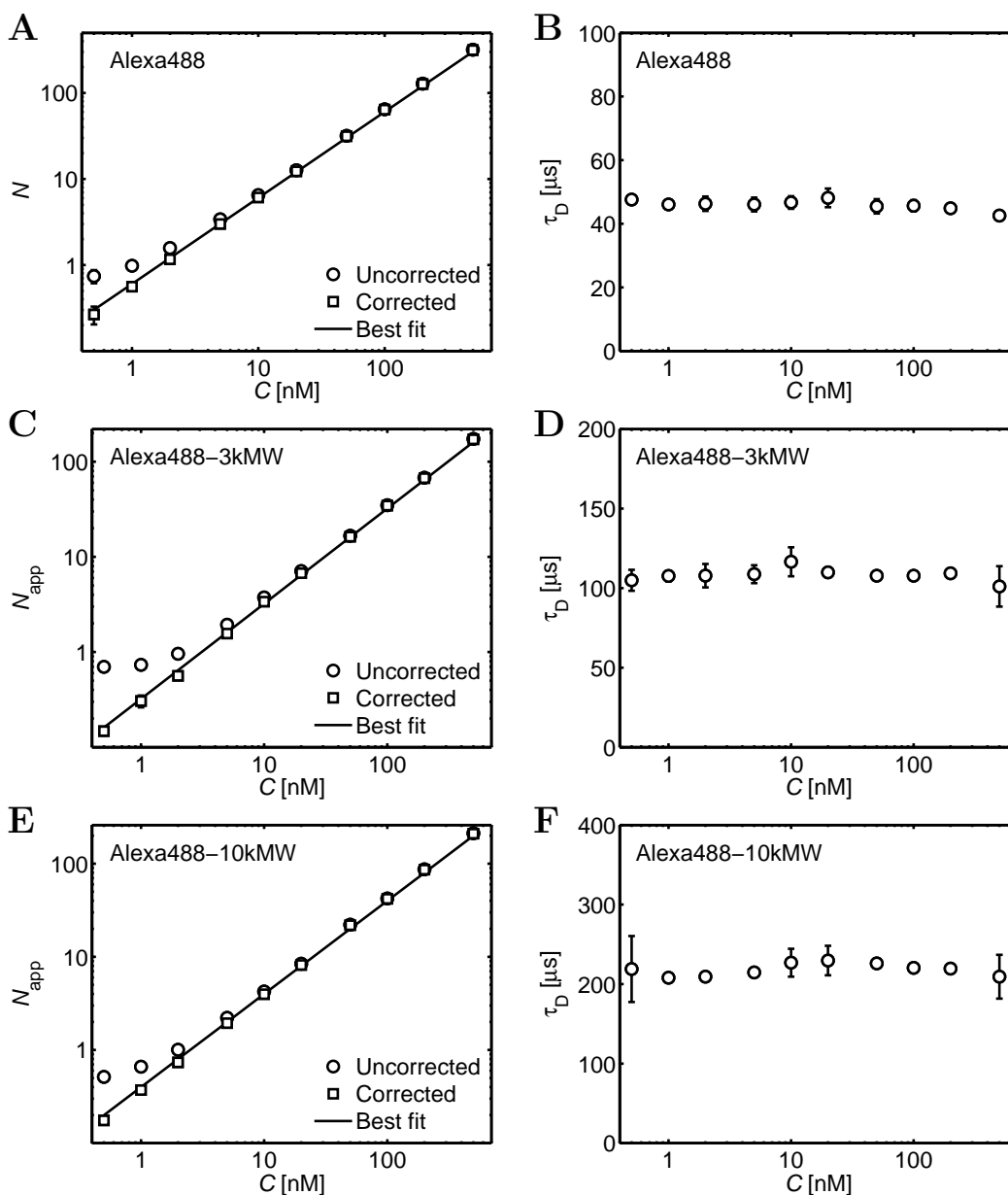
Figure 4.7: Free fluorescent molecules in HEPES buffer solution. (*A*, *C*, and *E*) The mean number of fluorescent molecules in the excitation volume, N, as a function of molar concentration, C, for Alexa 488 (*A*), Alexa488-3kMW (*C*), or Alexa488-10kMW (*E*). As Alexa488-3kMW and Alexa488-10kMW are a type of fluorescent molecules with variable brightness, their mean molecule numbers are only apparent. Both uncorrected and background-corrected mean molecules numbers are included in the plots. The straight lines are the best fits to the background-corrected data. (*B*, *D*, and *F*) Diffusion time, τ_{D}, of the fluorescent molecules as a function molar concentration, C, for the same experiments. In all panels, the data are the average of three separate experiments. Error bars show the standard deviations. The error bars are not shown when they are smaller than the symbols.
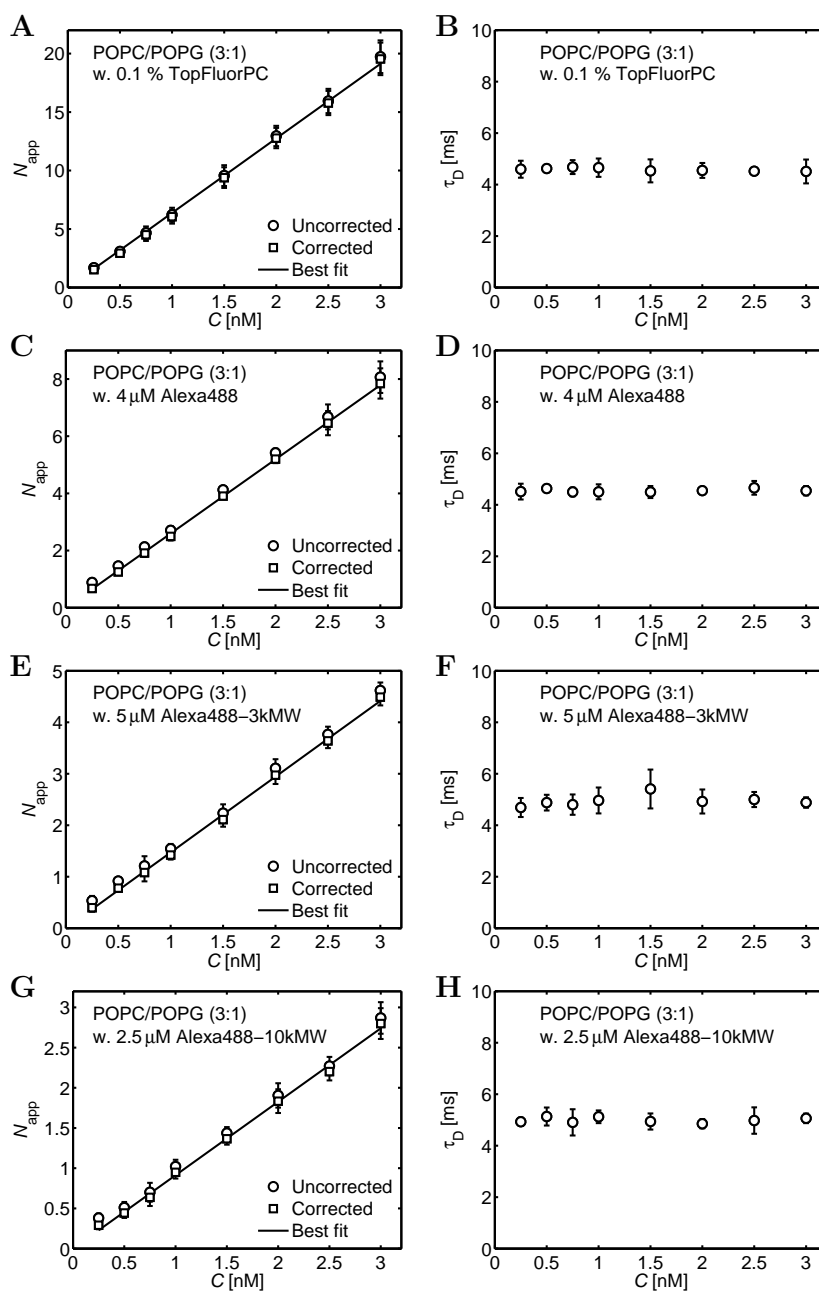
Figure 4.8: POPC/POPG (3:1) LUVs dispersed in HEPES buffer. (*A, C, E, G*) Apparent mean number of POPC/POPG (3:1) LUVs, N_{app}, as a function of lipid molar concentration, C, for LUVs labeled with 0.1 % TopFluor PC (*A*), or entrapping 4 μM Alexa488 (*C*), 5 μM Alexa488-3kMW (*E*), or 2.5 μM Alexa488-10kMW (*G*). Both uncorrected and background-corrected LUV numbers are shown. The straight lines are the best fits to the background-corrected data. (*B, D, F, H*) LUV diffusion time, τ_{D}, as a function of lipid molar concentration, C, for the same experiments. In all panels, the data are the average of three separate experiments. Error bars show the standard deviations. The error bars are not shown when they are smaller than the symbols.

in the figure. For the background-corrected numbers, a linear relationship between N_{app} and C is achieved. Diffusion times of the LUVs as a function of lipid molar concentrations are shown in Fig. 4.8, *B*, *D*, *F*, and *H*. Across the entire concentration range, no changes in diffusion times were observed, indicating that the vesicles were not interacting with each other. Typical diffusion times of LUVs were found to be ~ 4800 µs, corresponding to a hydrodynamic radius of ~ 56 nm, albeit small variations between individual batches were observed.

4.7.3   Autocorrelation curves for varying fractions of entrapped molecules

Method

In the article, we described how we prepared a number of samples with variable percentages of Alexa488, Alexa488-3kMW, or Alexa488-10kMW entrapped in POPC/POPG (3:1) LUVs by mixing (i) a stock sample with 1 mM POPC/POPG (3:1) LUVs entrapping 4 µM Alexa488, 5 µM Alexa488-3kMW or 2.5 µM Alexa488-10kMW with (ii) a stock sample with free Alexa488, Alexa488-3kMW, or Alexa488-10kMW in buffer, respectively, with molar concentrations identical to those of samples in which 0.1 % Triton X-100 had induced complete release from 1 mM POPC/POPG (3:1) LUVs entrapping 4 µM Alexa488, 5 µM Alexa488-3kMW or 2.5 µM Alexa488-10kMW, respectively.

Results

Representative examples of autocorrelation curves recorded from these samples are shown in Fig. 4.9, *A*, *C*, and *E*, together with the best fits of Eq. 4.5 to these curves. Increasing the ratio of unentrapped to entrapped fluorescent molecules shifted the diffusion times of the autocorrelation curves towards smaller values mirroring the much higher diffusion coefficient of unentrapped fluorescent molecules as compared to entrapped fluorescent molecules which are restricted to diffuse together with the LUVs. In addition, the amplitude of the autocorrelation curves also decreased when the fraction of unentrapped fluorescent molecules increased. In Fig. 4.9, *B*, *D*, and *F*, the autocorrelation curves are all normalized to the same amplitude to further allow visualization of the shift of diffusion times as the fraction of percentage of entrapped molecules is changed.

4.7.4   Dependence of brightness ratio on excitation intensity

Method

To test how the brightness ratio between entrapped and unentrapped fluorescent molecules, k, depends on the excitation power, we prepared a number of samples with 1 mM LUVs entrapping 4 µM Alexa488, 5 µM Alexa488-3kMW, or 2.5 µM Alexa488-10kMW. Additionally, we prepared a number samples with free Alexa488, Alexa488-3kMW, or Alexa488-10kMW in buffer solution. The concentrations of the samples with free molecules in buffer corresponded to those of samples in which 0.1 % Triton X-100 had induced complete leakage from 1 mM
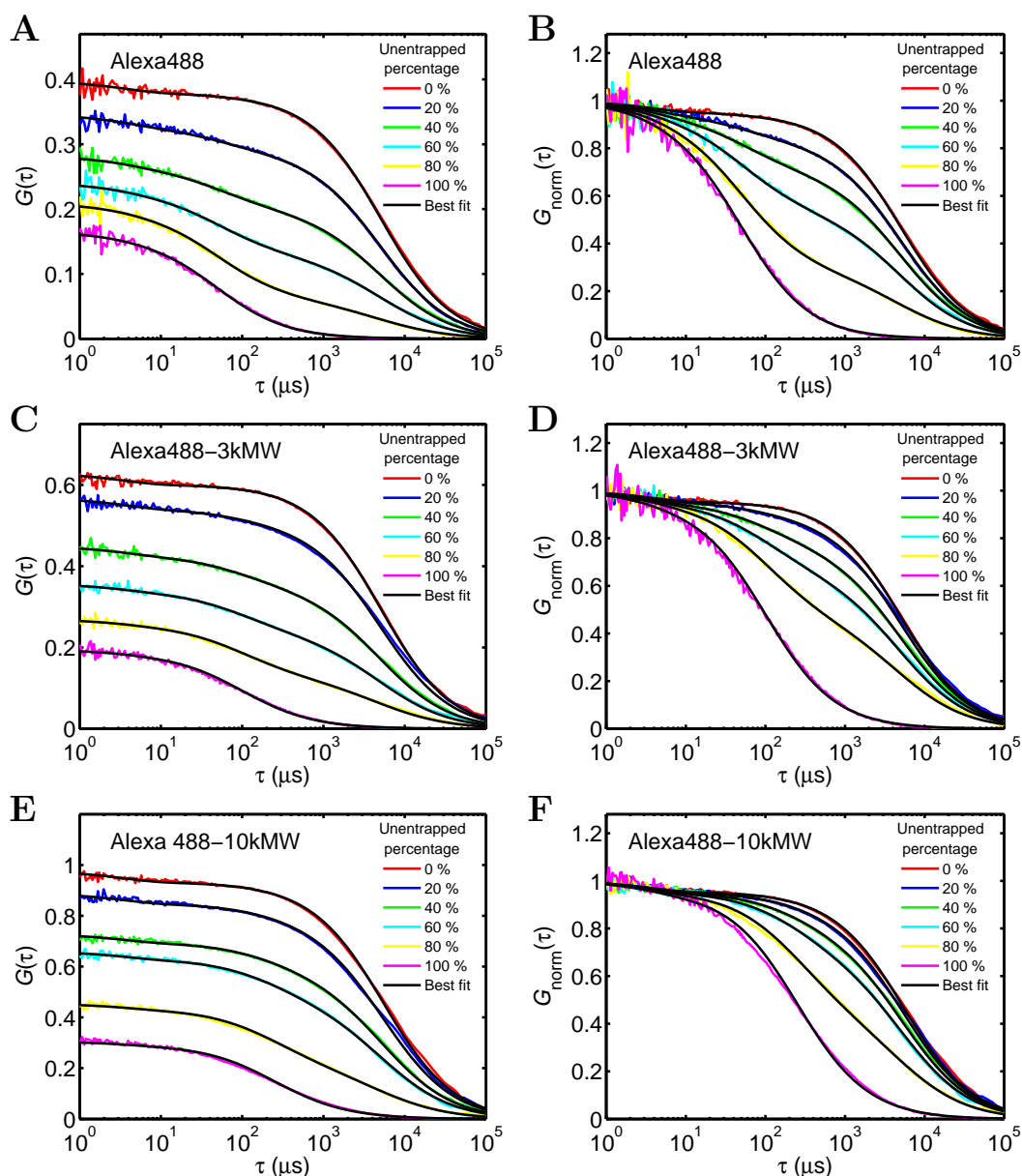
Figure 4.9: (*A*, *C*, and *E*) Autocorrelation curves recorded in samples with variable percentages of fluorescent molecules entrapped in POPC/POPG (3:1) LUVs. (*A*) Free Alexa488 and POPC/POPG (3:1) LUVs with 4 µM Alexa488. (*C*) Free Alexa488-3kMW and POPC/POPG (3:1) LUVs with 5 µM Alexa488-3kMW. (*E*) Free Alexa488-10kMW and POPC/POPG (3:1) LUVs with 2.5 µM Alexa488-10kMW. The black lines represent the best fit of Eq. 4.5. (*B*, *D*, and *F*) Autocorrelation curves normalized to an amplitude of 1 to allow for more clear visualization of the shift in diffusion times associated with changes in the percentage of unentrapped fluorescent molecules.

Figure 4.10: The brightness ratio between entrapped and unentrapped fluorescent molecules, k, vs the excitation power, P, for Alexa488 (*A*), Alexa488-3kMW (*B*), or Alexa488-10kMW (*C*). The values of k in this figure are all normalized with respect to the value of k obtained at $P = 0.74$ µW. Consequently, this data point is by definition set to 1. The data in all panels are the average of three separate experiments.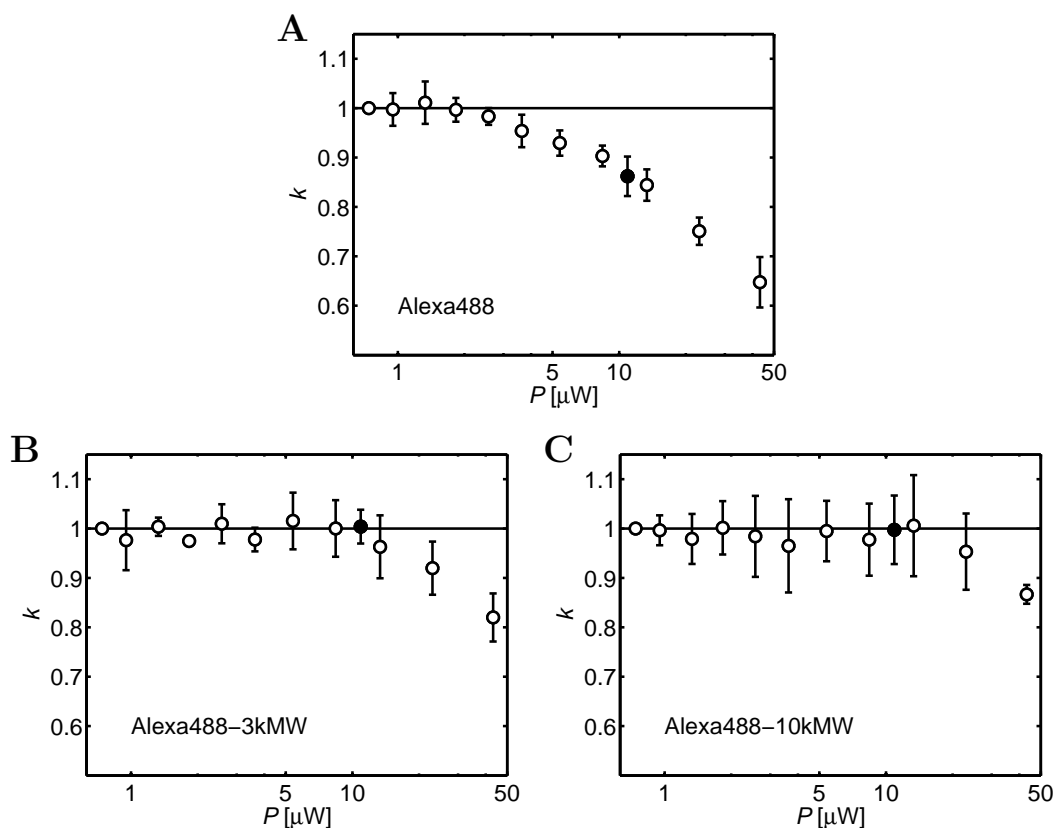 The error bars show the standard deviations. Error bars are not shown if they are smaller than the symbols. The black data points correspond to our standard choice of excitation power for the leakage experiments in the article.

LUVs entrapping 4 µM Alexa488, 5 µM Alexa488-3kMW, or 2.5 µM Alexa488-10kMW. All samples were then transferred to the µ-slide 8 wells for examination by FCS.

All samples were subject to varying excitation powers, and the brightness ratio, k, was calculated by the equation

$$k = \frac{B_0 - B_{\mathrm{b}}}{B_{100} - B_{\mathrm{b}}} \tag{4.31}$$

where B_0 is the photon count rate from the samples in which all fluorescent molecules were entrapped in LUVs, B_{100} is the photon count rate from the samples in which all fluorescent molecules were freely diffusing in buffer, and B_{b} is the uncorrelated background photon count rate as determined from measurements in pure buffer. Since the preparation procedure of the samples with free molecules might lead to small uncertainties in concentrations, all values of k were normalized by dividing them with the value of k obtained from the lowest excitation

power of 0.74 μW. In that way, k is by definition set to 1 when $P = 0.74$ μW and any uncertainties in k due to uncertainties in concentrations of free molecules are eliminated.

Results

Fig. 4.10 shows the determined brightness ratio, k, as a function of the excitation power. Especially for Alexa488, k is found to be dependent on the excitation power. However, also in the cases of Alexa488-3kMW and Alexa488-10kMW, high excitation powers might impact k. The black data points in Fig. 4.10 represent our standard choice of excitation power for the leakage experiments. Please note that Fig. 4.10 is primarily presented for illustrative purposes. The values of k actually used for calculations in the article are calculated directly from 1 mM LUV solutions with or without Triton X-100 or MPX to induce complete leakage so as to avoid the normalization step described in the Methods section.

4.7.5   Kinetics of MPX-induced leakage

Method

To investigate MPX-induced leakage from POPC/POPG (3:1) LUVs, variable volumes of MPX stock solutions were transferred to Protein LoBind tubes containing POPC/POPG (3:1) LUVs entrapping 4 μM Alexa488, 5 μM Alexa488-3kMW, or 2.5 μM Alexa488-10kMW. The final LUV concentrations of these samples were always 1 mM. Immediately after addition of MPX, each sample was vigorously vortexed for a few seconds and subsequently incubated at room temperature. After 10 min, 20 min, 1 h or ~18 h incubation, the samples were transferred to the μ-slide 8 wells for examination by FCS. Experiments were conducted with an excitation power of 10.9 μW. Leakage values were calculated using Eq. 4.10.

Results

Fig. 4.11 shows MPX-induced leakage after 10 min, 20 min, 1 h, or ~18 h incubation time for selected [P]/[L] ratios. The figure shows that values of leakage are essentially always identical after 10 min, 20 min, and 1 h incubation. Thus, MPX-induced leakage from POPC/POPG (3:1) LUVs is a transient process, in which a rapid burst of leakage within the first few minutes is followed by a dramatic slowing down or complete cessation of marker efflux. Therefore, values of leakage recorded after 1 h incubation essentially represent the leakage that occurs within the first few minutes after MPX addition to the LUVs. However, the values of leakage recorded after ~18 h incubation of MPX with LUVs reveal that leakage, after the initial rapid burst of leakage, in some cases persists at a much slower rate. The slower rate seems to be a function of the [P]/[L] ratio; the higher the [P]/[L] ratio, the higher the rate of this secondary release process.
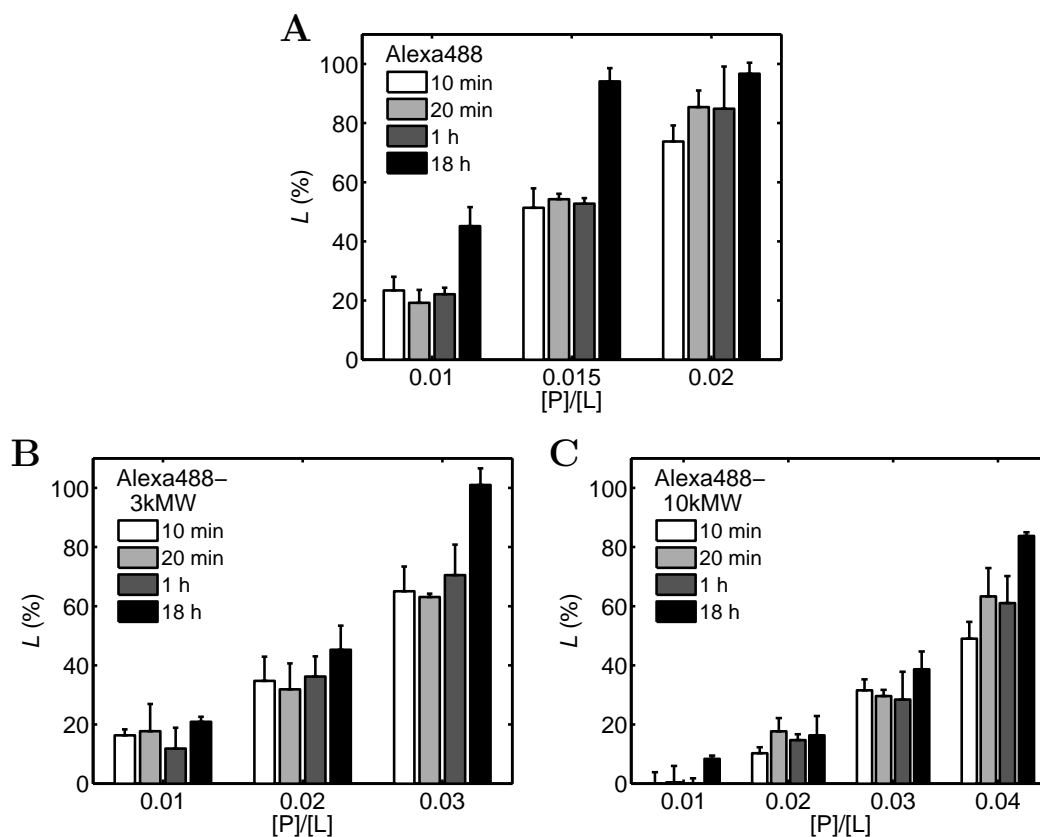
Figure 4.11: MPX-induced leakage, L, after incubation of MPX with 1 mM POPC/POPG (3:1) LUVs for 10 min, 20 min, 1 h, and ~ 18 h. (*A*) Leakage from LUVs entrapping 4 µM Alexa488. (*B*) Leakage from LUVs entrapping 5 µM Alexa488-3kMW. (*C*) Leakage from LUVs entrapping 2.5 µM Alexa488-10kMW. In all panels, the data are the average of three separate experiments. Error bars represent standard deviations. Leakage is a biphasic process, in which a rapid burst of leakage within the first few minutes after MPX addition is followed by a dramatic slowing down or complete cessation of leakage.

4.7.6 Investigation of leakage by equilibrium dialysis

Materials

Fast Micro-Equilibrium DIALYZER casettes with 500 µL half-cells and cellulose acetate 300 kDa MWCO membranes for equilibrium dialysis were purchased from Harvard Apparatus (Scandicat, Odder, Denmark).

Method

Variable volumes of MPX stock solutions were transferred to Protein LoBind tubes containing POPC/POPG (3:1) LUVs entrapping 20 µM Alexa488-3kMW. The final LUV concentrations were always 1 mM. After addition of MPX, samples were vigorously vortexed and subse-

Figure 4.12: Equilibrium dialysis experiments to study MPX-induced leakage of Alexa488-3kMW. (*A*) White bars are value of leakage as determined b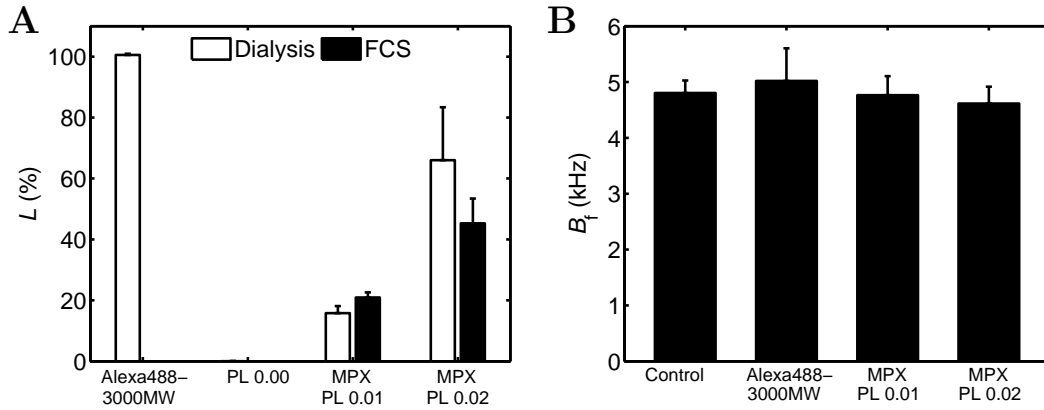y Eq. 4.32. The sample "Alexa488-3kMW" is a control sample to check equilibration of 60 nM Alexa488-3kMW across the dialysis membrane. For this sample, an L-value of 100 % indicates complete equilibration. The black data bars are leakage as determined by FCS; therefore, such black bars are not available for the "Alexa488-3kMW"-sample. For $[P]/[L] = 0$, the black bar is by definition 0 %. Within the experimental uncertainty, leakage values determined from dialyzed samples and from FCS on non-dialyzed samples are in good agreement. (*B*) Apparent brightness values, B_{f}, of Alexa488-3kMW samples taken from the buffer-containing half-cells. The sample 'Control' is a sample with 30 nM Alexa488-3kMW that was not incubated in the dialysis cassettes. B_{f} is found to be identical for all samples. Data are the average of two to five separate experiments. Error bars show the standard deviations.

quently incubated at room temperature for ∼30 min. The samples were then transferred to the half-cells of equilibrium dialysis cassettes in which the other half cell was filled with buffer. A cassette in which the one half cell contained 60 nM free Alexa488-3kMW together with 1 mM unlabeled POPC/POPG (3:1) LUVs and the other half-cell contained buffer was also prepared to check that Alexa488-3kMW equilibrated across the dialysis membrane. The cassettes were incubated for ∼ 20 h before the contents of the cassettes were transferred to the µ-slide 8 wells for examination by FCS. Experiments were conducted with excitation power of 10.9 µW.

From the photon count rates of the FCS measurements, the percentage of Alexa488-3kMW that had leaked out of the vesicles, L, could be calculated by the formula

$$L = \frac{2\left(B_{\mathrm{buf}} - B_{\mathrm{b}}\right)}{\left(B_{\mathrm{LUV}} - B_{\mathrm{buf}}\right)k^{-1} + 2\left(B_{\mathrm{buf}} - B_{\mathrm{b}}\right)} \tag{4.32}$$

where B_{buf} is the photon count rate of the sample from the buffer-containing half-cell, B_{LUV} is the photon count rate of MPX/LUV-containing half-cell, B_{b} is the background photon count rate, and k is the usual brightness ratio between entrapped and unentrapped Alexa488-3kMW.

Results

In the equilibrium dialysis experiments, we investigated MPX-induced leakage of Alexa488-3kMW from POPC/POPG (3:1) LUVs at two different [P]/[L] ratios of 0.01 and 0.02. At these [P]/[L] ratios, after the initial rapid burst of leakage, no additional leakage of Alexa488-3kMW was observed during a ~ 18 h incubation period (Fig. 4.11 *B*). Accordingly, the role of the equilibrium dialysis experiments was simply to separate the Alexa488-3kMW-molecules that were released during the initial rapid burst of leakage from the Alexa488-3kMW-molecules that remained entrapped during this burst. In other words, the equilibrium dialysis leakage data should be representative of the leakage that occurred during the initial rapid burst of leakage. Consequently, leakage as determined from the dialyzed samples using Eq. 4.32 should be directly comparable to leakage determined by FCS performed on non-dialyzed samples. Fig. 4.12 *A* confirms that within the experimental uncertainties, this notion is true, albeit we note that leakage as determined from the dialyzed samples at a [P]/[L] ratio of 0.02 is associated with a rather high experimental uncertainty.

The Alexa488-3kMW molecules that had diffused to the buffer-containing half-cells during equilibration must then be representative of the Alexa488-3kMW molecules that are released during the initial rapid burst of leakage. Therefore, by performing FCS on the samples from the buffer-containing half-cells, it is possible to check whether B_f of Alexa488-3kMW is constant for different values of leakage. Fig. 4.12 *B* confirms that B_f of Alexa488-3kMW in the buffer containing half-cells is indeed constant for different values of leakage, meaning that the probability of a given Alexa488-3kMW molecule being released during the initial rapid burst of leakage is not dependent on the number of fluorescent labels on the Alexa488-3kMW molecules. Consequently, we conclude that our FCS-based protocol is fully applicable to study release of Alexa488-3kMW from LUVs. Unfortunately, since Alexa488-10kMW only equilibrates very slowly across the dialysis membranes, we were not capable of performing the same type of experiments on leakage of Alexa488-10kMW. However, given the fact that the value of B_f for Alexa488-3kMW was found to be *completely* unbiased during leakage, we consider it unlikely that the B_f-value of Alexa488-10kMW will be strongly biased during leakage.

Single-vesicle analysis of antimicrobial peptide-induced leakage

The following chapter contains a manuscript in preparation. The manuscript is entitled "Single-vesicle analysis of leakage induced by cationic membrane-active peptides". The manuscript is based on work carried out in collaboration with Nicky Ehrlich. Nicky Ehrlich also wrote part of Section 5.3.4 for the manuscript.

5.1 Abstract

The mechanisms by which cationic membrane-active peptides interact with lipid bilayers have for years been subject to significant scientific attention. In particular, great efforts have been put into studying the mechanisms by which cationic membrane-active peptides permeabilize lipid bilayers. In this article, we combine two powerful techniques to study membrane permeabilization induced by the three α-helical cationic membrane-active peptides mastoparan X, melittin, and magainin 2. Specifically, fluorescence correlation spectroscopy to quantify leakage from a bulk collection of large unilamellar lipid vesicles in aqueous solution was combined with confocal imaging to visualize leakage from individual surface-immobilized large unilamellar lipid vesicles. Our results show the all three peptides induce partial transient permeabilization of POPC/POPG (3:1) bilayers by the formation of transmembrane pores. Additionally, our results show that on the single-vesicle level this leakage process is heterogenous in the sense that some vesicles are completely emptied and some vesicles are only partly emptied.

5.2 Introduction

Cationic membrane-active polypeptides have been studied for years as candidates for becoming a novel class of anti-infective therapeutics (6, 8). In particular, a great deal of effort has been put into understanding the mechanisms by which cationic membrane-active pep-

tides destabilize cellular membranes, as these destabilizing activities have been suggested to play a central role for the antimicrobial and cytotoxic activities of cationic membrane-active peptides (5, 10, 14, 28). To study these membrane-destabilizing activities, synthetic lipid vesicles are often employed as minimal models of cellular membranes. In one of the most popular assays with such synthetic lipid vesicles, size-homogenous unilamellar lipid vesicles with a diameter of 100 nm (LUVs) are loaded with high self-quenching concentrations of fluorophores, such as calcein or carboxyfluorescein (169, 170). These LUVs are then mixed with peptides. If the peptides induce permeabilization of the vesicle membranes, the encapsulated fluorophores will leak out of the vesicles, and the fluorescence emission will increase due to dequenching of the fluorophores that escape the vesicle lumen.

One of the major limitations of the conventional quenching-based leakage assays is that they only provide average information about leakage from an ensemble of vesicles. Therefore, to study heterogeneities in leakage between individual LUVs, more sophisticated experimental methods have been designed. These methods have especially been focussed on whether peptide-induced leakage is a graded process, in which all of the vesicles release a similar fraction of their contents, or an all-or-none process, in which part of the vesicles release all of their contents and part of the vesicles release no contents. In one of these methods, the self-quenching of the fluorophores that remain inside the vesicles during the leakage process is used to assess whether leakage occurs via a graded process or an all-or-none process (171, 172). In another method, the dye/quencher pair ANTS/DPX is used to assess whether leakage occurs via a graded process or an all-or-none process (49, 150, 151, 173). In yet another method, the fluorescence lifetime of calcein inside vesicles is analyzed to assess the leakage mechanism (174, 175).

However, all of these methods to study heterogeneities in leakage between individual LUVs are based on indirect analyses. To directly visualize peptide-induced leakage on the single-vesicle level, giant unilamellar lipid vesicles (GUVs) with a diameter of 5 μm or more have been employed instead of LUVs (46–48). Due to the large size of the GUVs, fluxes of fluorescent markers into or out of the GUVs are directly visible by optical microscopy. By binning the degrees of fillings of individual GUVs, it is then, for example, possible to deduce whether a given peptide induces leakage by a graded process or an all-or-none process (176, 177). However, an important limitation of the GUV experiments, as compared to the LUV experiments, is that it is very difficult to control the experimental lipid concentration and, thereby, also the experimental peptide-to-lipid ratio.

In this article, we study peptide-induced leakage from LUVs using two less conventional techniques. The first technique is fluorescence correlation spectroscopy (FCS) (156, 157). In FCS, fluctuations in emission intensity from fluorescent molecules diffusing across a small confocal volume are analyzed to obtain autocorrelation curves carrying information about concentrations, diffusion properties, and other things of fluorescent molecules in solution. We recently showed that FCS is applicable to quantitatively study peptide-induced leakage of fluorescent markers from LUVs in solution (Chapter 4), including leakage of fluorescent markers of different sizes. Thereby, FCS provide a high level of insight into the mechanisms by which cationic membrane-active peptides induce leakage from LUVs. However, just like for the conventional quenching based leakage assays, one major limitation of FCS is that

the technique only provides average information about the leakage process; no information about heterogeneity in leakage between LUVs is available by FCS.

Therefore, we also employed a second experimental technique to obtain information about leakage on the single-vesicle level. In this technique, LUVs, labeled with a lipid-anchored fluorophore and loaded with a spectrally separated fluorescent marker, are immobilized on a cover glass slide, allowing individual LUVs to be visualized by confocal microscopy as diffraction-limited spots (178, 179). Thereby, the technique allows more direct observation of peptide-induced leakage from individual LUVs than what hitherto has been possible. In addition, the technique also allows us to study leakage of fluorescent markers of different sizes on the single-vesicle level; such studies remain so far as largely unexplored territory for LUVs. In order to ensure that this more direct observation of leakage did not come at the cost of poor control of the experimental peptide-to-lipid ratio, we designed a detailed experimental protocol in which peptides were added to and subsequently removed from LUVs before LUVs were immobilized.

By combining FCS with confocal imaging of surface-immobilized LUVs, we believe that we have introduced a powerful experimental approach to study peptide-induced leakage from LUVs. To demonstrate the potential of this approach, we considered the three archetypal antimicrobial cationic membrane-active peptides mastoparan X, melittin, and magainin 2. All these three peptides have in common that they are linear, small, and enriched in hydrophobic and, of course, cationic amino acid residues. In addition, all three peptides are known to fold into amphipathic α-helical structures upon association to phospholipid bilayers (111, 117, 120–123). Moreover, all three peptides have been found to induce leakage from lipid vesicles, and, for all three peptides, it has been extensively studied whether this leakage is characterizable as an all-or-none process or a graded process (47, 48, 51, 52, 122, 128, 130–133, 173, 180). For example, mastoparan X has previously been suggested to induce graded leakage from egg PC/egg PG (7:3) LUVs (51) and from POPC/POPG GUVs of varying POPG content (133), melittin has previously been suggested to induce all-or-none leakage from POPC LUVs (134), and magainin 2 has previously been suggested to induce graded leakage from egg PG LUVs (122) and all-or-none leakage from POPC/POPG (1:1) and POPC/POPG (7:3) LUVs (173) and from DOPG/DOPC GUVs of varying DOPG content (47). In this article, we study the interactions of these three peptides with POPC/POPG (3:1) LUVs. Our experimental data confirms previous observations that these peptides are indeed capable of permeabilizing lipid bilayers. In addition, our data also show that leakage considered on the single-vesicle level is a heterogenous process in the sense that some vesicles are completely emptied and some vesicles are only partly emptied. This heterogenous leakage profile is found regardless of the size of the encapsulated fluorescent marker.

5.3 Materials and methods

5.3.1 Materials

1-palmitoyl-2-oleoyl-*sn*-glycero-3-phosphocholine (POPC), 1-palmitoyl-2-oleoyl-*sn*-glycero-3-[phospho-rac-(1-glycerol)], sodium salt (POPG), 1,2-dioleoyl-*sn*-glycero-3-phosphoethanola-

mine-N-(cap biotinyl), sodium salt (DOPE-Biotin), and 1-palmitoyl-2-[11-(dipyrrometheneb-oron difluoride)undecanoyl]-*sn*-glycero-3-phosphocholine (TopFluor PC) were purchased from Avanti Polar Lipids (Alabaster, AL, USA). Bovine serum albumin (BSA), biotin-labeled bovine serum albumin (BSA-biotin), streptavidin from *Streptomyces avidinii*, N-(2-hydroxyet-hyl)piperazine-N'-(2-ethanesulfonic acid) (HEPES) and the corresponding sodium salt (HEP-ES-Na), and NaCl were purchased from Sigma-Aldrich (Brøndby, Denmark). 1,1'-dioctadecyl-3,3,3',3'-tetramethylindodicarbocyanine perchlorate (DiD), Alexa Fluor 488 hydrazide, sodium salt (Alexa488), Alexa Fluor 488 dextran, 3000 MW, anionic (Alexa488-3kMW), and Alexa Fluor 488 dextran, 10000 MW, anionic, fixable (Alexa488-10kMW) were purchased from Life Technologies (Nærum, Denmark). Melittin was purchased from Peptide 2.0 (Chantilly, VA, USA), and magainin 2 and mastoparan X were purchased from GL Biochem (Shang-hai, China). Mastoparan X was further purified by semi-preparative HPLC (Waters semi-preparative HPLC equipped with a Waters 600 pump & controller and a Waters 2489 UV/vis detector, Waters, Milford, MA, USA). The purity of all three peptides was checked by ana-lytical HPLC (Shimadzu LC-2010C analytical HPLC equipped with a UV/vis detector, Shi-madzu, Kyoto, Japan, or Gilson analytical HPLC equipped with a Gilson 321 HPLC pump and a Gilson 155 UV/vis detector, Gilson, Middleton, MI, USA) and the identity of the pep-tides was confirmed by MALDI-TOF (Bruker Reflex IV MALDI-TOF spectrometer, Bruker, Billerica, MA, USA).

5.3.2   Sample preparation

LUV preparation and characterization

Lipid solutions were prepared in chloroform/methanol (9:1). The organic solvent was removed under a gentle stream of nitrogen. The samples were subsequently kept in vacuum overnight to remove the residual solvent. The lipid films were hydrated in HEPES buffer (10 mM HEPES, 100 mM NaCl, pH 7.4) with vigorous vortexing every 5 min for a period of 30 min. To prepare dye-loaded vesicles, Alexa488, Alexa488-3kMW or Alexa488-10kMW were added to the buffer. (Concentrations of these fluorescent molecules were determined from the absorbance, recorded by a NanoDrop 2000c spectrophotometer (NanoDrop Products, Wilmington, DE, USA), assuming that (i) the extinction coefficient of Alexa488 at maximum absorption at ca. 495 nm is $71000 \, \text{cm}^{-1}\text{M}^{-1}$ and (ii) using the degree of labeling of Alexa488-3kMW and Alexa488-10kMW that was stated by the manufacturer). The hydrated lipid suspensions were then subject to 5 freeze-thaw cycles by alternately placing the sample vials in an isopropanol/dry ice bath and a warm water bath. Next, the lipid suspensions were extruded 21 times through a 100 nm polycarbonate filter (Whatman, Maidstone, UK) using a mini-extruder (Avanti Polar Lipids) to form LUVs. The size of the LUVs was checked by dynamic light scattering (ZetaPALS, Brookhaven Instruments, Holtsville, NY, USA). Phosphorous concentrations of the LUV solutions were determined using the method of Rouser et al. (144), albeit with slightly modified reagent concentrations. Phosphorous concentrations of dye-loaded vesicles were determined after the vesicles had been run on a size exclusion chromatography column (Sepharose CL-4B, GE Healthcare, VWR - Bie & Berntsen, Herlev, Denmark) to separate the free dye from the vesicles.

Peptide stock solutions

Peptide stock solutions were prepared in HEPES buffer. To prevent loss of peptides due to adsorption to tube walls and pipette tips, peptide stock solutions were generally handled in Protein LoBind tubes (Eppendorf, VWR - Bie & Berntsen) and at high concentrations of at least 100 µM. To determine the concentration of peptide stock solutions, the extinction coefficients of peptides at 220 nm were calculated to be 40100 cm^{-1}M^{-1} for mastoparan X, 46700 cm^{-1}M^{-1} for melittin, and 23900 cm^{-1}M^{-1} for magainin 2 by correlating the peptide concentrations determined by an Antek 8060 chemiluminescent nitrogen detector (PAC, Houston, TX, USA) to the absorbance of the same peptide samples, determined by a NanoDrop 2000c spectrophotometer. Given these extinction coefficients, peptide concentrations of stock solutions were then always determined by recording the absorbance at 220 nm using the NanoDrop 2000c spectrophotometer.

5.3.3   FCS experiments

The details of the FCS measurements and analysis were the same as previously described (Chapter 4).

Sample preparation

Varying volumes of 100 µM peptide stock solutions were added to varying volumes of POPC/POPG (3:1) LUV solutions in Protein LoBind tubes to a final LUV concentration of 1 mM. The LUVs were entrapping 4 µM Alexa488, 5 µM Alexa488-3kMW, or 2.5 µM Alexa488-10kMW, or labeled with 0.1 % TopFluor PC. Immediately upon addition of peptide, the samples were vigorously vortexed for a few seconds and subsequently incubated for 1 h. The samples were then transferred to 8-well chambered cover glasses (µ-slide 8 wells, ibidi, DFA Instruments, Glostrup, Denmark) for examination by FCS.

FCS measurements

FCS measurements were performed using a commercially available DCS-120 confocal scanning FLIM system (Becker & Hickl, Berlin, Germany) connected to a Zeiss Axio Observer Z1 inverted microscope equipped with a C-Apochromat 40x/1.2 W Corr UV-VIS-IR water immersion objective (Carl Zeiss, Jena, Germany). The excitation source for the system was a 473 nm picosecond diode laser (BDL-473-SMC, Becker & Hickl) operated at a pulse repetition rate of 50 MHz. The incident excitation power at the objective rear aperture was measured by a PM100D optical power meter (Thorlabs, Goteborg, Sweden). After passing through a 485 nm longpass filter (HQ485LP, Becker & Hickl) and a confocal pinhole, the fluorescence emission was detected with a HPM-100-40 hybrid detector connected to a SPC-150 module (Becker & Hickl). Lifetime-gating was used to partially suppress background noise. SPCM software (Becker & Hickl) was used to calculate the experimental autocorrelation curves. The curves were subsequently exported to be fitted by MATLAB (The MathWorks, Natick, MA, USA). All samples were measured by positioning the laser focus $\sim$ 50 µm above the top of the cover glass. The acquisition time for all FCS experiments

was 300 s. By calibration with Alexa488, the effective excitation volume was determined to be 1.0 fL and the structural S-parameter was determined to be 7.4. The S-parameter was always fixed to this value when fitting all other experimental autocorrelation curves. Expect for the experiments determining the S-parameter, all autocorrelation curves in this article were analyzed using unweighted least squares fitting. Autocorrelation curves dominated by single bright events were discarded in the data analysis.

Data analysis

For a single type of diffusing species in solution, the autocorrelation function, $G(\tau)$, is given by:

$$G(\tau) = \frac{1}{N}g(\tau) = \frac{1}{N}\left(1 + \frac{T}{1-T}\mathrm{e}^{-\tau/\tau_{\mathrm{T}}}\right)\left(1 + \frac{\tau}{\tau_{\mathrm{D}}}\right)^{-1}\left(1 + \frac{\tau}{S^2\tau_{\mathrm{D}}}\right)^{-\frac{1}{2}} \quad (5.1)$$

where τ is the lag time, N is the average number of fluorescent particles in the excitation volume, T is the fraction of fluorescent particles in the triplet state, τ_{T} is the characteristic triplet state lifetime, S is the ratio of the axial to radial dimensions of the excitation volume, and τ_{D} is the characteristic translational diffusion time of the fluorescent particles. For samples in which peptides had been added to TopFluor PC-labeled LUVs, this equation was used to fit the recorded autocorrelation curves. In that case, N was the apparent average number of LUVs in the excitation volume and τ_{D} was the characteristic diffusion time of the LUVs.

For a leaky solution of LUVs, there are two diffusing species: LUVs entrapping fluorescent molecules (index v) and free fluorescent molecules (index f). In that case, the autocorrelation function is given by

$$G(\tau) = \frac{B_{\mathrm{f}}^2 N_{\mathrm{f}} g_{\mathrm{f}}(\tau) + B_{\mathrm{v}}^2 N_{\mathrm{v}} g_{\mathrm{v}}(\tau)}{B_{\mathrm{tot}}^2} = A_{\mathrm{f}} g_{\mathrm{f}}(\tau) + A_{\mathrm{v}} g_{\mathrm{v}}(\tau) \quad (5.2)$$

where B_{f} and B_{v} are the apparent brightness (photon count rate per molecule) of the free fluorescent molecules and the LUVs, respectively, N_{f} and N_{v} are the apparent average number of the free fluorescent molecules and LUVs in the excitation volume, respectively, A_{f} and A_{v} are the amplitude of the free fluorescent molecules and the LUVs, respectively, and g_{f} and g_{v} are defined as given in Eq. 5.1.

During a leakage experiment, a certain fraction of the initially entrapped fluorescent molecules will leak out of the LUVs. This fraction, L, must be given by the equation

$$L = \frac{C_{\mathrm{f}} - C_{\mathrm{f0}}}{C_{\mathrm{f100}} - C_{\mathrm{f0}}} \quad (5.3)$$

where C_{f0} is the concentration of unentrapped fluorescent molecules before peptide addition, C_{f} is the concentration of unentrapped fluorescent molecules after peptide addition, and C_{f100} is the concentration of unentrapped fluorescent molecules at complete leakage. Using Eqs.

5.2 and 5.3, it is possible to derive a quadratic equation relating L to the output parameters of the FCS experiments:

$$L = \frac{A_\text{f} \left(B_\text{f} N_\text{f100} L + k B_\text{f} N_\text{f100} (1 - L) + B_\text{b} \right)^2 - A_\text{f0} \left(k B_\text{f} N_\text{f100} + B_\text{b} \right)^2}{A_\text{f100} \left(B_\text{f} N_\text{f100} + B_\text{b} \right)^2 - A_\text{f0} \left(k B_\text{f} N_\text{f100} + B_\text{b} \right)^2}. \tag{5.4}$$

In this equation, N_f100 is the background-corrected average number of free fluorescent molecules in the excitation volume of a sample displaying $100\ \%$ leakage, B_b is the background photon count rate, A_f is determined by fitting Eq. 5.2 to a autocorrelation curve acquired from a sample with unknown leakage, L, A_f0 and A_f100 are the values of A_f as determined from samples with $0\ \%$ leakage and $100\ \%$ leakage, respectively, and k is the brightness ratio between entrapped and free fluorescent molecules. Under our experimental conditions, we found that $k = 0.85$ for Alexa488, $k = 0.96$ for Alexa488-3kMW, and $k = 0.95$ for Alexa488-10kMW. Eq. 5.4 was then solved for L using Maple (Maplesoft, Waterloo, Ontario, Canada). For further details on how to derive and experimentally determine the parameters of Eq. 5.4, see Chapter 4.

5.3.4 Confocal imaging experiments

Sample preparation

Varying volumes of $100\ \mu$M peptide stock solutions were added to Protein LoBind tubes containing solutions of POPC/POPG (3:1) LUVs functionalized with $0.1\ \%$ DOPE-biotin, labeled with $0.1\ \%$ DiD, and loaded with either $200\ \mu$M Alexa488 or $200\ \mu$M Alexa488-10kMW. The final LUV concentrations of the samples were always 1 mM. Immediately upon addition of peptide, the samples were vigorously vortexed for a few seconds. After 1 h incubation, a large excess of unlabeled POPG LUVs was added to a final POPG LUV concentration of 6.7 mM and a final POPC/POPG (3:1) LUV concentration of 0.83 μM. Immediately after addition of the POPG LUVs, the samples were vortexed for a few seconds and then incubated overnight. The next day, the samples were transferred to 8-well chambered cover glasses (ibidi). These 8-well chambered cover glasses had been prepared by incubation with 1 g/l BSA-biotin/BSA (1:10) for 10 minutes and then incubation with 0.025 g/l streptavidin for 10 minutes. After each incubation step, the chambers were washed thoroughly with PBS buffer and finally with HEPES buffer. The biotinylated POPC/POPG (3:1) LUVs were then immobilized on the streptavidin functionalized surfaces by incubating the samples for 7-10 minutes followed by washing with HEPES buffer. The surface density of LUVs was varied by the amount of added sample.

Setup

Immobilized LUVs were imaged with a commercially available inverted confocal microscope (Leica TCS SP5 AOBS, Leica Microsystems, Wetzlar, Germany) using a water immersion objective (HCX PL APO CS 63.0x/1.20, Leica). The microscope stage was placed in an incubator box (Life Imaging Services, Basel, Switzerland), in which the temperature remained constant at 22° C. Micrographs from the membrane signal (DiD) and lumen signal (Alexa488

or Alexa488-10kMW) were acquired sequentially to avoid cross excitation. First, the lumen dye was excited using the 488 nm line of an argon laser, and the emission between 495 and 555 nm was collected with a PMT. A 633 nm diode laser was then used to excite the membrane dye, and the emission between 640 nm and 711 nm was collected. Imaging was repeated 15 times and a pinhole size of 1 AU was used. Additionally, for each image sequence, a bright field image for each laser was obtained for later correcting the fluorescence signal for laser fluctuations between different images, samples, and days. Images had a resolution of 1024 x 1024 pixel, with a physical pixel area of 72,9 x 72,9 nm^2 and a bit depth of 8. Specimens were scanned bidirectional with a speed of 100 Hz, corresponding to an exposure time in each sub-image of 9.8 μs for each pixel.

Data analysis

A custom made software routine in Igor Pro 6 (Wavemetrics, Lake Oswego, OR, USA) was used for single-vesicle analysis. Using the micrographs acquired from the membrane dye detector channel, the software routine localized single LUVs in the micrographs and fitted their fluorescence intensity distribution via a 3D Gaussian fit; thresholding, minimum vesicle area and ellipticity were used as tools for faithfully localizing LUVs, and only LUVs that had no overexposed pixels and for which the Gaussian fit matched the criteria of having an uncertainty below 10% and a width of 3.5 ± 0.5 pixels were included in the data analysis. These strict criteria assured us to have intact single LUVs with sufficient fluorescent signal for single-vesicle analysis. The lumen dye and membrane dye emission intensity of each individual localized LUV were then determined by integrating the pixel intensities of a 7×7 pixel area. For each experiment, between 200 to 1000 LUVs were typically localized and included in the data analysis.

The average background intensity and the detection threshold of the apparatus were for every image series determined by plotting a cumulative probability density histogram of single pixel intensities from image areas where no vesicles had been detected. Based on this cumulative probability density histogram, we then conducted a Monte Carlo simulation to determine the background intensity distribution of the 7×7 pixel areas; from this intensity distribution, the average background intensity and the detection threshold of the apparatus were determined.

To calculate the average fraction of markers released from LUVs in a sample of peptide-treated immobilized LUVs, L, we used the equation

$$L = 1 - \frac{I - I_\mathrm{b}}{I_0 - I_\mathrm{b}} \tag{5.5}$$

where I is the average lumen dye emission intensity per LUV of the given sample of peptide-treated immobilized LUVs, I_0 is the average lumen dye emission intensity per LUV of untreated LUVs, and I_b is the background intensity.

To calculate the fraction of LUVs that upon treatment by peptide had been completely emptied below the detection threshold of the apparatus, we used the equation

$$E = 1 - \frac{F}{F_0} \tag{5.6}$$

where E is the fraction of LUVs that had been emptied upon treatment by peptide, F is the fraction of non-empty LUVs of the peptide-treated sample, and F_0 is the fraction of non-empty LUVs of a sample of untreated LUVs.

5.4 Results and discussion

5.4.1 FCS experiments

First, we used FCS to study peptide-induced leakage from an ensemble of LUVs in solution. Fig. 5.1 shows leakage vs the peptide-to-lipid ratio as determined by FCS after 1 h incubation of peptides together with 1 mM POPC/POPG (3:1) LUV loaded with Alexa488, Alexa488-3kMW, or Alexa488-10kMW. These data demonstrate that leakage induced by mastoparan X (Fig. 5.1 *A*) and melittin (Fig. 5.1 *B*) is dependent on the size of the entrapped marker; both peptides induces much more effective release of Alexa488, with a molar mass of 570 Da, than of Alexa488-3kMW and Alexa488-10kMW, with nominal molar masses of 3 kDa and 10 kDa, respectively. In contrast, leakage induced by magainin 2 (Fig. 5.1 *C*) did not display the same dependency on the marker size.

Leakage was also checked for shorter incubation times. These data (not shown) demonstrate that leakage induced by mastoparan X, melittin, and magainin 2 is a partial transient process in which a rapid burst of leakage, over the course of a few minutes, is followed by dramatic slow down or complete cessation of leakage. In that way, the leakage values that we record after 1 h incubation is, by and large, representative of the rapid burst of leakage that occurs within the first few minutes after addition of peptide. It should be noted that such transient partial leakage is a commonly reported phenomenon for leakage induced by membrane-active peptides (45); however, the specific molecular details underlying partial transient leakage are still not completely understood

We also used FCS to evaluate the mechanism by which mastoparan X, melittin and magainin 2 induce leakage from POPC/POPG (3:1) LUVs. Fig. 5.2 shows the effect of the peptides on TopFluor PC-labeled POPC/POPG (3:1) LUVs as determined by FCS after 1 h incubation of peptides together with 1 mM LUV. For mastoparan X (Fig. 5.2, *A* and *B*) and melittin (Fig. 5.2, *C* and *D*) the apparent average number of LUVs in the excitation volume and diffusion times of the LUVs were largely constant for all peptide-to-lipid ratios. This strongly implies that leakage induced by mastoparan X and melittin is due to formation of transmembrane pores. For magainin 2 (Fig. 5.2, *E* and *F*), the apparent number of LUVs gradually decreased as a function of the peptide-to-lipid ratio, and, concurrently, the LUV diffusion times gradually increased as a function of the peptide-to-lipid ratio. These observations imply that magainin 2 induce aggregation or fusion of the POPC/POPG (3:1) LUVs. However, we do not believe that this aggregation/fusion process play a major role in the magainin 2-induced leakage. Thus, we note that magainin 2 induced almost complete leakage of all markers already at a peptide-to-lipid ratio of 0.01 (Fig. 5.1 *C*). At this peptide-to-lipid ratio, magainin 2 did not induce significant changes in the apparent average number of LUVs in the excitation volume and in the LUV diffusion times (Fig. 5.2, *E* and *F*), indicating the aggregation/fusion process to only play a minor role in magainin 2-induced
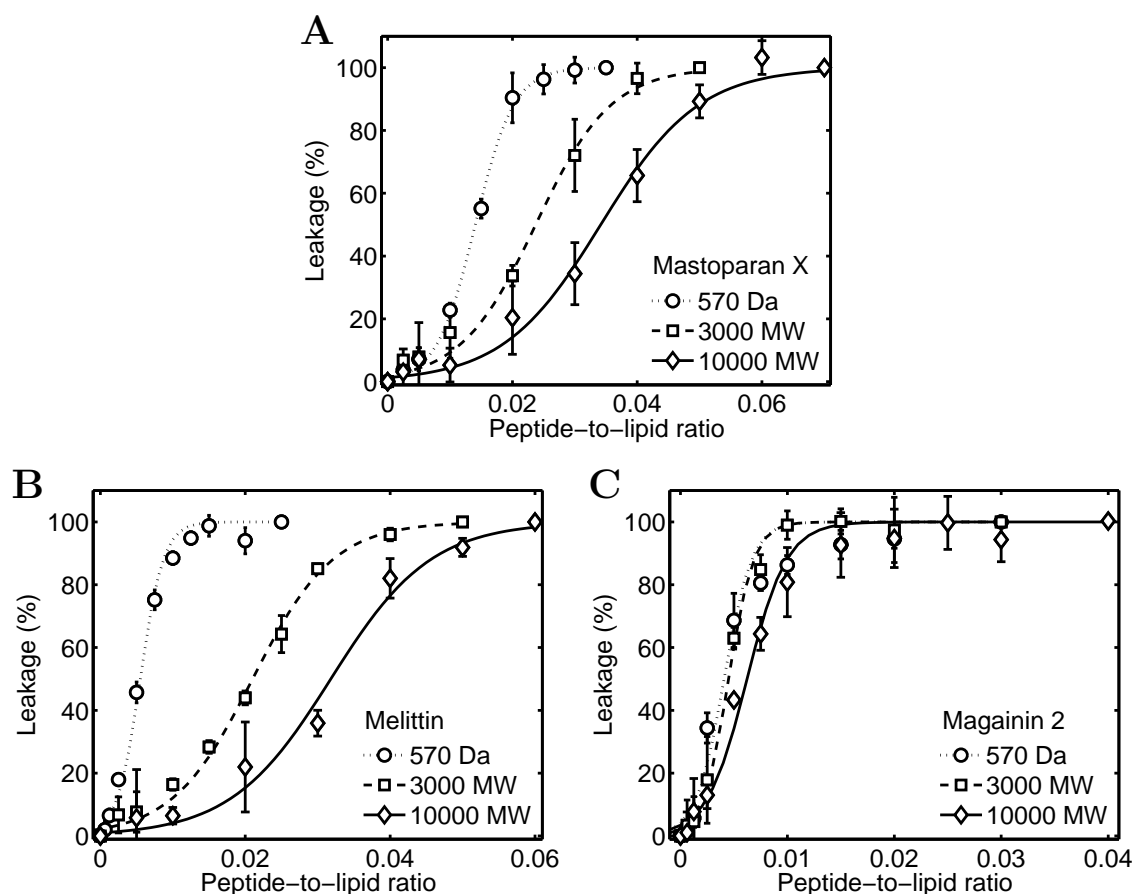
Figure 5.1: Peptide-induced leakage from 1 mM POPC/POPG (3:1) LUVs containing Alexa488 (molar mass of 570 Da), Alexa488-3kMW (nominal molar mass of 3 kDa), or Alexa488-10kMW (nominal molar mass of 10 kDa) as determined by FCS after 1 h incubation of peptides together with LUVs. In all panels, the data are the average of three separate experiments. The error bars show the standard deviations. The error bars are not shown when they are smaller than the symbols. The leakage values at the lowest and highest peptide-to-lipid ratios correspond to no leakage and complete leakage, respectively, and, therefore, they are, by definition, always set to $0\ \%$ and $100\ \%$, respectively. Trendlines are added to guide the eye. Leakage induced by mastoparan X (A) and melittin (B) is dependent on the size of the entrapped marker. Contrary, leakage induced by magainin 2 (C) is less dependent on size of the entrapped marker.

leakage. Therefore, we conclude that magainin 2, just like mastoparan X and melittin, induce leakage from POPC/POPG (3:1) LUVs by formation of transmembrane pores, and not by any other molecular processes, such as membrane fusion. Holding the conclusion that mastoparan X, melittin, and magainin 2 form transmembrane pores together with the observations in Fig. 5.1 that leakage from POPC/POPG (3:1) LUVs induced by magainin 2 is less dependent on the marker size than leakage induced by mastoparan X and melittin, we deduce that magainin 2 must form larger and/or more stable transient pores during

partial transient leakage from POPC/POPG (3:1) LUVs than melittin and mastoparan X. The questions is then whether these differences in pores size and/or stability will also give rise to differences in the leakage profiles on the single-vesicle level.

5.4.2 Confocal imaging experiments

In the confocal imaging experiments, we considered POPC/POPG (3:1) LUVs functionalized with DOPE-biotin, labeled with DiD, and loaded with either Alexa488 or Alexa488-10kMW. 1 mM of these LUVs were incubated together with peptides for 1 h in solution. After this incubation time, a large excess of POPG LUVs was added to the solutions. As mastoparan X, melittin and magainin 2, just like cationic membrane-active peptides in general, all exhibit high affinity for partitioning onto such anionic POPG LUVs (110, 112, 128, 129, 181), they will dissociate from the POPC/POPG (3:1) LUVs and instead partition onto the POPG LUVs. To ensure maximal transfer of peptide from the POPC/POPG (3:1) LUVs to the POPG LUVs, the samples were incubated overnight. The next day, the LUVs were immobilized to cover glasses for visualization by confocal imaging. Fig. 5.3 *A* shows a schematic drawing of a surface-immobilized LUV. Fig. 5.3, *B-E*, shows a few representative confocal images of the surface-immobilized LUVs.

The POPG-induced removal of peptides from the POPC/POPG (3:1) LUVs served two purposed. First, the POPG-induced removal of peptides from the POPC/POPG (3:1) LUVs completely halted the leakage process (see Fig. 5.8 in the Supporting material), thereby ensuring that leakage observed from the immobilized LUVs was representative of peptide-induced leakage that had occurred from LUVs in solution during the 1 h incubation period before POPG had been added. Second, the fact that peptides had been removed from the POPC/POPG (3:1) LUVs ensured that all LUVs were immobilized under identical experimental conditions, i.e., removal of peptides from the POPC/POPG (3:1) LUVs ensured that peptides partitioned onto the POPC/POPG (3:1) LUVs could not influence the immobilization process. Since FCS control experiments in addition had shown that adding DOPE-biotin and DiD to the POPC/POPG (3:1) LUVs did not perturb the leakage process (see Fig. 5.7 in the Supporting material), the confocal imaging data should then be directly comparable to the FCS data. To confirm that this notion is true, we used Eq. 5.5 to calculate the average percentage of released fluorescent markers from collections of surface-immobilized LUVs and compared it to the leakage percentages determined by FCS. Fig. 5.4 shows the calculated average leakage percentages of the surface-immobilized LUVs as a function of the peptide-to-lipid ratio. For the Alexa488-containing LUVs, very good agreement between leakage calculated from the surface-immobilized LUVs and FCS was achieved. For the Alexa488-10kMW-containing LUVs, reasonably good agreement between leakage calculated from the surface-immobilized LUVs and FCS was achieved, albeit leakage determined from the surface-immobilized LUVs was generally slightly lower than in FCS. The small deviations in leakage of Alexa488-10kMW observed between the surface-immobilized LUVs and FCS might be due to differences in experimental conditions between the two techniques. For instance, the molar concentration of 200 μM Alexa488-10kMW inside the immobilized LUVs corresponds to a relatively high mass concentration; we can not rule out that such high mass concentrations impact the kinetics of the leakage process, for example, because
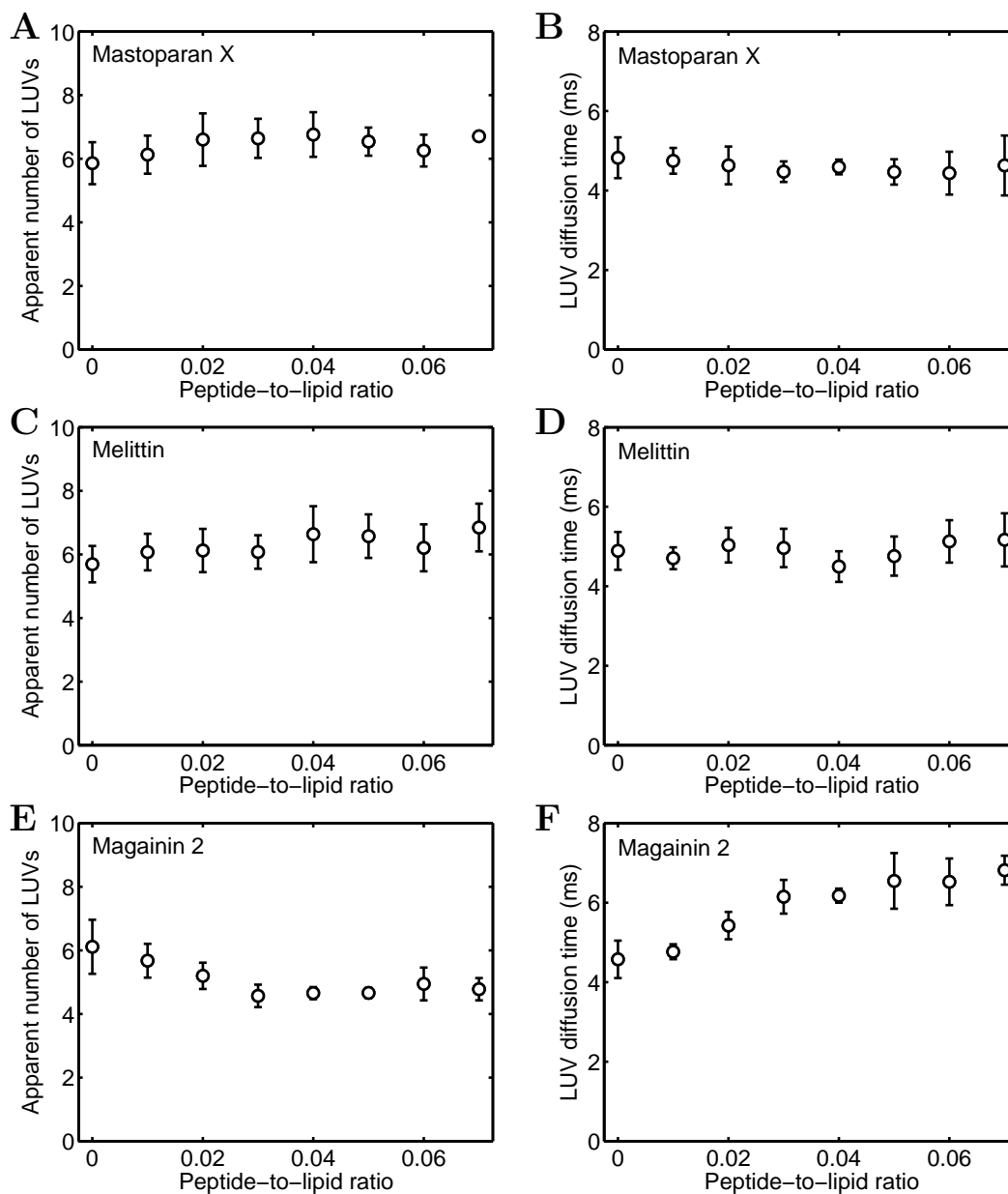
Figure 5.2: Effect of peptides on TopFluor PC-labeled POPC/POPG (3:1) LUVs as determined by FCS after 1 h of incubation of peptides together with 1 mM LUVs. In all panels, the data are the average of three separate experiments. The error bars show the standard deviations. The error bars are not shown when they are smaller than the symbols. For mastoparan X (*A* and *B*) and melittin (*C* and *D*), the apparent average number of LUVs in the excitation volume and the diffusion times of the LUVs were largely constant for all peptide-to-lipid ratios. In contrast, for magainin 2 (*E* and *F*), the apparent number of LUVs gradually decreased and the LUV diffusion times gradually increased as a function of the peptide-to-lipid ratio. By comparison with Fig. 5.1, we conclude that leakage induced by all three peptides must be due to formation of transmembrane pores.
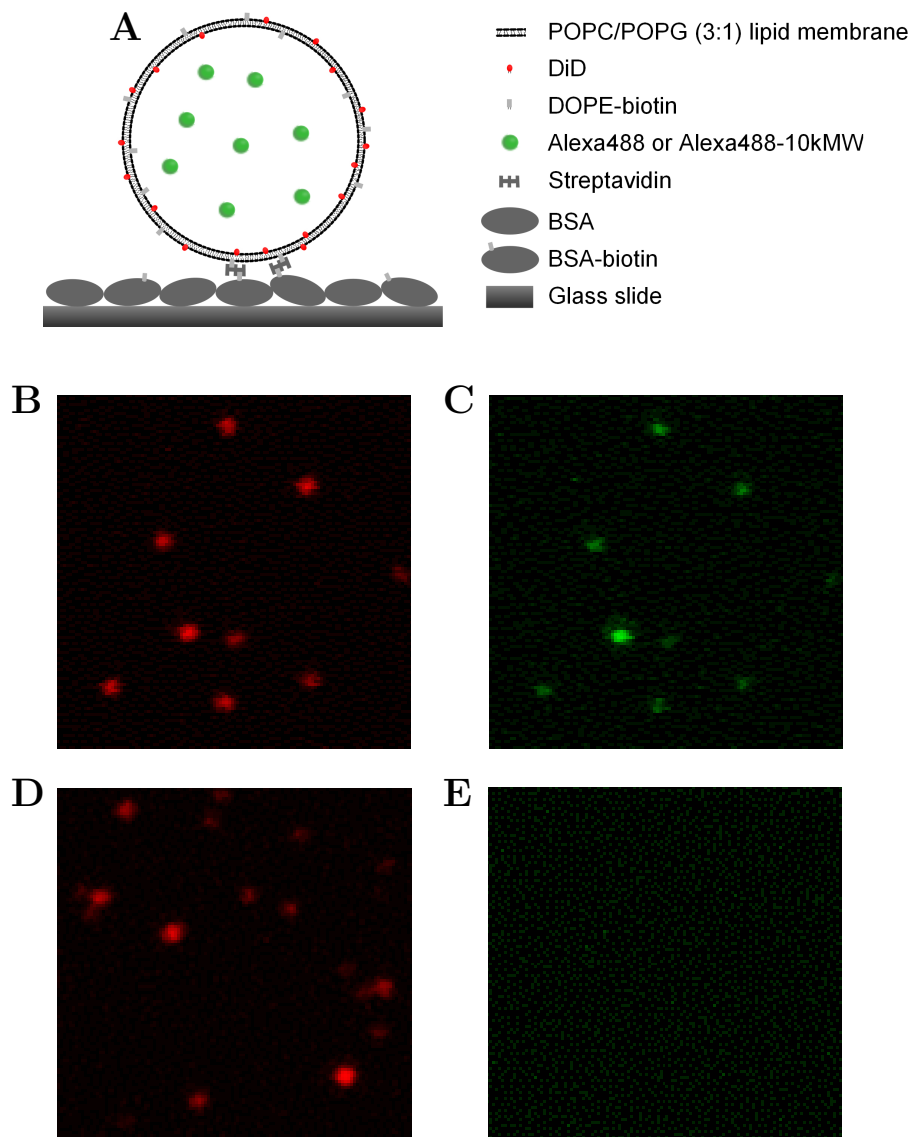
Figure 5.3: (*A*) Schematic drawing of a surface-immobilized POPC/POPG (3:1) LUV. The LUVs were functionalized with DOPE-biotin, labeled with the membrane dye DiD, and loaded with Alexa488 or Alexa488-10kMW. The LUVs were immobilized to cover glass slides by biotin/streptavidin coupling only after treatment with peptide. They could then be visualized as diffraction-limited spots by confocal microscopy. (*B*) and (*C*) Representative confocal images of immobilized DiD-labeled Alexa488-loaded LUVs that had not been treated with peptide (i.e., corresponding to a peptide-to-lipid ratio of 0) before surface-immobilization. A high degree of colocalization between the DiD detector channel (*B*) and the Alexa488 detector channel (*C*) was observed, demonstrating that almost all LUVs contained Alexa488. (*D*) and (*E*) Representative confocal images of immobilized DiD-labeled Alexa488-loaded LUVs that had been treated with mastoparan X (peptide-to-lipid ratio of 0.018) before surface-immobilization. Now, the LUVs were completely void of Alexa488 signal, demonstrating that mastoparan X induced release of Alexa488 from the LUVs. Sizes of the confocal images shown in (*B-E*) are 8.7×8.7 μm. In order to allow the reader to clearly visualize individual LUVs in the images, the contrast of the confocal images in (*B-E*) was enhanced.
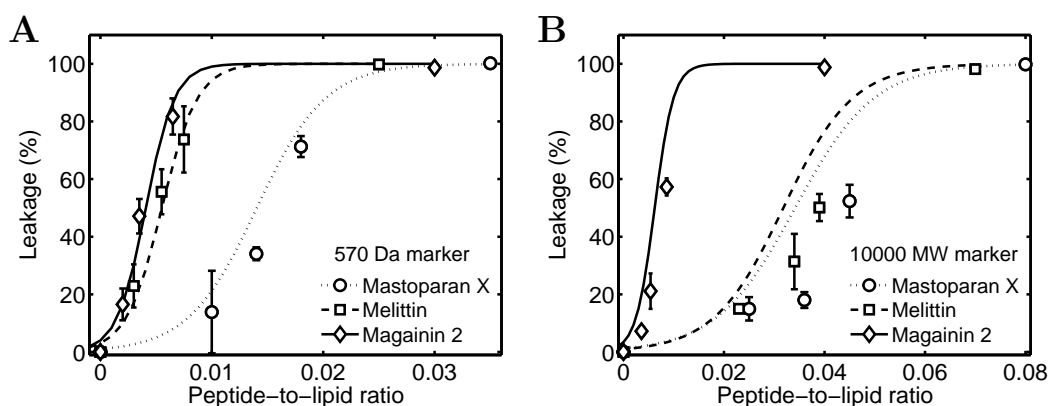
Figure 5.4: Average leakage percentage from the surface-immobilized POPC/POPG (3:1) LUVs as a function of the peptide-to-lipid ratio. In all panels, the data are the average of two separate experiments. The error bars show the standard deviations. The error bars are not shown when they are smaller than the symbols. By definition, the leakage values determined at peptide-to-lipid ratios of 0 are set 0 %. The trendlines are taken from the FCS leakage data in Fig. 5.1 to allow for direct comparison to FCS data. (*A*) Peptide-induced leakage of Alexa488 from the LUVs. Very good agreement between the leakage percentages calculated from the immobilized LUVs and the FCS experiments is observed. (*B*) Peptide-induced leakage of Alexa488-10kMW from the LUVs. Reasonably good agreement between the leakage percentages calculated from the immobilized LUVs and the FCS experiments is observed, albeit the leakage determined from the immobilized LUVs is generally slightly lower than leakage determined by FCS.

of intermolecular interactions between the dextran molecules.

From the surface-immobilized LUVs, we can then obtain insight into peptide-induced leakage on the single-vesicle level by considering the intensity distributions of the immobilized vesicles. Fig. 5.5 shows a few representative examples of such single-vesicle intensity distributions. Specifically, Fig. 5.5 *A* shows the Alexa488 single-vesicle intensity distributions of two samples of unperturbed (peptide-to-lipid ratio 0) and mastoparan X-treated (peptide-to-lipid ratio 0.014) LUVs, respectively. For the mastoparan X-treated LUVs, a large fraction of LUVs were completely emptied of Alexa488 below the detection limit of the apparatus. In contrast, such an empty fraction of LUVs was not observed in the untreated sample. Fig. 5.5 *B* shows the DiD single-vesicle intensity distributions of the same two samples. Interestingly, the DiD single-vesicle intensity distributions were identical for the untreated LUVs and for the mastoparan X-treated LUVs. This observation implies that the LUVs remained intact upon treatment of mastoparan X, and thereby that mastoparan X-induced leakage must be due to the formation of transmembrane pores. In fact, for peptides at all peptide-to-lipid ratios, we always found that the DiD single-vesicle intensity distributions appeared largely identical. This observation corroborates the conclusion that leakage studied in this article is due formation of transmembrane pores.

To systematize the observations from the single-vesicle intensity distributions, we used Eq. 5.6 to calculate the percentage of LUVs that had been completely emptied of lumen dye during leakage induced by mastoparan X, melittin, or magainin 2. Fig. 5.6 *A*
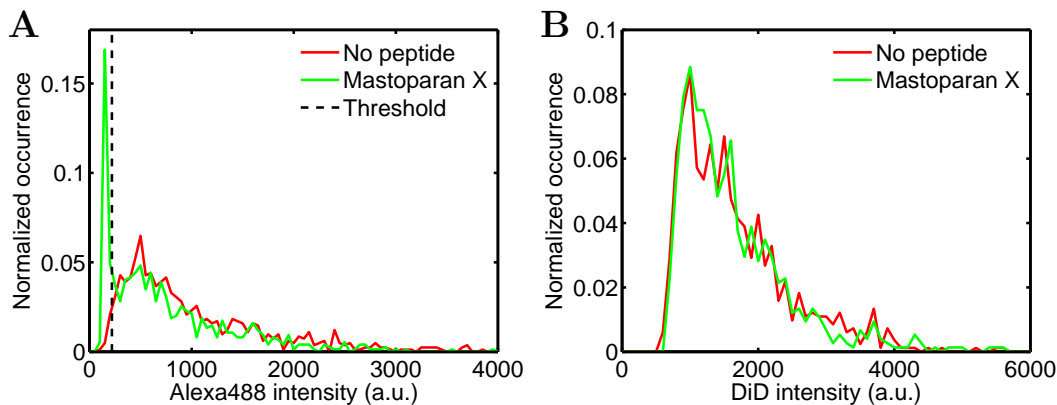
Figure 5.5: Representative examples of single-vesicle intensity distribution of surface-immobilized DiD-labeled Alexa488-containing POPC/POPG (3:1) LUVs. Two different LUV batches were considered: untreated LUVs (peptide-to-lipid ratio of 0) and mastoparan X-treated LUVs (peptide-to-lipid ratio of 0.014). (*A*) Alexa488 single-vesicle intensity distributions. The vertical dashed line show the detection threshold of the apparatus. A large fraction of the LUVs were completely emptied of Alexa488 upon treatment by mastoparan X. (*B*) DiD single-vesicle intensity distributions. The DiD intensity distributions did not change upon treatment by mastoparan X, indicating that the LUVs remained intact.

shows a plot of the percentage of emptied LUVs vs the average percentage leakage from Alexa488-containing LUVs. The plot shows that the three peptides do not induce leakage from Alexa488-containing POPC/POPG (3:1) LUVs by an ideal all-or-none process. If that would have been the case, then the data points in the plot would have been positioned along the diagonal line. Rather, the peptides induce leakage of Alexa488 from POPC/POPG (3:1) LUVs by a strongly heterogenous process in which a fraction of the LUVs are completely emptied and another fraction of the LUVs are only partly emptied. The same type of heterogenous peptide-induced leakage is also observed from LUVs containing Alexa488-10kMW (Fig. 5.6 *B*). Thus, this heterogenous leakage process occurs regardless of the size of the lumen dye. Interestingly, even though magainin 2 by FCS was found to form larger pores than mastoparan X and melittin, our data demonstrates that on the single-vesicle level, magainin 2-induced leakage is similar to leakage induced by mastoparan X and melittin in the sense that all three peptides entail these heterogenous leakage profiles. One could perhaps have expected that the larger and/or more stable magainin 2 pores would lead to leakage by an all-or-none-type process since the larger and/or more stable pores would allow for complete emptying of individual LUV. However, the data in Fig. 5.6 show that this notion is not true, at least for magainin 2-induced leakage from POPC/POPG (3:1) LUVs.

The question is then what molecular processes that might provide an explanation for the heterogenous leakage process that was observed on the single-vesicle level. In order to come up with a possible explanation, we consider a model in which cationic membrane-active peptides will initially bind to the outer leaflet of the LUVs to create an asymmetric tension in the bilayers, promoting the formation of transmembrane pores (75). Upon equilibration of the peptides across the membranes, the internal tension in the membranes is reduced and,
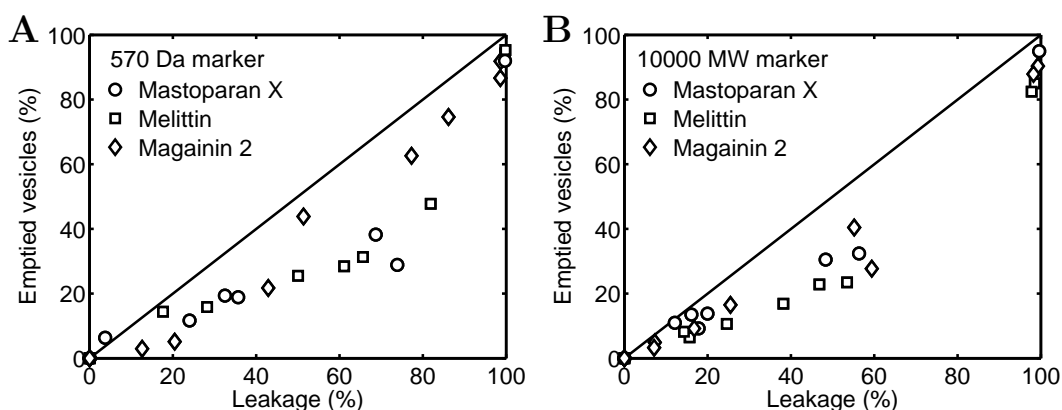
Figure 5.6: The percentage of emptied LUVs vs the average percentage of leakage as determined from confocal imaging of peptide-treated surface-immobilized POPC/POPG (3:1) LUVs containing Alexa488 (*A*) or Alexa488-10kMW (*B*). Each data point corresponds to an individual experiment at a specific peptide-to-lipid ratio. The solid lines represent ideal all-or-none leakage. The data demonstrates that all three peptides induce a heterogenous type of leakage. This heterogenous leakage persists regardless of the size of the lumen dye.

therefore, the transmembrane pores shrink in size or completely closes. Assuming that this model is valid, we conjecture that the heterogenous leakage profiles that we observed on the single-vesicle level imply that the pores that are transiently opened as a result of the asymmetric tension have a distribution of sizes and/or lifetimes. To be more specific, we conjecture that the transiently opened pores might sometimes be sufficiently large and/or long-lived to induce complete leakage of the LUV contents. In other cases, the transiently opened pores will be of a size that restricts the leakage of LUV contents, or they will be so short-lived that the LUVs are only partially emptied before the pores once again close. Thus, in other words, we conjecture that the transient transmembrane pores are not characterizable by one single well-defined radius and one single well-defined lifetime. To corroborate the notion of the transmembrane pores having a distribution of sizes and/or lifetimes, we note that heterogenous leakage was also identified for the two membrane-active peptides CpreTM and NpreTM in a study using GUVs (176).

However, it should be noted that the above scheme only represents a hypothesis. That is, there might also be other explanations for the heterogenous single-vesicle leakage profiles. For example, heterogeneity in leakage on the single-vesicle level could also be a result of heterogeneity in the properties of individual LUVs. For instance, there is no guarantee that the POPC/POPG ratio is completely identical for all LUVs. Indeed, variations in lipid composition would most likely also result in heterogenous single-vesicle leakage profiles. Also, even though LUVs are often assumed to be completely monodisperse, reality is that there will be some polydispersity in samples of LUVs. Differences in sizes between individual LUVs would probably also lead to heterogenous single-vesicle leakage profiles, for example, because of differences in lumen volumes between individual LUVs and because of differences in the membrane curvature between individual LUVs (160). Thus, further efforts are required to

fully understand how to interpret the data in Fig. 5.6 to corroborate or dismiss the hypothesis that transient pores formed by mastoparan X, melittin, and magainin 2 have a distribution of sizes and/or lifetimes.

5.5 Concluding remarks

In this article, we used two techniques to study partial transient leakage of fluorescent markers of different sizes from POPC/POPG (3:1) LUVs induced by the three α-helical cationic membrane-active peptides mastoparan X, melittin, and magainin 2. FCS was used to study peptide-induced leakage on the bulk level. From the FCS experiments we noticed that magainin 2 forms larger and/or more stable pores than mastoparan X and melittin. Confocal imaging of surface-immobilized LUVs was used to study peptide-induced leakage on the single-vesicle level. The confocal imaging experiments were designed so that peptide-induced leakage as observed from the surface-immobilized LUVs was directly representable of peptide-induced leakage from LUVs in solution as observed by FCS. Thereby, the surface-immobilized vesicles provided a more direct and flexible way to observe peptide-induced leakage from individual LUVs than what hitherto has been possible. The data from the surface-immobilized LUVs show that leakage induced by mastoparan X, melittin, and magainin 2 follows a heterogenous process in which some LUVs are completely emptied and some LUVs are only partly emptied, and that this type of leakage is always identified, regardless of the size of the entrapped marker.

5.6 Supporting material

5.6.1 Perturbation induced by DOPE-biotin and DiD

Method

Varying volumes of 100 µM peptide stock solutions were added to varying volumes of POPC/POPG/DOPE-biotin/DiD (74.9:24.9:0.1:0.1) LUV solutions in Protein LoBind tubes to a final LUV concentration of 1 mM. The LUVs were entrapping 4 µM Alexa488 or 2.5-5 µM Alexa488-10kMW. Immediately upon addition of peptide, the samples were vigorously vortexed for a few seconds and subsequently incubated for 1 h. The samples were then transferred to the 8-well chambered cover glasses for examination by FCS. The FCS setup was as described in the main document, albeit with the small difference that an additional 520-550 nm bandpass filter (HQ535/30, Becker & Hickl) was inserted before the pinhole to filter away emission from DiD. From the acquired autocorrelation data, peptide-induced leakage from the POPC/POPG/DOPE-biotin/DiD (74.9:24.9:0.1:0.1) LUVs was then calculated using Eq. 5.4 as described in the main document.

Results

Fig. 5.7 shows leakage vs peptide-to-lipid ratio as determined by FCS after 1 h incubation of peptides together with 1 mM POPC/POPG/DOPE-biotin/DiD (74.9:24.9:0.1:0.1) LUVs
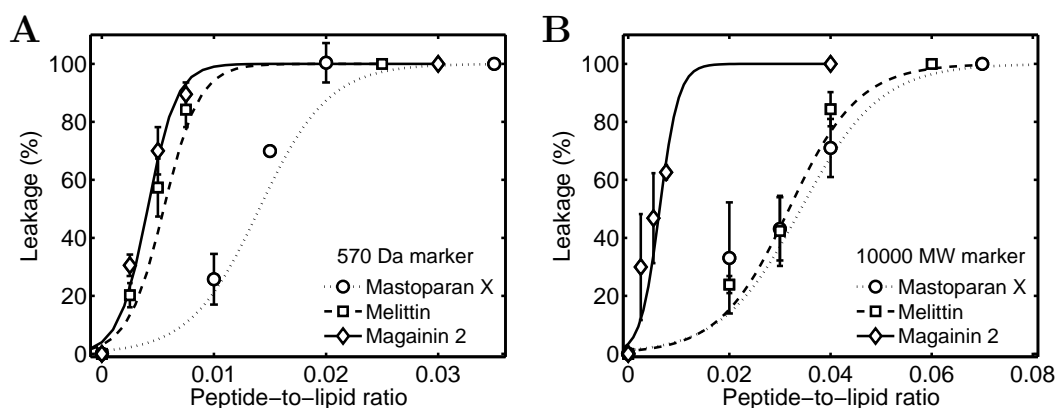
Figure 5.7: Peptide-induced leakage from 1 mM POPC/POPG/DOPE-biotin/DiD (74.9:24.9:0.1:0.1) LUVs containing Alexa488 (*A*) or Alexa488-10kMW (*B*) as determined by FCS after 1 h incubation of peptides together with LUVs. In both panels, the data are the average of three separate experiments. The error bars show the standard deviations. The error bars are not shown when they are smaller than the symbols. The leakage values at the lowest and highest peptide-to-lipid ratios correspond to no leakage and complete leakage, respectively, and, therefore, they are, by definition, always set to 0 % and 100 %, respectively. Trendlines are those of the FCS experiments in Fig 5.1. The data demonstrate that addition of 0.1 % DOPE-biotion and 0.1 % DiD to POPC/POPG (3:1) LUVs induce no perturbations in the leakage process.

loaded with Alexa488 or Alexa488-10kMW. The data demonstrate that addition of 0.1 % DOPE-biotion and 0.1 % DiD to the POPC/POPG (3:1) LUVs does not induce significant changes in leakage as compared to unfunctionalized and unlabeled POPC/POPG (3:1) LUVs.

5.6.2 Effect of POPG addition

Method

Varying volumes of 100 µM peptide stock solutions were added to varying volumes of POPC/POPG/DOPE-biotin/DiD (74.9:24.9:0.1:0.1) LUV solutions in Protein LoBind tubes to a final LUV concentration of 1 mM. The LUVs were entrapping 4 µM Alexa488 or 2.5-5 µM Alexa488-10kMW. Immediately upon addition of peptide, the samples were vigorously vortexed for a few seconds and subsequently incubated for 1 h. After 1 h incubation, a large excess of POPG LUVs was added to a final POPG LUV concentration of 6.7 mM and a final POPC/POPG (3:1) LUV concentration of 0.83 µM. Immediately after addition of the POPG LUVs, the samples were vortexed for a few seconds and then incubated overnight. The next day, the samples were transferred to 8-well chambered cover glasses for examination by FCS. The FCS setup was as described in the main document, albeit with the small difference that an additional 520-550 nm bandpass filter (HQ535/30, Becker & Hickl) was inserted before the pinhole to filter away emission from DiD. From the acquired autocorrelation data, leakage from the POPC/POPG/DOPE-biotin/DiD (74.9:24.9:0.1:0.1) LUVs was then calculated using Eq. 5.4 as described in the main document.
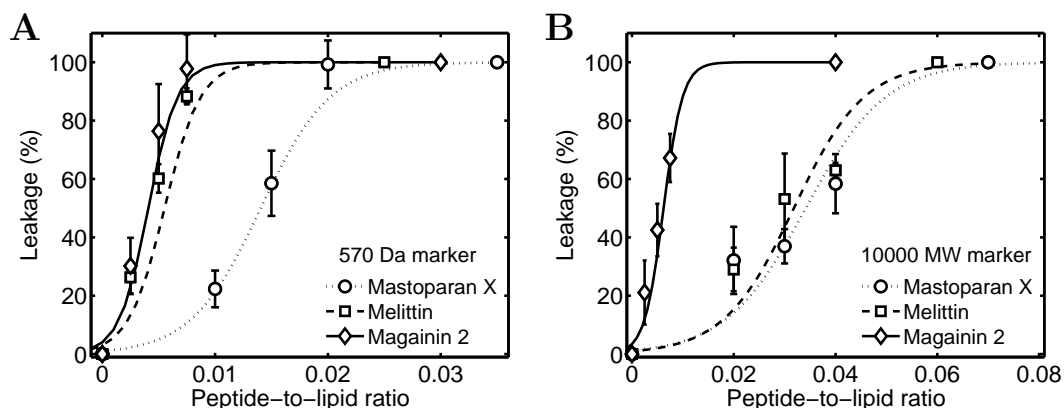
Figure 5.8: Peptide-induced leakage from 1 mM POPC/POPG/DOPE-biotin/DiD (74.9:24.9:0.1:0.1) LUVs containing Alexa488 (*A*) or Alexa488-10kMW (*B*) as determined by FCS conducted on samples in which peptides and LUVs are incubated for 1 h before peptides are removed from the LUVs by addition of a large excess of POPG followed by overnight incubation. In both panels, the data are the average of three separate experiments. The error bars show the standard deviations. The error bars are not shown when they are smaller than the symbols. The leakage values at the lowest and highest peptide-to-lipid ratios correspond to no leakage and complete leakage, respectively, and, therefore, they are, by definition, always set to 0 % and 100 %, respectively. Trendlines are those of the FCS experiments in Fig. 5.1. The data demonstrate leakage is completely halted upon addition of POPG LUVs.

Results

Fig. 5.7 shows leakage vs peptide-to-lipid ratio as determined by FCS conducted on samples in which peptides had been incubated for 1 h together with 1 mM POPC/POPG/DOPE-biotin/DiD (74.9:24.9:0.1:0.1) LUV loaded with Alexa488 or Alexa488-10kMW before a large excess of POPG had been added for overnight incubation. The data shows that upon addition of POPG, no further leakage occurs from the POPC/POPG/DOPE-biotin/DiD (74.9:24.9:0.1:0.1) LUVs.

Conclusions and future perspectives

6.1 Conclusions

A number of specific conclusions were presented at the end of Chapters 3-5. However, for completeness, the three following sections will briefly again summarize the conclusions of this thesis. Specifically, each the three following sections will summarize the conclusions obtained from the three experimental techniques that were employed in this thesis.

6.1.1 Analytical HPLC

Analytical HPLC was used in Chapter 3 to study adsorption of mastoparan X, melittin, and magainin 2 to solid surfaces of glass and plastic. Using this technique, we found that each of the three peptides readily adsorb to both glass and plastic surfaces. Especially alarming is the finding that at typical experimental concentrations of 1-2 µM, $90~\%$ or more of the peptides might be adsorbed to the surfaces of disposable glass and plastic containers. Thus, surface adsorption of antimicrobial peptides is clearly an effect that has to be taken into account when designing experiments on antimicrobial peptides.

6.1.2 FCS

FCS was considered in Chapters 4 and 5 as a technique for quantifying antimicrobial peptide-induced leakage of fluorescent markers from LUVs in solution. Specifically, in Chapter 4, the mathematical theory required for this purpose was derived. In addition, Chapter 4 also considered a number of experimental pitfalls that might compromise the correctness of the leakage values determined by FCS. It was shown that if all of these pitfalls were avoided, then FCS can be used to accurately quantify leakage of fluorescent markers from LUVs in solution, including leakage of fluorescent markers of different sizes. In Chapter 4, mastoparan X was then used to demonstrate that FCS is indeed applicable to study antimicrobial peptide-induced leakage from LUVs in solution.

In Chapter 5, FCS was used to compare partial transient leakage induced by mastoparan X, melittin, and magainin 2 from POPC/POPG (3:1) LUVs. Thus, it was found that leakage

induced from POPC/POPG (3:1) LUVs by all three peptides is due to formation of trans-membrane pores. Furthermore, it was found that magainin 2 on average induced larger pores and/or more stable pores than did mastoparan X and melittin.

6.1.3 Confocal imaging of immobilized LUVs

Confocal imaging was used in Chapter 5 to study antimicrobial peptide-induced leakage of fluorescent markers from surface-immobilized LUVs. To that end, an experimental protocol was developed that allowed the leakage data from the surface-immobilized LUVs to be directly correlated to leakage data determined by FCS on LUVs in solution. Thereby, the surface-immobilized LUVs could be used to gain a higher level of insight into antimicrobial peptide-induced leakage from LUVs on the single-vesicle level than what so far has been achieved by other techniques. For example, the surface-immobilized vesicles could be used for single-vesicle studies of leakage of fluorescent markers of different sizes; such studies on LUVs have hitherto remained as unexplored territory.

The surface-immobilized LUVs were then used to study partial transient leakage induced by mastoparan X, melittin, and magainin 2. The obtained leakage data revealed that on the single-vesicle level, all three peptides induced leakage through a strongly heterogenous process in which some LUVs are completely emptied and some LUVs are only partly emptied. This heterogenous leakage profile is observed regardless of the size of the fluorescent encapsulant. This observations lead to the hypothesis that transmembrane pores formed by mastoparan X, melittin, and magainin 2 might have a distribution of pores and/or lifetimes. However, further work is need to corroborate or dismiss that hypothesis.

6.2 Future perspectives

In the following, it is briefly discussed how the work presented in this thesis might in the future be used to elucidate the mechanisms of antimicrobial peptide-lipid membrane interactions.

6.2.1 Analytical HPLC

As mentioned in Section 2.5, a major goal for research on antimicrobial peptide-lipid membrane interactions is to quantitatively relate the physicochemical properties of the peptides to their mode of membrane interactions. However, for such quantitative relations to be established, it is a prerequisite that the experimental peptide-to-lipid ratio is well-known. The information given in Chapter 3 provides knowledge on how to control this experimental peptide-to-lipid ratio, and thereby also provides a basis for conducting quantitative investigations relating physicochemical properties of the peptides to their mode of membrane interactions.

However, for completeness, it should be noted that in order for the physicochemical properties of the peptides to be quantitatively related to the mode of membrane interactions of the peptides, it is also important to have information about the concentrations of the peptides *in* the lipid membranes. In order to deduce these membrane-bound concentrations, it is necessary to know the partition coefficient for the partitioning of the peptides from water

into the lipid membranes. However, information about partition coefficients is not as such available by any of the techniques presented in this thesis. Instead other techniques could be used for the purpose of determining the partition coefficients, for example, techniques based on intrinsic tryptophan fluorescence (182), isothermal titration calorimetry (64), or equilibrium dialysis combined with analytical HPLC (183).

6.2.2 FCS

A great advantage of FCS is that the technique can be used as a medium-throughout technique for quantifying peptide-induced leakage from LUVs of fluorescent probes of different sizes. Thereby, the technique is applicable for performing quantitative systematic studies to investigate the influence of peptide amino acid residue sequence and lipid composition on the characteristic size of transmembrane pores. Additionally, in cases where leakage is independent on the marker size (168), FCS is applicable to reveal whether leakage occurs due to formation of transmembrane pores or due to membrane solubilization. Thus, FCS is highly applicable for conducting systematic quantitative studies that aim at relating the physicochemical properties of antimicrobial peptides to their mode of membrane interactions.

Another advantage of FCS is that the technique only requires a very low concentration of encapsulated fluorescent markers. Consequently, the experimental conditions in the FCS experiments are much more freely varied than they are in the conventional quenching-based leakage assay, in which very high concentrations of fluorescent markers are encapsulated. In particular, in FCS experiments, it is possible to vary freely the buffer conditions on both the inside and the outside of LUVs. Thereby, FCS would be suitable for studying the impact of osmotic pressure differences between the inside and outside of the vesicle lumen on the leakage process. Another interesting possibility of the FCS experiments would be to evaluate the impact of transmembrane potentials on the leakage process (184). Information about how these parameters influence pore size and leakage mechanism would help to shed light on the mechanisms underlying antimicrobial peptide-lipid membrane interactions.

6.2.3 Confocal imaging of immobilized LUVs

Leakage induced by mastoparan X, melittin, and magainin 2 from POPC/POPG (3:1) LUVs was on the single-vesicle level a heterogenous process for all three peptides. However, it would in future be very interesting to investigate how the leakage process on the single-vesicle level depends on the peptide amino acid residue sequence and the lipid composition of the LUVs; that is, it would be interesting to investigate whether leakage is always a heterogenous process on the single-vesicle level, independent on the peptide sequence and lipid composition, or whether leakage sometimes might be characterized as an ideal all-or-none-type process. Such studies could provide insight into the nature of the transmembrane pores formed by antimicrobial peptides and possibly also a quantitative link between the physicochemical properties of antimicrobial peptides and their behavior in different lipid membranes.

Finally, it should be noted that confocal imaging of surface-immobilized LUVs, when compared to the conventional quenching-based leakage assays, requires relatively low concen-

trations of fluorescent markers. Thereby, it might be possible to use the surface-immobilized LUVs to conduct systematic studies on the effect of osmotic pressure differences and transmembrane potentials on the leakage process on the single-vesicle level, just like FCS is applicable to study the effect of osmotic pressure differences and transmembrane potentials on the leakage process on the bulk level. Systematic studies on the influence of osmotic pressure differences and transmembrane potentials on the leakage process on the single-vesicle level might provide new and interesting insights into the mechanisms by which antimicrobial peptides interact with phospholipid membranes.

References

[1] J. Davies and D. Davies. Origins and evolution of antibiotic resistance. *Microbiol. Mol. Biol. Rev.*, 74:417–433, 2010.

[2] U. Theuretzbacher. Global antibacterial resistance: the never-ending story. *J. Global Antimicrob. Resist.*, 1:63–69, 2013.

[3] D. Jabes. The antibiotic R&D pipeline: an update. *Curr. Opin. Microbiol.*, 14:564–569, 2011.

[4] T. B. Stanton. A call for antibiotic alternatives research. *Trends Microbiol.*, 21: 111–113, 2013.

[5] M. Zasloff. Antimicrobial peptides of multicellular organisms. *Nature*, 415:389–395, 2002.

[6] H. Jenssen, P. Hamill, and R. E. W. Hancock. Peptide antimicrobial agents. *Clin. Microbiol. Rev.*, 19:491–511, 2006.

[7] A. K. Marr, W. J. Gooderham, and R. E. W. Hancock. Antibacterial peptides for therapeutic use: obstacles and realistic outlook. *Curr. Opin. Pharmacol.*, 6:468–472, 2006.

[8] A. T. Y. Yeung, S. L. Gellatly, and R. E. W. Hancock. Multifunctional cationic host defence peptides and their clinical applications. *Cell. Mol. Life Sci.*, 68:2161–2176, 2011.

[9] A. Giuliani, G. Pirri, and S. F. Nicoletto. Antimicrobial peptides: an overview of a promising class of therapeutics. *Cent. Eur. J. Biol.*, 2:1–33, 2007.

[10] W. C. Wimley and K. Hristova. Antimicrobial peptides: successes, challenges and unanswered questions. *J. Membr. Biol.*, 239:27–34, 2011.

[11] N. Papo and Y. Shai. Can we predict biological activity of antimicrobial peptides from their interactions with model phospholipid membranes? *Peptides*, 24:1693–1703, 2003.

[12] K. A. Brogden. Antimicrobial peptides: pore formers or metabolic inhibitors in bacteria? *Nature Rev. Microbiol.*, 3:238–250, 2005.

[13] G. Wang, X. Li, and Z. Wang. APD2: the updated antimicrobial peptide database and its application in peptide design. *Nucleic Acids Res.*, 37:D933–D937, 2009.

[14] M. Pasupuleti, A. Schmidtchen, and M. Malmsten. Antimicrobial peptides: key components of the innate immune system. *Crit. Rev. Biotechnol.*, 32:143–171, 2012.

[15] V. Nizet, T. Ohtake, X. Lauth, J. Trowbridge, J. Rudisill, R. A. Dorschner, V. Pestonjamasp, J. Piraino, K. Huttner, and R. L. Gallo. Innate antimicrobial peptide protects the skin from invasive bacterial infection. *Nature*, 414:454–457, 2001.

[16] N. H. Salzman, D. Ghosh, K. M. Huttner, Y. Paterson, and C. L. Bevins. Protection against enteric salmonellosis in transgenic mice expressing a human intestinal defensin. *Nature*, 422:522–526, 2003.

[17] K. Pütsep, G. Carlsson, H. G. Boman, and M. Andersson. Deficiency of antibacterial peptides in patients with morbus Kostmann: an observation study. *Lancet*, 360:1144–1149, 2002.

[18] C. B. Park, H. S. Kim, and S. C. Kim. Mechanism of action of the antimicrobial peptide buforin II: buforin II kills microorganisms by penetrating the cell membrane and inhibiting cellular functions. *Biochem. Biophys. Res. Commun.*, 244:253–257, 1998.

[19] H. G. Boman, B. Agerberth, and A. Boman. Mechanisms of action on *Escherichia coli* of cecropin P1 and PR-39, two antibacterial peptides from pig intestine. *Infect. Immun.*, 61:2978–2984, 1993.

[20] S. Cociancich, A. Ghazi, C. Hetru, J. A. Hoffmann, and L. Letellier. Insect defensin, an inducible antibacterial peptide, forms voltage-dependent channels in *Micrococcus luteus*. *J. Biol. Chem.*, 268:19239–19245, 1993.

[21] T. Schneider, T. Kruse, R. Wimmer, I. Wiedemann, V. Sass, U. Pag, A. Jansen, A. K. Nielsen, P. H. Mygind, D. S. Raventós, S. Neve, B. Ravn, A. M. J. J. Bonvin, L. De Maria, A. S. Andersen, L. K. Gammelgaard, H. G. Sahl, and H. H. Kristensen. Plectasin, a fungal defensin, targets the bacterial cell wall precursor Lipid II. *Science*, 328:1168–1172, 2010.

[22] K. Kavanagh and S. Dowd. Histatins: antimicrobial peptides with therapeutic potential. *J. Pharm. Pharmacol.*, 56:285–289, 2004.

[23] U. H. N. Dürr, U. S. Sudheendra, and A. Ramamoorthy. LL-37, the only human member of the cathelicidin family of antimicrobial peptides. *Biochim. Biophys. Acta*, 1758:1408–1425, 2006.

[24] V. Teixeira, M. J. Feio, and M. Bastos. Role of lipids in the interaction of antimicrobial peptides with membranes. *Prog. Lipid Res.*, 51:149–177, 2012.

[25] J. P. S. Powers and R. E. W. Hancock. The relationship between peptide structure and antibacterial activity. *Peptides*, 24:1681–1691, 2003.

[26] J. Johansson, G. H. Gudmundsson, M. E. Rottenberg, K. D. Berndt, and B. Agerberth. Conformation-dependent antibacterial activity of the naturally occurring human peptide LL-37. *J. Biol. Chem.*, 273:3718–3724, 1998.

[27] Z. Oren and Y. Shai. Selective lysis of bacteria but not mammalian cells by diastereomers of melittin: structure-function study. *Biochemistry*, 36:1826–1835, 1997.

[28] M. R. Yeaman and N. Y. Yount. Mechanisms of antimicrobial peptide action and resistance. *Pharmacol. Rev.*, 55:27–55, 2003.

[29] M. Dathe, H. Nikolenko, J. Meyer, M. Beyermann, and M. Bienert. Optimization of the antimicrobial activity of magainin peptides by modification of charge. *FEBS Lett.*, 501:146–150, 2001.

[30] A. Giangaspero, L. Sandri, and A. Tossi. Amphipathic α helical antimicrobial peptides. *Eur. J. Biochem.*, 268:5589–5600, 2001.

[31] M. Pasupuleti, B. Walse, B. Svensson, M. Malmsten, and A. Schmidtchen. Rational design of antimicrobial C3a analogues with enhanced effects against Staphylococci using an integrated structure and function-based approach. *Biochemistry*, 47:9057–9070, 2008.

[32] R. Bessalle, H. Haas, A. Goria, I. Shalit, and M. Fridkin. Augmentation of the antibacterial activity of magainin by positive-charge chain extension. *Antimicrob. Agents Chemother.*, 36:313–317, 1992.

[33] T. Wieprecht, M. Dathe, M. Beyermann, E. Krause, W. L. Maloy, D. L. MacDonald, and M. Bienert. Peptide hydrophobicity controls the activity and selectivity of magainin 2 amide in interaction with membranes. *Biochemistry*, 36:6124–6132, 1997.

[34] Y. Chen, M. T. Guarnieri, A. I. Vasil, M. L. Vasil, C. T. Mant, and R. S. Hodges. Role of peptide hydrophobicity in the mechanism of action of α-helical antimicrobial peptides. *Antimicrob. Agents Chemother.*, 51:1398–1406, 2007.

[35] H. T. Chou, T. Y. Kuo, J. C. Chiang, M. J. Pei, W. T. Yang, H. C. Yu, S. B. Lin, and W. J. Chen. Design and synthesis of cationic antimicrobial peptides with improved activity and selectivity against *Vibrio* spp. *Int. J. Antimicrob. Agents*, 32:130–138, 2008.

[36] Y. Shai. Mechanism of the binding, insertion and destabilization of phospholipid bilayer membranes by α-helical antimicrobial and cell non-selective membrane-lytic peptides. *Biochim. Biophys. Acta*, 1462:55–70, 1999.

[37] K. Matsuzaki. Control of cell selectivity of antimicrobial peptides. *Biochim. Biophys. Acta*, 1788:1687–1692, 2009.

[38] Y. Miyazaki, M. Aoki, Y. Yano, and K. Matsuzaki. Interaction of antimicrobial peptide magainin 2 with gangliosides as a target for human cell binding. *Biochemistry*, 51: 10229–10235, 2012.

[39] R. Sood, Y. Domanov, M. Pietiäinen, V. P. Kontinen, and P. K. J. Kinnunen. Binding of LL-37 to model biomembranes: insight into target *vs* host cell recognition. *Biochim. Biophys. Acta*, 1778:983–996, 2008.

[40] R. Sood and P. K. J. Kinnunen. Cholesterol, lanosterol, and ergosterol attenuate the membrane association of LL-37(W27F) and temporin L. *Biochim. Biophys. Acta*, 1778:1460–1466, 2008.

[41] D. Allende, S. A. Simon, and T. J. McIntosh. Melittin-induced bilayer leakage depends on lipid material properties: evidence for toroidal pores. *Biophys. J.*, 88:1828–1837, 2005.

[42] K. Matsuzaki, K. Sugishita, N. Fujii, and K. Miyajima. Molecular basis for membrane selectivity of an antimicrobial peptide, magainin 2. *Biochemistry*, 34:3423–3429, 1995.

[43] M. N. Melo, R. Ferre, and M. A. R. B. Castanho. Antimicrobial peptides: linking partition, activity and high membrane-bound concentrations. *Nat. Rev. Microbiol.*, 7: 245–250, 2009.

[44] J. R. Henriksen and T. L. Andresen. Thermodynamic profiling of peptide membrane interactions by isothermal titration calorimetry: a search for pores and micelles. *Biophys. J.*, 101:100–109, 2011.

[45] W. C. Wimley. Describing the mechanism of antimicrobial peptide action with the interfacial activity model. *ACS Chem. Biol.*, 5:905–917, 2010.

[46] G. Fuertes, A. J. García-Sáez, S. Esteban-Martín, D. Giménez, O. L. Sánchez-Muñoz, P. Schwille, and J. Salgado. Pores formed by Baxα5 relax to a smaller size and keep at equilibrium. *Biophys. J.*, 99:2917–2925, 2010.

[47] Y. Tamba and M. Yamazaki. Magainin 2-induced pore formation in the lipid membranes depends on its concentration in the membrane interface. *J. Phys. Chem. B*, 113:4846–4852, 2009.

[48] Y. Tamba, H. Ariyama, V. Levadny, and M. Yamazaki. Kinetic pathway of antimicrobial peptide magainin 2-induced pore formation in lipid membranes. *J. Phys. Chem. B*, 114:12018–12026, 2010.

[49] S. M. Gregory, A. Cavenaugh, V. Journigan, A. Pokorny, and P. F. F. Almeida. A quantitative model for the all-or-none permeabilization of phospholipid vesicles by the antimicrobial peptide cecropin A. *Biophys. J.*, 94:1667–1680, 2008.

[50] K. Matsuzaki, O. Murase, N. Fujii, and K. Miyajima. Translocation of a channel-forming antimicrobial peptide, magainin 2, across lipid bilayers by forming a pore. *Biochemistry*, 34:6521–6526, 1995.

[51] K. Matsuzaki, S. Yoneyama, O. Murase, and K. Miyajima. Transbilayer transport of ions and lipids coupled with mastoparan X translocation. *Biochemistry*, 35:8450–8456, 1996.

[52] K. Matsuzaki, O. Murase, and K. Miyajima. Kinetics of pore formation by an antimicrobial peptide, magainin 2, in phospholipid bilayers. *Biochemistry*, 34:12553–12559, 1995.

[53] M. T. Lee, W. C. Hung, F. Y. Chen, and H. W. Huang. Mechanism and kinetics of pore formation in membranes by water-soluble amphipathic peptides. *Proc. Natl. Acad. Sci. USA*, 105:5087–5092, 2008.

[54] G. Kokot, M. Mally, and S. Svetina. The dynamics of melittin-induced membrane permeability. *Eur. Biophys. J.*, 41:461–474, 2012.

[55] M. T. Lee, T. L. Sun, W. C. Hung, and H. W. Huang. Process of inducing pores in membranes by melittin. *Proc. Natl. Acad. Sci. USA*, 110:14243–14248, 2013.

[56] S. J. Ludtke, K. He, W. T. Heller, T. A. Harroun, L. Yang, and H. W. Huang. Membrane pores induced by magainin. *Biochemistry*, 35:13723–13728, 1996.

[57] C. C. Lee, Y. Sun, S. Qian, and H. W. Huang. Transmembrane pores formed by human antimicrobial peptide LL-37. *Biophys. J.*, 100:1688–1696, 2011.

[58] S. J. Ludtke, K. He, Y. Wu, and H. W. Huang. Cooperative membrane insertion of magainin correlated with its cytolytic activity. *Biochim. Biophys. Acta*, 1190:181–184, 1994.

[59] H. W. Huang. Molecular mechanism of antimicrobial peptides: the origin of cooperativity. *Biochim. Biophys. Acta*, 1758:1292–1302, 2006.

[60] S. Ludtke, K. He, and H. W. Huang. Membrane thinning caused by magainin 2. *Biochemistry*, 34:16764–16769, 1995.

[61] H. W. Huang, F. Y. Chen, and M. T. Lee. Molecular mechanism of peptide-induced pores in membranes. *Phys. Rev. Lett.*, 92:198304–1–198304–4, 2004.

[62] M. L. Longo, A. J. Waring, L. M. Gordon, and D. A. Hammer. Area expansion and permeation of phospholipid membrane bilayers by influenza fusion peptides and melittin. *Langmuir*, 14:2385–2395, 1998.

[63] M. R. Wenk and J. Seelig. Magainin 2 amide interaction with lipid membranes: calorimetric detection of peptide binding and pore formation. *Biochemistry*, 37:3909–3916, 1998.

[64] G. Klocek, T. Schulthess, Y. Shai, and J. Seelig. Thermodynamics of melittin binding to lipid bilayers. Aggregation and pore formation. *Biochemistry*, 48:2586–2596, 2009.

[65] L. Yang, T. M. Weiss, R. I. Lehrer, and H. W. Huang. Crystallization of antimicrobial pores in membranes: magainin and protegrin. *Biophys. J.*, 79:2002–2009, 2000.

[66] L. Yang, T. A. Harroun, T. M. Weiss, L. Ding, and H. W. Huang. Barrel-stave model or toroidal model? A case study on melittin pores. *Biophys. J.*, 81:1475–1485, 2001.

[67] S. Qian, W. Wang, L. Yang, and H. W. Huang. Structure of transmembrane pore induced by Bax-derived peptide: evidence for lipidic pores. *Proc. Natl. Acad. Sci. USA*, 105:17379–17383, 2008.

[68] K. Bertelsen, J. Dorosz, S. K. Hansen, N. C. Nielsen, and T. Vosegaard. Mechanisms of peptide-induced pore formation in lipid bilayers investigated by oriented ^{31}P solid-state NMR spectroscopy. *PLoS ONE*, 7:e47745, 2012.

[69] D. Sengupta, H. Leontiadou, A. E. Mark, and S. J. Marrink. Toroidal pores formed by antimicrobial peptides show significant disorder. *Biochim. Biophys. Acta*, 1778:2308–2317, 2008.

[70] T. Lazaridis, Y. He, and L. Prieto. Membrane interactions and pore formation by the antimicrobial peptide protegrin. *Biophys. J.*, 104:633–642, 2013.

[71] M. Mihajlovic and T. Lazaridis. Antimicrobial peptides bind more strongly to membrane pores. *Biochim. Biophys. Acta*, 1798:1494–1502, 2010.

[72] K. Matsuzaki, K. Sugishita, N. Ishibe, M. Ueha, S. Nakata, K. Miyajima, and R. M. Epand. Relationship of membrane curvature to the formation of pores by magainin 2. *Biochemistry*, 37:11856–11863, 1998.

[73] S. Bobone, D. Roversi, L. Giordano, M. De Zotti, F. Formaggio, C. Toniolo, Y. Park, and L. Stella. The lipid dependence of antimicrobial peptide activity is an unreliable experimental test for different pore models. *Biochemistry*, 51:10124–10126, 2012.

[74] A. J. García-Sáez, S. Chiantia, J. Salgado, and P. Schwille. Pore formation by a Bax-derived peptide: effect on the line tension of the membrane probed by AFM. *Biophys. J.*, 93:103–112, 2007.

[75] G. Fuertes, D. Giménez, S. Esteban-Martín, O. L. Sánchez-Muñoz, and J. Salgado. A lipocentric view of peptide-induced pores. *Eur. Biophys. J.*, 40:399–415, 2011.

[76] E. Karatekin, O. Sandre, H. Guitouni, N. Borghi, P. H. Puech, and F. Brochard-Wyart. Cascades of transient pores in giant vesicles: line tension and transport. *Biophys. J.*, 84:1734–1749, 2003.

[77] K. He, S. J. Ludtke, D. L. Worcester, and H. W. Huang. Neutron scattering in the plane of membranes: structure of alamethicin pores. *Biophys. J.*, 70:2659–2666, 1996.

[78] K. He, S. J. Ludtke, W. T. Heller, and H. W. Huang. Mechanism of alamethicin insertion into lipid bilayers. *Biophys. J.*, 71:2669–2679, 1996.

[79] S. Qian, W. Wang, L. Yang, and H. W. Huang. Structure of the alamethicin pore reconstructed by X-ray diffraction analysis. *Biophys. J.*, 94:3512–3522, 2008.

[80] M. Mihajlovic and T. Lazaridis. Antimicrobial peptides in toroidal and cylindrical pores. *Biochim. Biophys. Acta*, 1798:1485–1493, 2010.

[81] A. Pokorny, T. H. Birkbeck, and P. F. F. Almeida. Mechanism and kinetics of δ-lysin interaction with phospholipid vesicles. *Biochemistry*, 41:11044–11056, 2002.

[82] A. Pokorny and P. F. F. Almeida. Kinetics of dye efflux and lipid flip-flop induced by δ-lysin in phosphatidylcholine vesicles and the mechanism of graded release by amphipathic, α-helical peptides. *Biochemistry*, 43:8846–8857, 2004.

[83] A. Pokorny and P. F. F. Almeida. Permeabilization of raft-containing lipid vesicles by δ-lysin: a mechanism for cell sensitivity to cytotoxic peptides. *Biochemistry*, 44: 9538–9544, 2005.

[84] R. Rathinakumar and W. C. Wimley. Biomolecular engineering by combinatorial design and high-throughput screening: small, soluble peptides that permeabilize membranes. *J. Am. Chem. Soc.*, 130:9849–9858, 2008.

[85] R. Rathinakumar, W. F. Walkenhorst, and W. C. Wimley. Broad-spectrum antimicrobial peptides by rational combinatorial design and high-throughput screening: the importance of interfacial activity. *J. Am. Chem. Soc.*, 131:7609–7617, 2009.

[86] E. Gazit I. R. Miller, Phil C. Biggin, M. S. P. Sansom, and Y. Shai. Structure and orientation of the mammalian antibacterial peptide cecropin P1 within phospholipid membranes. *J. Mol. Biol.*, 258:860–870, 1996.

[87] N. Papo and Y. Shai. Exploring peptide membrane interaction using surface plasmon resonance: differentiation between pore formation versus membrane disruption by lytic peptides. *Biochemistry*, 42:458–466, 2003.

[88] Y. Shai. Mode of action of membrane active antimicrobial peptides. *Biopolymers*, 66: 236–248, 2002.

[89] E. S. Salnikov, A. J. Mason, and B. Bechinger. Membrane order perturbation in the presence of antimicrobial peptides by ^{2}H solid-state NMR spectroscopy. *Biochimie*, 91:734–743, 2009.

[90] R. F. Epand, G. Wang, B. Berno, and R. M. Epand. Lipid segregation explains selective toxicity of a series of fragments derived from the human cathelicidin LL-37. *Antimicrob. Agents Chemother.*, 53:3705–3714, 2009.

[91] R. F. Epand, W. L. Maloy, A. Ramamoorthy, and R. M. Epand. Probing the "charge cluster mechanism" in amphipathic helical cationic antimicrobial peptides. *Biochemistry*, 49:4076–4084, 2010.

[92] A. Arouri, M. Dathe, and A. Blume. Peptide induced demixing in PG/PE lipid mixtures: a mechanism for the specificity of antimicrobial peptides towards bacterial membranes? *Biochim. Biophys. Acta*, 1788:650–659, 2009.

[93] R. F. Epand, L. Maloy, A. Ramamoorthy, and R. M. Epand. Amphipathic helical cationic antimicrobial peptides promote rapid formation of crystalline states in the presence of phosphatidylglycerol: lipid clustering in anionic membranes. *Biophys. J.*, 98:2564–2573, 2010.

[94] R. M. Epand and R. F. Epand. Bacterial membrane lipids in the action of antimicrobial agents. *J. Pept. Sci.*, 17:298–305, 2011.

[95] R. M. Epand and R. F. Epand. Lipid domains in bacterial membranes and the action of antimicrobial agents. *Biochim. Biophys. Acta*, 1788:289–294, 2009.

[96] P. Joanne, C. Galanth, N. Goasdoué, P. Nicolas, S. Sagan, S. Lavielle, G. Chassaing, C. El Amri, and I. D. Alves. Lipid reorganization induced by membrane-active peptides probed using differential scanning calorimetry. *Biochim. Biophys. Acta*, 1788:1772–1781, 2009.

[97] B. Bechinger and K. Lohner. Detergent-like actions of linear amphipathic cationic antimicrobial peptides. *Biochim. Biophys. Acta*, 1758:1529–1539, 2006.

[98] B. Bechinger. Rationalizing the membrane interactions of cationic amphipathic antimicrobial peptides by their molecular shape. *Curr. Opin. Colloid Interface Sci.*, 14: 349–355, 2009.

[99] E. F. Haney, S. Nathoo, H. J. Vogel, and E. J. Prenner. Induction of non-lamellar lipid phases by antimicrobial peptides: a potential link to mode of action. *Chem. Phys. Lipids*, 163:82–93, 2010.

[100] K. Hilpert, M. R. Elliott, R. Volkmer-Engert, P. Henklein, O. Donini, Q. Zhou, D. F. H. Winkler, and R. E. W. Hancock. Sequence requirements and an optimization strategy for short antimicrobial peptides. *Chem. Biol.*, 13:1101–1107, 2006.

[101] A. J. Krauson, J. He, A. W. Wimley, A. R. Hoffmann, and W. C. Wimley. Synthetic molecular evolution of pore-forming peptides by iterative combinatorial library screening. *ACS Chem. Biol.*, 8:823–831, 2013.

[102] R. Rathinakumar and W. C. Wimley. High-throughput discovery of broad-spectrum peptide antibiotics. *FASEB J.*, 24:3232–3238, 2010.

[103] C. D. Fjell, H. Jenssen, K. Hilpert, W. A. Cheung, N. Pante, R. E. W. Hancock, and A. Cherkasov. Identification of novel antibacterial peptides by chemoinformatics and machine learning. *J. Med. Chem.*, 52:2006–2015, 2009.

[104] C. D. Fjell, J. A. Hiss, R. E. W. Hancock, and G. Schneider. Designing antimicrobial peptides: form follows function. *Nat. Rev. Drug Discovery*, 11:37–51, 2012.

[105] A. J. Krauson, J. He, and W. C. Wimley. Determining the mechanism of membrane permeabilizing peptides: identification of potent, equilibrium pore-formers. *Biochim. Biophys. Acta*, 1818:1625–1632, 2012.

[106] N. B. Last and A. D. Miranker. Common mechanism unites membrane poration by amyloid and antimicrobial peptides. *Proc. Natl. Acad. Sci. USA*, 110:6382–6387, 2013.

[107] P. F. Almeida and A. Pokorny. Mechanisms of antimicrobial, cytolytic, and cell-penetrating peptides: from kinetics to thermodynamics. *Biochemistry*, 48:8083–8093, 2009.

[108] A. N. McKeown, J. L. Naro, L. J. Huskins, and P. F. Almeida. A thermodynamic approach to the mechanism of cell-penetrating peptides in model membranes. *Biochemistry*, 50:654–662, 2011.

[109] K. S. Clark, J. Svetlovics, A. N. McKeown, L. Huskins, and P. F. Almeida. What determines the activity of antimicrobial and cytolytic peptides in model membranes. *Biochemistry*, 50:7919–7932, 2011.

[110] T. Etzerodt, J. R. Henriksen, P. Rasmussen, M. H. Clausen, and T. L. Andresen. Selective acylation enhances membrane charge sensitivity of the antimicrobial peptide mastoparan-x. *Biophys. J.*, 100:399–409, 2011.

[111] H. Raghuraman and A. Chattopadhyay. Melittin: a membrane-active peptide with diverse functions. *Biosci. Rep.*, 27:189–223, 2007.

[112] K. Matsuzaki. Magainins as paradigm for the mode of action of pore forming polypeptides. *Biochim. Biophys. Acta*, 1376:391–400, 1998.

[113] T. Higashijima, K. Wakamatsu, M. Takemitsu, M. Fujino, T. Nakajima, and T. Miyazawa. Conformational change of mastoparan from wasp venom on binding with phospholipid membrane. *FEBS Lett.*, 152:227–230, 1983.

[114] W. C. Wimley and S. H. White. Experimentally determined hydrophobicity scale for proteins at membrane interfaces. *Nat. Struct. Biol.*, 3:842–848, 1996.

[115] Y. M. Crandall and M. D. Bruch. Characterization of the structure and dynamics of mastoparan-X during folding in aqueous TFE by CD and NMR spectroscopy. *Biopolymers*, 89:197–209, 2008.

[116] D. Marion, M. Zasloff, and A. Bax. A two-dimensional NMR study of the antimicrobial magainin 2. *FEBS Lett.*, 227:21–26, 1988.

[117] B. Bechinger, M. Zasloff, and S. J. Opella. Structure and orientation of the antibiotic peptide magainin in membranes by solid-state nuclear magnetic resonance spectroscopy. *Protein Sci.*, 2:2077–2084, 1993.

[118] Y. Miura. NMR studies on the monomer-tetramer transition of melittin in an aqueous solution at high and low temperatures. *Eur. Biophys. J.*, 41:629–636, 2012.

[119] T. Higashijima, K. Wakamatsu, K. Saito, M. Fujino, T. Nakajima, and T. Miyazawa. Molecular aggregation and conformational change of wasp venom mastoparan as induced by salt in aqueous solution. *Biochim. Biophys. Acta*, 802:157–161, 1984.

[120] Y. Todokoro, I. Yumen, K. Fukushima, S. W. Kang, J. S. Park, T. Kohno, K. Wakamatsu, H. Akutsu, and T. Fujiwara. Structure of tightly membrane-bound mastoparan-X, a G-protein-activating peptide, determined by solid-state NMR. *Biophys. J.*, 91: 1368–1379, 2006.

[121] K. Wakamatsu, A. Okada, T. Miyazawa, M. Ohya, and T. Higashijima. Membrane-bound conformation of mastoparan-X, a G-protein-activating peptide. *Biochemistry*, 31:5654–5660, 1992.

[122] K. Matsuzaki, O. Murase, H. Tokuda, S. Funakoshi, N. Fujii, and K. Miyajima. Orientational and aggregational states of magainin 2 in phospholipid bilayers. *Biochemistry*, 33:3342–3349, 1994.

[123] M. R. Hartings, H. B. Gray, and J. R. Winkler. Probing melittin helix-coil equilibria in solutions and vesicles. *J. Phys. Chem. B*, 112:3202–3207, 2008.

[124] J. A. Whiles, R. Brasseur, K. J. Glover, G. Melacini, E. A. Komives, and R. R. Vold. Orientation and effects of mastoparan X on phospholipid bicelles. *Biophys. J.*, 80: 280–293, 2001.

[125] G. Schwarz and G. Beschiaschvili. Thermodynamic and kinetic studies on the association of melittin with a phospholipid bilayer. *Biochim. Biophys. Acta*, 979:82–90, 1989.

[126] N. Hellmann and G. Schwarz. Peptide-liposome association. A critical examination with mastoparan-X. *Biochim. Biophys. Acta*, 1369:267–277, 1998.

[127] K. Fujita, S. Kimura, and Y. Imanishi. Self-assembly of mastoparan X derivative having fluorescence probe in lipid bilayer membrane. *Biochim. Biophys. Acta*, 1195:157–163, 1994.

[128] L. E. Yandek, A. Pokorny, and P. F. F. Almeida. Wasp mastoparans follow the same mechanism as the cell-penetrating peptide transportan 10. *Biochemistry*, 48:7342–7351, 2009.

[129] G. Beschiaschvili and J. Seelig. Melittin binding to mixed phosphatidylglycerol/phosphatidylcholine membranes. *Biochemistry*, 29:52–58, 1990.

[130] A. Arbuzova and G. Schwarz. Pore-forming action of mastoparan peptides on liposomes: a quantitative analysis. *Biochim. Biophys. Acta*, 1420:139–152, 1999.

[131] S. Rex and G. Schwarz. Quantitative studies on the melittin-induced leakage mechanism of lipid vesicles. *Biochemistry*, 37:2336–2345, 1998.

[132] S. Rex. Pore formation induced by the peptide melittin in different lipid vesicle membranes. *Biophys. Chem.*, 58:75–85, 1996.

[133] M. P. dos Santos Cabrera, D. S. Alvares, N. B. Leite, B. M. de Souza, M. S. Palma, K. A. Riske, and J. R. Neto. New insight into the mechanism of action of wasp mastoparan peptides: lytic activity and clustering observed with giant vesicles. *Langmuir*, 27:10805–10813, 2011.

[134] T. Benachir and M. Lafleur. Study of vesicle leakage induced by melittin. *Biochim. Biophys. Acta*, 1235:452–460, 1995.

[135] E. E. Ambroggio, F. Separovic, J. H. Bowie, G. D. Fidelio, and L. A. Bagatolli. Direct visualization of membrane leakage induced by the antibiotic peptides: Maculatin, Citropin, and Aurein. *Biophys. J.*, 89:1874–1881, 2005.

[136] R. Dimova, S. Aranda, N. Bezlyepkina, V. Nikolov, K. A. Riske, and R. Lipowsky. A practical guide to giant vesicles. Probing the membrane nanoregime via optical microscopy. *J. Phys.: Condens. Matter*, 18:S1151–S1176, 2006.

[137] F. Milletti. Cell-penetrating peptides: classes, origin, and current landscape. *Drug Discov. Today*, 17:850–860, 2012.

[138] C. Bechara and S. Sagan. Cell-penetrating peptides: 20 years later, where do we stand? *FEBS Lett.*, 587:1693–1702, 2013.

[139] D. Persson, P. E. G. Thorén, M. Herner, P. Lincoln, and B. Nordén. Application of a novel analysis to measure the binding of the membrane-translocating peptide penetratin to negatively charged liposomes. *Biochemistry*, 42:421–429, 2003.

[140] D. E. Chico, R. L. Given, and B. T. Miller. Binding of cationic cell-permeable peptides to plastic and glass. *Peptides*, 24:3–9, 2003.

[141] M. R. Duncan, J. M. Lee, and M. P. Warchol. Influence of surfactants upon protein/peptide adsorption to glass and polypropylene. *Int. J. Pharm.*, 120:179–188, 1995.

[142] H. M. L. J. Joosten and M. Nuñez. Adsorption of nisin and enterocin 4 to polypropylene and glass surfaces and its prevention by Tween 80. *Lett. Appl. Microbiol.*, 21:389–392, 1995.

[143] S. L. Law and C. L. Shih. Adsorption of calcitonin to glass. *Drug. Dev. Ind. Pharm.*, 25:253–256, 1999.

[144] G. Rouser, A. N. Siakotos, and S. Fleischer. Quantitative analysis of phospholipids by thin-layer chromatography and phosphorus analysis of spots. *Lipids*, 1:85–86, 1966.

[145] M. Duncan, M. Gilbert, J. Lee, and M. Warchol. Development and comparison of experimental assays to study protein/peptide adsorption onto surfaces. *J. Colloid Interface Sci.*, 165:341–345, 1994.

[146] K. Nakanishi, T. Sakiyama, and K. Imamura. On the adsorption of proteins on solid surfaces, a common but very complicated phenomenon. *J. Biosci. Bioeng.*, 91:233–244, 2001.

[147] J. H. Livesey and M. G. Nicholls. Stickiness to hydrophobic surfaces varies widely among peptides and proteins. *J. Immunoassay. Immunochem.*, 33:302–313, 2012.

[148] M. T. Tosteson, S. J. Holmes, M. Razin, and D. C. Tosteson. Melittin lysis of red cells. *J. Membr. Biol.*, 87:35–44, 1985.

[149] E. Grant Jr., T. J. Beeler, K. M. P. Taylor, K. Gable, and M. A. Roseman. Mechanism of magainin 2a induced permeabilization of phospholipid vesicles. *Biochemistry*, 31: 9912–9918, 1992.

[150] A. S. Ladokhin, W. C. Wimley, and S. H. White. Leakage of membrane vesicle contents: determination of mechanism using fluorescence requenching. *Biophys. J.*, 69:1964–1971, 1995.

[151] A. S. Ladokhin, W. C. Wimley, K. Hristova, and S. H. White. Mechanism of leakage of contents of membrane vesicles determined by fluorescence requenching. *Meth. Enzymol.*, 278:474–486, 1997.

[152] K. Matsuzaki, S. Yoneyama, and K. Miyajima. Pore formation and translocation of melittin. *Biophys. J.*, 73:831–838, 1997.

[153] A. Pramanik, P. Thyberg, and R. Rigler. Molecular interactions of peptides with phospholipid vesicle membranes as studied by fluorescence correlation spectroscopy. *Chem. Phys. Lipids*, 104:35–47, 2000.

[154] L. Yu, J. L. Ding, B. Ho, S. S. Feng, and T. Wohland. Investigation of the mechanisms of antimicrobial peptides interacting with membranes by fluorescence correlation spectroscopy. *The Open Chemical Physics Journal*, 1:62–79, 2008.

[155] L. Yu, L. Guo, J. L. Ding, B. Ho, S. S. Feng, J. Popplewell, M. Swann, and T. Wohland. Interaction of an artificial antimicrobial peptide with lipid membranes. *Biochim. Biophys. Acta*, 1788:333–344, 2009.

[156] O. Krichevsky and G. Bonnet. Fluorescence correlation spectroscopy: the technique and its applications. *Rep. Prog. Phys.*, 65:251–297, 2002.

[157] J. Ries and P. Schwille. Fluorescence correlation spectroscopy. *Bioessays*, 34:361–368, 2012.

[158] M. Magzoub, K. Oglęcka, A. Pramanik, L. E. G. Eriksson, and A. Gräslund. Membrane perturbation effects of peptides derived from the N-termini of unprocessed prion proteins. *Biochim. Biophys. Acta*, 1716:126–136, 2005.

[159] Y. Hirai, M. Kuwada, T. Yasuhara, H. Yoshida, and T. Nakajima. A new mast cell degranulating peptide homologous to mastoparan in the venom of Japanese hornet (*Vespa xanthoptera*). *Chem. Pharm. Bull. (Tokyo)*, 27:1945–1946, 1979.

[160] G. Schwarz and A. Arbuzova. Pore kinetics reflected in the dequenching of a lipid vesicle entrapped fluorescent dye. *Biochim. Biophys. Acta*, 1239:51–57, 1995.

[161] A. Arbuzova and G. Schwarz. Pore kinetics of mastoparan peptides in large unilamellar vesicles. *Prog. Colloid Polym. Sci.*, 100:345–350, 1996.

[162] Y. O. Posokhov, M. V. Rodnin, L. Lu, and A. S. Ladokhin. Membrane insertion pathway of annexin B12: thermodynamic and kinetic characterization by fluorescence correlation spectroscopy and fluorescence quenching. *Biochemistry*, 47:5078–5087, 2008.

[163] S. Rüttinger, V. Buschmann, B. Krämer, R. Erdmann, R. MacDonald, and F. Koberling. Comparison and accuracy of methods to determine the confocal volume for quantitative fluorescence correlation spectroscopy. *J. Microsc.*, 232:343–352, 2008.

[164] L. Rusu, A. Gambhir, S. McLaughlin, and J. Rädler. Fluorescence correlation spectroscopy studies of peptide and protein binding to phospholipid vesicles. *Biophys. J.*, 87:1044–1053, 2004.

[165] T. Wohland, R. Rigler, and H. Vogel. The standard deviation in fluorescence correlation spectroscopy. *Biophys. J.*, 80:2987–2999, 2001.

[166] S. T. Hess and W. W. Webb. Focal volume optics and experimental artifacts in confocal fluorescence correlation spectroscopy. *Biophys. J.*, 83:2300–2317, 2002.

[167] M. P. Bohrer, W. M. Deen, C. R. Robertson, J. L. Troy, and B. M. Brenner. Influence of molecular configuration on the passage of macromolecules across the glomerular capillary wall. *J. Gen. Physiol.*, 74:583–593, 1979.

[168] A. S. Ladokhin and S. H. White. 'Detergent-like' permeabilization of anionic lipid vesicles by melittin. *Biochim. Biophys. Acta*, 1514:253–260, 2001.

[169] T. M. Allen and L. G. Cleland. Serum-induced leakage of liposome contents. *Biochim. Biophys. Acta*, 597:418–426, 1980.

[170] J. N. Weinstein, S. Yoshikami, P. Henkart, R. Blumenthal, and W. A. Hagins. Liposome-cell interaction: transfer and intracellular release of a trapped fluorescent marker. *Science*, 195:489–492, 1977.

[171] J. N. Weinstein, R. D. Klausner, T. Innerarity, E. Ralston, and R. Blumenthal. Phase transition release, a new approach to the interaction of proteins with lipid vesicles. Application to lipoproteins. *Biochim. Biophys. Acta*, 647:270–284, 1981.

[172] K. Matsuzaki, M. Fukui, N. Fujii, and K. Miyajima. Permeabilization and morphological changes in phosphatidylglycerol bilayers induced by an antimicrobial peptide, tachyplesin I. *Colloid Polym. Sci.*, 271:901–908, 1993.

[173] S. M. Gregory, A. Pokorny, and P. F. F. Almeida. Magainin 2 revisited: a test of the quantitative model for the all-or-none permeabilization of phospholipid vesicles. *Biophys. J.*, 96:116–131, 2009.

[174] H. Patel, C. Tscheka, and H. Heerklotz. Characterizing vesicle leakage by fluorescence lifetime measurements. *Soft Matter*, 5:2849–2851, 2009.

[175] H. Patel, C. Tscheka, K. Edwards, G. Karlsson, and H. Heerklotz. All-or-none membrane permeabilization by fengycin-type lipopeptides from *Bacillus subtilis* QST713. *Biochim. Biophys. Acta*, 1808:2000–2008, 2011.

[176] B. Apellániz, J. L. Nieva, P. Schwille, and A. J. García-Sáez. All-or-none versus graded: single-vesicle analysis reveals lipid composition effects on membrane permeabilization. *Biophys. J.*, 99:3619–3628, 2010.

[177] S. A. Wheaten, A. Lakshmanan, and P. F. Almeida. Statistical analysis of peptide-induced graded and all-or-none fluxes in giant vesicles. *Biophys. J.*, 105:432–443, 2013.

[178] S. M. Christensen and D. G. Stamou. Sensing-applications of surface-based single vesicle arrays. *Sensors*, 10:11352–11368, 2010.

[179] S. R. Tabaei, M. Rabe, V. P. Zhdanov, N. J. Cho, and F. Höök. Single vesicle analysis reveals nanoscale membrane curvature selective pore formation in lipid membranes by an antiviral α-helical peptide. *Nano Lett.*, 12:5719–5725, 2012.

[180] G. van den Bogaart, J. T. Mika, V. Krasnikov, and B. Poolman. The lipid dependence of melittin action investigated by dual-color fluorescence burst analysis. *Biophys. J.*, 93:154–163, 2007.

[181] A. S. Ladokhin, M. E. Selsted, and S. H. White. Bilayer interactions of indolicidin, a small antimicrobial peptide rich in tryptophan, proline, and basic amino acids. *Biophys. J.*, 72:794–805, 1997.

[182] A. S. Ladokhin, S. Jayasinghe, and S. H. White. How to measure and analyze tryptophan fluorescence in membranes properly, and why bother? *Anal. Biochem.*, 285:235–245, 2000.

[183] W. C. Wimley and S. H. White. Quantitation of electrostatic and hydrophobic membrane interactions by equilibrium dialysis and reverse-phase HPLC. *Anal. Biochem.*, 213:213–217, 1993.

[184] D. Terrone, S. L. W. Sang, L. Roudaia, and J. R. Silvius. Penetratin and related cell-penetrating cationic peptides can translocate across lipid bilayers in the presence of a transbilayer potential. *Biochemistry*, 42:13787–13799, 2003.